January 2014

X-Ray Fluorescence Analysis Of The Bakken And Three Forks Formations Of The Williston Basin, North Dakota And Well Logging Applications

Russell James Carr

[How does access to this work benefit you? Let us know!](#)

Follow this and additional works at: https://commons.und.edu/theses

Recommended Citation

Carr, Russell James, "X-Ray Fluorescence Analysis Of The Bakken And Three Forks Formations Of The Williston Basin, North Dakota And Well Logging Applications" (2014). *Theses and Dissertations*. 1514.
https://commons.und.edu/theses/1514

X-RAY FLUORESCENCE ANALYSIS OF THE BAKKEN AND THREE FORKS
FORMATIONS OF THE WILLISTON BASIN, NORTH DAKOTA AND WELL
LOGGING APPLICATIONS

by

Russell James Carr

Bachelor of Science, University of Nevada, Reno, 2012

A Thesis

Submitted to the Graduate Faculty

of the

University of North Dakota

in partial fulfillment of the requirements

for the degree of

Master of Science

Grand Forks, North Dakota
May
2014

This thesis, submitted by Russell J. Carr in partial fulfillment of the requirements for the Degree of Master of Science from the University of North Dakota, has been read by the Faculty Advisory Committee under whom the work has been done and is hereby approved.

_____
Lance D. Yarbrough, Ph.D., P.E.-Chairperson

_____
Scott F. Korom, Ph.D., P.E.-Committee Member

_____
Steven A. Benson, Ph.D.-Committee Member

This thesis is being submitted by the appointed advisory committee as having met all of the requirements of the School of Graduate Studies at the University of North Dakota and is hereby approved.

_____
Wayne Swisher
Dean of the School of Graduate Studies

_____
Date

PERMISSION

Title   X-Ray Fluorescence Analysis of the Bakken and Three Forks Formations
             of the Williston Basin, North Dakota and Well-Logging Applications

Department   Geological Engineering

Degree   Master of Science

      In presenting this thesis in partial fulfillment of the requirements for a graduate degree from the University of North Dakota, I agree that the library of this University shall make it freely available for inspection. I further agree that permission for extensive copying for scholarly purposes may be granted by the professor who supervised my thesis work or, in his absence, by the Chairperson of the department or the dean of the School of Graduate Studies. It is understood that any copying or publication use shall not be allowed without my written permission. It is also understood that due recognition shall be given to me and to the University of North Dakota in any scholarly use which may be made of any material in my thesis.

<div style="margin-left:50%;">

Russell J. Carr, E.I., G.I.T.

5/17/2014

Date

</div>

TABLE OF CONTENTS

LIST OF FIGURES

LIST OF TABLES

LIST OF EQUATIONS

ACKNOWLEDGEMENTS

I want to sincerely thank Dr. Lance Yarbrough for his mentorship and friendship during my tenure in graduate school. I also want to thank Lance, Buffie, and Ezekiel Yarbrough for making my stay in Grand Forks warm and comfortable. I want to thank Dr. Scott Korom for his support and encouragement during my career as a graduate student. I want to thank Dr. Steven Benson, Dr. Srivats Srinivasachar, and Mrs. Shanna Corbett for their help and kindness. I also want to thank Dr. Yarbrough, Dr. Korom, and Dr. Benson for serving on my committee and helping me improve as an engineer.

I want to thank my parents James and Janice Carr. I also would like to thank Elsie, Robert, and Anna Carr for always supporting me. I love you. I want to thank Steven, Barbara, and Joshua Oxley for their support and encouragement.

I want to thank Janine Oxley for everything that she has done for me. I love her more than any words can describe.

ABSTRACT

The ability to characterize subsurface lithology is critical for hydrocarbon identification and subsequent production. Well-logging methods currently used in industry typically incorporate gamma ray, spontaneous potential, resistivity, porosity, acoustic and mud logging principles. Relatively little focus has been placed on using x-ray fluorescence (XRF) to identify the geochemical signatures of hydrocarbon bearing strata. The exploitation of petroleum bearing shale will demand greater stratigraphic resolution; x-ray fluorescence well-logging (XRFWL) will accurately and efficiently identify geochemical signatures of hydrocarbon bearing lithological units in both vertical and horizontal drilling applications. Geosteering applications will also be able to benefit from higher stratigraphic resolution provided by XRFWL.

This thesis research analyzed nine core sections representing The Lower Bakken and Three Forks Formation of the Williston Basin in North Dakota using x-ray fluorescence. The Charlotte 1-22H core sequence from Continental Resources was also included to assess the elemental composition of the stratigraphic interval spanning the Lodgepole, Bakken, Pronghorn, and Three Forks Formations. Core samples were obtained from the North Dakota Industrial Commission (NDIC) Wilson B. Laird Core and Sample Library at the University of North Dakota. Core sections were exposed to x-ray at 15 keV and 45 keV excitation voltages to provide elemental spectra; count rate values were obtained and elemental ratios were then calculated to assess the geochemical

composition and diagenetic changes within each stratigraphic interval. The results of the

analyses were then used to create XRF well-logs representing the subsurface lithology of

the Williston Basin. XRF well-logs were then compared with industry logging-while-

drilling (LWD) and wireline logs to assess the physical differences between conventional

logging and fluorescence logging measurements.

Results of x-ray fluorescence analysis of Williston Basin core include detailed

well-logs showing the vertical distribution of lightweight, mid-range, and trace metal

elements. Overwhelmingly, the evidence presented in this thesis shows that x-ray

fluorescence ratios can uniquely chronicle autonomous lithostratigraphic units with

higher efficiency than conventional wireline or logging-while drilling technology. The x-

ray fluorescence elemental ratios of Fe:Mn can more precisely determine formation

contacts on core sections than conventional gamma ray or spontaneous potential methods.

Furthermore, x-ray fluorescence will allow for unique identification of members and thin

beds within larger formations. Elemental Kα fluorescence ratios of Fe:Mn, Fe:Ca, Fe:Rb,

Fe:S, and S:Cl can precisely identify the Bakken Formation. Ratios of Ca:Mg, Ca:Rb,

Ca:Zn, and Ca:Ti can precisely identify the Lodgepole, Three Forks, and Middle Bakken

Formation. Furthermore, the ratio of Fe:Mn can be applied to the Middle Member of the

Bakken Formation to identify unique lithofacies. Although this thesis only analyzed

Williston Basin core, the results provided imply that calcium Kα fluorescence ratios can

be used to identify carbonate lithologies; iron Kα fluorescence ratios can be used to

identify shale lithologies.

Industrial applications of x-ray fluorescence well-logging could include accurate

lithological identification with higher stratigraphic resolution than current methods,

determinations of petroleum bearing strata, and improved efficiency during mud-logging analysis. The academic sector will benefit immensely from the use of XRF; research results will include lithofacies mapping and identification, thermal maturity determinations, mineral deposition and composition, basin origin and progression, depositional histories of formations, and genetic mapping of fluorescence values on cores throughout the Williston Basin. This thesis provides data, methodology, and discussions regarding the applications of x-ray fluorescence for geologic analysis in the Williston Basin of North Dakota.

CHAPTER I

INTRODUCTION

The Mississippian-Devonian Bakken Formation has been a source of continual academic research since being declared a 'Tremendous source of oil production' in the early 1970's by Dow (1974, p. 1253). Although numerous publications have discussed the depositional environments, lithology, and hydrocarbon resource potential (Meissner, 1984; LeFever et al., 1991; Smith and Bustin, 1995; Gaswirth, 2008; Sonnenberg and Pramudito, 2009; Pollastro, 2013), few publications have discussed x-ray fluorescence chemostratigraphic analysis of Williston Basin Core. This main objective of this thesis was to assess the feasibility of using active x-ray fluorescence elemental Kα count ratios as a high precision lithologic indicator using core sections from the Lodgepole, Bakken, and Three Forks Formations. Elemental fluorescence count ratios were then compared with industry wireline and logging-while- drilling (LWD) logs to determine if fluorescence and conventional well-logging methods are correlative. Fluorescence ratio data are then scrutinized and compared with Bakken literature to determine if depositional, diagenetic, or geologic interpretations can be extracted from core fluorescence data.

This thesis outlined a new method, using analytical chemostratigraphy, to address questions regarding the formation, deposition, and hydrocarbon production of the Bakken and Three Forks Formations of the Williston Basin, North Dakota. The

analytical method applied in this thesis was x-ray fluorescence (XRF); ionizing electromagnetic radiation is used to analyze the chemical composition of core sections throughout the hydrocarbon producing sections of the Williston Basin. To assess the feasibility of using XRF for geologic analysis, scientific objectives were developed to examine and summarize the applicability of this method for answering both academic and industrial questions. The objectives of this thesis focused on large-scale scientific questions; future research could utilize the method presented in this thesis to answer small-scale (i.e. regional/Giga-scale) scientific questions.

The objectives of this thesis will provide answers to the following scientific questions: The first objective of this thesis was to determine whether analytical XRF is capable of distinguishing unique geologic lithology. Core sections from the Lodgepole Formation (carbonate), Upper Bakken Member (shale), Middle Bakken Member (mixed siliciclastic and shale), Lower Bakken Member (shale), Pronghorn Member (mixed sandstone and shale), and Three Forks Formation (carbonate) will be subjected to x-ray to determine if each unique lithology is chemically distinguishable. If analytical XRF is capable of distinguishing unique geologic lithology, XRF could theoretically be incorporated as a well-logging or mud-logging tool. The ability to identify lithology down hole is fundamentally necessary for producing oil; a precise analytical tool for lithology identification would be industrially useful.

The second objective of this thesis was to determine whether analytical XRF is capable of distinguishing different geologic formations that consist of the same lithology. The second objective also answered the question of whether unique lithofacies can be distinguished within larger formations. If the first objective proves to be unsuccessful, the

second objective will also be unsuccessful. In this thesis fluorescence values of the Upper Bakken Member and Lower Bakken Member will be compared to examine whether visually identical lithology can be chemically identified and separated. Fluorescence values from the Middle Bakken Member and Three Forks Formations will be collected to assess whether individual lithofacies can be identified in a larger-scale member. If analytical XRF is capable of distinguishing thin lithofacies within larger members, XRF could theoretically outline thin beds of low permeability beds, such as shale. Precise identification of low permeability zones could allow for improved production through improved geo-steering and hydraulic fracturing design.

The third objective of this thesis was to determine whether whether analytical XRF is capable of precisely determining formation contacts with greater precision than current geophysical methods. Current well-logging methods will provide, at best, a two-foot vertical resolution. This question will be answered using a one-foot vertical resolution. Core section formation contacts were analyzed using XRF to establish whether fluorescence values can identify formation changes. The formation contacts analyzed in this thesis will include Lodgepole-Bakken and Bakken-Three Forks; member contacts within the Bakken Formation will also be collected (Upper-Middle Bakken Members, Middle-Lower Bakken Members, and Lower Bakken-Pronghorn Members). If analytical XRF is capable of determining unique lithology with high precision using drill cuttings alone, it could become a permanent mud-logging tool.

The fourth objective of this thesis was to quantify correlations between analytical XRF and current geophysical well-logging methods. This thesis used LWD and wireline logs to calculate various geologic parameters; shale volume, water saturation, and bulk

resistivity values were calculated and used to assess the hydrocarbon saturation down bore. These values were then compared with fluorescence values to determine whether XRF analysis can lead to the same geologic interpretations of other well-logging methods. If analytical XRF is capable of determining lithology, water saturation, oil saturation, and resistivity of core sections it will be a potentially useful well-logging tool.

The fifth objective of this thesis was to determine whether analytical XRF can be used as a tool to help determine paleoenvironments, sediment source providence, and diagenetic alteration of Williston Basin formations through geologic time. Building from the second thesis objective, if visually identical lithology can be distinguished using fluorescence, analytical XRF could also be used to determine sediment providence, basin subduction through geologic time, and diagenetic alteration throughout the Williston Basin. Genetic identification of geologic sections proves useful for numerous research topics including lithofacies mapping and identification, thermal maturity determinations, mineral deposition and compaction, basin origin and progression, and genetic mapping. Academic questions regarding Williston Basin core in hydrocarbon bearing strata are inherently useful to the industrial sector; analytical XRF could also benefit the petroleum industry.

The sixth and final objective of this thesis was to answer the question of why increased stratigraphic precision is necessary for petroleum production in the Williston Basin of North Dakota. To complete this objective the increased rate of horizontal drilling and oil production in the Williston Basin was summarized. This thesis showed that increased oil production is a function of drilling within permeable lithology; finding zones of higher permeability is necessary for higher levels of oil production.

To accomplish the objectives and answer the scientific questions included, this thesis first summarized the geology of the Williston Basin in North Dakota. Extensive research efforts have characterized every stratigraphic interval inside of the basin; this thesis only summarized the most fundamental literature describing the Upper, Middle, and Lower Members of the Bakken Formation and the Three Forks Formation. Understanding the lithology of the Bakken and Three Forks Formation is fundamentally necessary to determine whether x-ray fluorescence spectroscopy can adequately forecast abrupt formation contacts. Publications regarding the subsidence history, spatial extent, and resource utilization of the Williston Basin were quickly summarized to provide proper context for this thesis.

The United States Geologic Survey (USGS) hydrocarbon resource assessment of the Williston Basin was summarized to show the large amount of technically recoverable oil within Bakken-Three Forks reservoirs. The chronological development of horizontal drilling within the basin is quantified to show the exponential growth of both oil production and drilling within the State of North Dakota. Further formation data shows that the most productive horizontal wells have been drilled in the Middle Bakken Member of the Bakken Formation. Data from the North Dakota Industrial Commission (NDIC) will be presented to show that annual oil production from the Williston Basin quadrupled from 2009-2013. Quantifying and presenting the development of petroleum exploration, drilling, and production is necessary to provide evidence that more precise methods of lithological identification would greatly benefit industrial applications.

This thesis then explained the fundamental physics regarding x-ray fluorescence spectroscopy; thoroughly comprehending the principles of energy dispersive Kα

fluorescence is necessary should x-ray fluorescence becomes an industrially viable logging method in the next several years. Publications regarding the historical use of x-ray fluorescence in the earth sciences were discussed to dissect interpretation methods; additional sources outside of the earth sciences will also be examined to bridge the gap between x-ray fluorescence use in the earth sciences and other scientific disciplines. Describing the working principles of x-ray fluorescence is necessary to support data collection methodology used within this thesis.

Key portions of this thesis involved explanations between conventional and unconventional hydrocarbon resources. The Bakken-Three Forks oil pool of North Dakota is an example of an unconventional hydrocarbon resource; due to the lack of structural traps characteristic of conventional reservoirs, this thesis will provide evidence that unconventional hydrocarbon exploitation requires more precise stratigraphic location identification than conventional counterparts. Conventional well-logging methods, specifically wireline and logging-while-drilling methods, are described and to show which methods can be effectively utilized within the Williston Basin. This thesis will show evidence that neither wireline nor LWD methods provide a clear and distinct advantage for hydrocarbon identification. Finally, wireline and LWD data from Williston Basin core will be examined to conclude this thesis.

The methods behind all data collection, processing, and well-log calculations are presented so that results found in this thesis research are scientifically sound and repeatable. After procedures are explained, this thesis was broken into two distinct sections. The first section examined the results found in nine Bakken-Three Forks contact core sections throughout the Williston Basin; the second section focused on the

Continental Resources', Inc. Charlotte 1-22H core section representing the Lodgepole, Bakken, and Three Forks Formations. The first section also presented x-ray fluorescence as a means of assessing a formation contact; the Charlotte 1-22H well was included to support the initial findings and provide additional geologic insight. The goal of both sections is to provide evidence to support the claim that x-ray fluorescence can adequately locate changes of lithology on an unprecedented scale; to prove that x-ray fluorescence has an added advantage over gamma logging, it will have to offer a one-foot vertical resolution. Currently the best resolution logs offer a two-foot vertical resolution. Data from this thesis showed that Middle Bakken horizontal wells are the most productive unconventional wells within the Williston Basin, the one-foot or less vertical resolution offered by x-ray fluorescence would be especially useful for horizontal drilling within the Middle Member of the Bakken. Knowing that the well bore is located within the siliciclastic Middle Member of the Bakken would only benefit industry, x-ray fluorescence can indicate shale lithology before gamma ray methods.

This thesis concluded by acknowledging the shortcomings and limitations of data. As of 2014 x-ray fluorescence is not an established well-logging method so there are challenges that need to be identified and overcome with respect to using the method. Large-scale and collaborative research and development efforts are needed to incorporate x-ray fluorescence into a wireline or LWD package. If x-ray fluorescence is adopted by the oil and gas industry within the next several years, it will most likely be incorporated as a mud-logging tool of drill cuttings returned from bit. This thesis showed that x-ray fluorescence is a viable lithology identification tool; future use will allow for precise stratigraphic determinations allowing additional hydrocarbon production and efficiency.

This thesis concluded by showing that Fe:Mn, Fe:Ca, Fe:S, Fe:Rb, and S:Cl elemental ratios can effectively be applied during core analysis to determine shale lithology within the Bakken Formation. Ca:Mg, Ca:Ti, and Ca:Rb elemental Kα fluorescence ratios can be effectively applied to core analysis of carbonate lithology; although data from this thesis represented only Williston Basin core, the former fluorescence ratios can be utilized for all carbonate and shale lithologies, respectively.

CHAPTER II

GEOLOGY OF THE WILLISTON BASIN

This thesis provided new insight to arguments regarding the paleogeography, paleoenvironment, and depositional histories of the Bakken and Three Forks Formations in the Williston Basin of North Dakota by outlining a new method of core logging. Ionizing electromagnetic x-ray fluorescence elemental count data will allow for a more thorough examination of the chemostratigraphy of the Upper Bakken, Middle Bakken, Lower Bakken, and Three Forks Formations. This data will allow for comparisons between the results found in this thesis and the differing conclusions (See Chapter II-"Sequence Stratigraphy of the Mississippian Devonian Bakken Formation) of previous Bakken authors: (LeFever et al., 1991; Meissner, 1984; Smith and Bustin, 1995; Smith and Bustin, 1996; and Thrasher, 1987). In addition to adding insight to previous academic research, this thesis will also attempt to assess the feasibility of more precise stratigraphic identification during horizontal and vertical drilling operations. To adequately answer the former thesis objectives, it is necessary to summarize the petroleum geology of the Williston Basin, the petroleum resource assessment of the Williston Basin, the chronological development of horizontal drilling in the Williston Basin, the sequence stratigraphy of the Mississippian-Devonian Bakken Formation, and finally the sequence stratigraphy of the Devonian Three Forks Formation. This thesis highlights the fact that hydrocarbon production from the Williston Basin is increasing at

9

an exponential rate; precisely knowing the stratigraphic location while drilling in the vertical and horizontal directions will be important as production continues to increase. Technological advancements, such as the use of ionizing electromagnetic energy down bore, will ultimately allow for increased oil production in the Williston Basin of North Dakota.

The Williston Basin is an intracratonic sedimentary basin with the deepest Precambrian basement located near Williston, North Dakota (Webster, 1984). The spatial extent of the Williston Basin is widely considered to be contained within Montana, North Dakota, South Dakota, and South-Central Canada (Gerhard, 1982). Major structural features in the Williston Basin include the Nesson Anticline, the Billings Anticline, the Cedar Creek Anticline, the Welson Fault, and the Brockton-Froid Fault Zone. The Nesson and Cedar Creek Anticlines have been regarded as prolific conventional structural traps; major zones of production include the Beaver Lodge, Sanish, and West Tioga oil fields. Although the Nesson Anticline is historically regarded as a conventional structural trap, the Nesson Anticline appears to be a tensional structural feature caused by the dissolution of Prairie Formation salts (Smith and Bustin, 1995). Most of the hydrocarbons produced are from reservoir and source rocks deposited during the Paleozoic Era; significant producers include (but are not limited to) the Mississippian Lodgepole Formation, the Mississippian-Devonian Bakken Formation, the Devonian Three Forks Formation, and the Devonian Duperow Formation (LeFever, 1987). The North Dakota Industrial Commission (NDIC) records the cumulative oil production (over the entire history of petroleum production in the state) in the North Dakota portion of the Williston Basin; as of December 2013 the cumulative oil produced was 2.251 billion

barrels of oil. The most productive formations include the Bakken Formation (546.5 million barrels through 5,380 wells), the Red River Formation (250.4 million barrels in Member A and B through 1,265 wells), the Madison Group (931.4 million barrels in the Lodgepole, Mission Canyon, and Charles Formations through 5,547 wells), the Duperow Formation (51.4 million barrels through 345 wells), and the Three Forks Formation (142.9 million barrels of oil through 1,642 wells).

Age (Mya)	Era	Period	Sequence	Group	Formation	Members
320	Paleozoic	Mississippian	Kaskaskia	Big Snowy	Otter	
					Kibbey	
				Madison	Charles Fm.	
					Mission Canyon	
					Lodgepole	
345					Bakken	Upper Bakken
						Middle Bakken
		Devonian				Lower Bakken
						Pronghorn
					Three Forks	
				Jefferson	Birdbear	
					Duperow	
				Manitoba	Souris River	
					Dawson Bay	
				Elk Point	Prairie	
					Winnipegosis	

Figure 1. Stratigraphic Column of the Kaskaskia Sequence. The Kaskaskia Sequence of the Paleozoic Era extends geographically across the Williston Basin and thickens towards the center of the Basin. The inclusion of the Pronghorn Member as the lowermost member of the Bakken Formation is based off the revised nomenclature of (LeFever et al., 2011).

Universally all publications regarding the Bakken and Three Forks Formations of the Williston Basin agree that the Bakken Formation is overlain by Mississippian Madison Group carbonates. The Lodgepole Formation, Mission Canyon Formation, and Charles Formations overlay the Bakken Formation in the North Dakota Portion of the Williston Basin. All cited publications also agree that the Bakken Formation overlays the Devonian Three Forks Formation; with the Three Forks Formation overlying the Birdbear or Nisku Formation. Due to the breadth of knowledge available regarding the Bakken Formation in both the United States and Canada (also known as the Exshaw Formation), this paper will focus only on the North Dakota portion of the Bakken Formation. However, the Three Forks Formation will be discussed in both North Dakota and Manitoba. When discussing the actual Bakken Formation, most authors agree that the Bakken Formation is composed of a black, organic-rich, upper and lower shale member. Furthermore, most authors agree that the middle Bakken Formation exists between the Upper and Lower Shale members and is composed of varying lithofacies of dolomite, siltstone, dolomitic siltstone, and light shale. All authors also agree on several lithological characteristics of the Three Forks Formation; it is composed of dolomite, shale, and siltstone with alternating zones of anoxic and oxidized deposition. Although formation lithology agreement is common between authors, large-scale disagreements exist over the depositional history, thicknesses, and nomenclature in each formation. This thesis will attempt to answer questions regarding the paleogeography, paleoenvironment, and depositional history of the Bakken and Three Forks Formations.

Petroleum Resource Assessment of the Williston Basin

On April 30, 2013 the United States Geological Survey (USGS) estimated that the

Bakken-Three Forks oil pool in the Williston Basin of North Dakota, South Dakota, and

Montana holds a total of 7.4 billion barrels of undiscovered and technically recoverable

oil (Gaswirth et al., 2013). This updated assessment was completed subsequently to the

April, 2008 USGS assessment that listed the Bakken-Three Forks oil pool at 3.65 billion

barrels of undiscovered and technically recoverable oil (Pollastro et al., 2008). Five years

after the initial resource assessment the USGS increased the amount of technically

recoverable oil in the Bakken-Three Forks oil pool a total of 3.75 billion barrels; this

dramatic increase was due to new horizontal drilling technology, a substantial increase in

the number of wells tapping the Bakken-Three Forks oil pool (4,000 additional wells

added between April 2008 and April 2013), and increased cooperation from industry in

providing geologic, exploration, and production data. The 2013 resource assessment also

included hydrocarbons held in the reservoir carbonates of the Three Forks Formation into

the assessment. The 2013 USGS resource assessment concludes with a catalog of the

total amount of technically recoverable oil in the Williston Basin by State: South Dakota

holds 1.4 million barrels, Montana holds 1.583 billion barrels, and North Dakota holds

5.798 billion barrels. The USGS resource assessment is important because it outlines the

fact that despite technological advancements in geologic analysis since the beginning of

the personal computing revolution, the total amount of oil within the Bakken Formation

and the amount of oil that will ultimately be recovered is ultimately an abstract estimate

at best. Although calculating the absolute amount of recoverable oil in the Bakken-Three

Forks oil pool is seemingly impossible, academic and industrial partners have proven that huge amounts of recoverable oil still exist in the Williston Basin. As the ability to precisely map the stratigraphy while drilling increases with technological advancement, the ultimate recoverable oil will increase. This statement will be proven by showing the chronological development of horizontal drilling in the Williston Basin; horizontal well bores that have reached zones with high effective porosity have been recorded as prolific hydrocarbon producers.

Chronological Development of Horizontal Drilling

As of September, 2013 the North Dakota Industrial Commission (NDIC) reports 6,376 horizontal wells in the State of North Dakota. Formation data exists for each horizontal well: 231 horizontal wells have been completed into the Upper Bakken Member, 2 horizontal wells have been completed into the Lodgepole Formation, 70 horizontal wells have been completed into areas where the Middle Bakken and Three Forks Formations contact (primarily in the northwest corner of the state along the Canadian Border), 1,610 horizontal wells have been completed into the Lower Bakken and Three Forks Formation contact zone, and finally 4,463 horizontal wells have been completed into the Middle Bakken member of the Bakken Formation. Based on these data alone it is apparent that companies have been targeting the Middle Member of the Bakken Formation and the Three Forks Formation; higher porosity, effective porosity, and permeability allow for hydrocarbon production. Permeability measurements within the Bakken Formation and the Three Forks Formation suggest that effective porosity increases outside of the shale: the average Bakken shale permeability is 1.8mD, the average Middle Bakken permeability is 5.6mD, and the average Three Forks permeability

is 4.3mD (Nicolas, 2006). The average porosity of the entire Bakken Formation is14.7%

and the average porosity of the entire Three Forks Formation is 16.5% (Nicolas, 2006).

Horizontal well development is a relatively new practice when compared to the

history of the Williston Basin. As of September, 2013 the total horizontal oil production

in North Dakota has been 730.36 million barrels of oil (32% of total cumulative oil

production in the Williston Basin history). Today oil is arguably the most important

natural resource produced in North Dakota; oil was first discovered in the state in 1951

when Amerada Hess Corporation completed the Clarence Iverson #1 on the Nesson

Anticline in the Silurian Interlake Formation (Heck et al., 1998). In the interval between

1951 and 1986 no horizontal wells were completed in the Williston Basin, for the lack of

technology and ingenuity prevented progress.

Table 1. Chronological Development of Horizontal Drilling in the Williston Basin. From
January, 2011 through October, 2013 the number of new horizontal wells completed was
greater than the combined total from the previous 60 years.

Chronological Development of Horizontal Drilling-Williston Basin, North Dakota		
Timeline	Number of Completed Horizontal Wells	Number of New Horizontal Wells
1951-March 1986	1	1
March 1986-July 1991	146	145
July 1991-December 2001	227	82
December 2001-December 2008	943	716
January 2009-December 2010	2,189	1,246
January 2011-October 2013	6,377	4,188
Based on Non-Confidential NDIC data from 1951-September, 2013.		

Table 2. Cumulative Horizontal Oil Production by Formation in the Williston Basin. Horizontal wells targeting the Middle Bakken Formation have been the most prolific unconventional hydrocarbon producers in the Williston Basin; the high permeability and effective porosity allows high production yield.

Cumulative Oil Production By Formation From Horizontal Wells-Williston Basin, North Dakota		
Formation	Total Number of Horizontal Wells	Barrels of Oil (Bbls)
Upper Bakken Formation	237	24,520,000
Three Forks Formation	1,610	142,980,000
Middle Bakken Formation	4,469	554,990,000
MB-TF (Shale Absent)	76	7,810,000
Lodgepole Formation	2	34,500
Based on Non-Confidential NDIC data from 1951-October, 2013.		

The first horizontal well, Froholm #1-18 completed by Phillip D. Armstrong Inc., was completed into the Upper Bakken Member on March 29th, 1986. This well produced a total of 41,273 barrels of oil, a relatively small production total. Between 1986 and July, 1991, 145 additional horizontal wells were completed into the Upper Bakken Member; the total oil production was 15.67 million barrels of oil. The first horizontal well targeting the Three Forks Formation, AMU H-517 HR by Hess Corporation, was completed on July 23rd, 1991 and produced only 2,763 barrels of oil. Between July, 1991 and December, 2001 81 additional wells were completed into the Upper Bakken Member, these wells produced 8.19 million barrels and raised the cumulative Upper Bakken Production to 23.86 million barrels. Fifty years after the first oil was discovered in the Williston Basin, only 227 horizontal wells had been drilled.

Horizontal drilling in the Williston Basin experienced the birth of a renaissance on March 4th, 2004 when Continental Resources, Inc. drilled the first horizontal well, named Robert Heuer 1-17R, into the Middle Bakken Formation. This well produced

109,147 barrels of oil and convinced operators that drilling into the porous lithofacies of the Middle Bakken Formation would yield greater effective porosity and hence greater oil production. In the period between March 4th, 2004 and December 31st, 2008, 713 additional horizontal wells were completed in the Williston Basin: 631 were drilled in the Middle Bakken (total oil production of 113.35 million barrels), 78 were drilled into the Three Forks (total oil production of 10.12 million barrels), and the forgotten Upper Bakken Member only had four new horizontal completions (total production of 658 thousand barrels). Between January 1, 2009 and December 31st, 2010 1,246 new horizontal wells were completed in the Williston Basin. The Middle Bakken was again targeted far more than any other formation; 964 new horizontal wells produced 168.26 million barrels of oil. The Three Forks Formation was also targeted again during this period, producing approximately 36.77 million barrels of oil from 281 horizontal wells. The Upper Bakken formation remained forgotten between 2009 and 2010.

The explosion in the number of horizontal wells in the Williston Basin truly began in 2011 and continues into the present day. Between 1951 and January 1st, 2011 a total of 2,189 horizontal wells were drilled in the Williston Basin. Between January 1st, 2011 and October 11th, 2013 4,188 wells were drilled into the Bakken-Three Forks oil pool of the Williston Basin, raising the total number of non-confidential horizontal wells registered with the North Dakota Industrial Commission to 6,377. Building off the successes seen between 2009 and 2010, the majority of producing wells were completed into the Middle Bakken and Three Forks Formations. From 2011–2013, 1,254 horizontal wells have been completed into the Three Forks Formation, accounting for 96.09 million barrels of oil production. During this same interval, 2,933 horizontal wells were

completed into the Middle Bakken Formation, accounting for 280.89 million barrels of

oil production. During this period no wells were completed into the Upper Bakken

Member, operators quickly realized that profit would come from the permeable units

within the Three Forks.

Table 3. Annual North Dakota Oil Production, 2009-2013. The average daily oil
production in the State of North Dakota quadrupled (by a factor of 3.77) between 2009
and 2013. The dramatic increase in oil production is due to increased horizontal drilling
(Tables One and Two).

Annual Oil Production-State of North Dakota (2009-2013)		
Year	Total Oil Production (Bbls)	Average Daily Production (Bbls/Day)
January-August, 2013	198,200,000	823,333
2012	243,200,000	728,060
2011	152,900,000	418,897
2010	113,000,000	309,679
2009	79,700,000	218,500
Based on Non-Confidential NDIC data from 2009-August, 2013.		

To conclude this section a brief summary of cumulative oil production from the

horizontal wells by formation will be presented over the history of the Williston Basin:

Since 1986, Upper Bakken Formation horizontal wells have produced 24.52 million

barrels of oil from 237 wells (average of 103,459 barrels per well). Since 1991, Three

Forks Formation horizontal wells have produced 142.98 million barrels of oil from 1,610

wells (average of 88,807 barrels per well). Since 2004, Middle Bakken Formation

horizontal wells have produced 554.99 million barrels of oil from 4,469 wells (average of

124,186 barrels per well). Since 2005, horizontal wells representing the Middle Bakken-

Three Forks Formation (where the Lower Bakken Member is absent) have produced 7.81

million barrels of oil from 76 wells (average of 102,763 barrels per well). Since 2009,

Lodgepole Formation horizontal wells have produced 34,500 barrels of oil from 2 wells (average of 17,250 barrels of oil per well).

These statistics show that historical oil production in North Dakota relied heavily on conventional drilling techniques based on structural traps centered along the Nesson Anticline. Approximately 931.4 million total barrels of oil were produced from the Madison Group (Lodgepole, Charles, and Mission Canyon Formation) between 1951 and 2013. As the number of operators in the Williston Basin and the demand for domestic oil increases, future oil production (as seen between the interval of 2009–2013) will likely focus on Bakken-Three Forks horizontal wells. From 1951–2013 the conventional type reservoirs of the Madison Group produced 931.4 million barrels, averaging approximately 15.78 million barrels of production per year. From 2004–2013 the Middle Bakken Formation produced 554.99 million barrels of oil, averaging approximately 61.67 million barrels of production per year. Whether the dramatic oil production seen in the Bakken-Three Forks oil pool is due to technological advancement or the increased amount of drilling, the oil demand of the developing world will continue to increase over the next several decades.

Analyzing the chronological development of horizontal drilling in the North Dakota portion of the Williston Basin and the historical production of petroleum is important to establish a baseline; should the future economic and political needs of the United States continue to call for increased domestic production, continued horizontal drilling in the Bakken-Three Forks oil pool will provide the best opportunity for million-barrel per day production. To make horizontal drilling as efficient as possible, accurate sequence stratigraphic interpretations throughout the Williston Basin are needed. For

example, by analyzing the total amount of oil produced from horizontal wells it becomes apparent that horizontal drilling will yield more oil in the Middle Bakken Formation than in the Upper Bakken Member. Knowing the local sequence stratigraphy of each unit will allow for precise well-log analysis and correlation; knowing the borehole geophysical properties of each formation more accurately will allow for precise placement of horizontal legs during lateral drilling.

Stratigraphy of the Mississippian-Devonian Bakken Formation

The Bakken Formation of the Williston Basin is commonly broke into three main members: an upper shale member, am siltstone member, and a lower Shale Member. The thickness of the Bakken Formation can vary greatly, but typically is thickest near the center of the basin and progressively thins towards the edges of the basin. The thickness of the Bakken Formation is listed at up to 140 feet in the thickest part, and less than 1 foot thick towards the basin edge (Meissner, 1984). The Upper and Lower Bakken Members are reported to be very identical in composition; typically composed of hard, glossy, metamorphosed shale. The Lower Bakken Member is reported to become less organic rich than the Upper Bakken Member; more clay and silt dominate between the Lower Bakken and Three Forks contact (Meissner, 1984). This description agrees with the typically higher gamma-ray reading seen with the Lower Bakken Member. Both the Upper and Lower Bakken Members are described as black, fissile, with few fossils, and highly organic-rich.

Although the lithology is much less controversial than the Middle Member of the Bakken Formation, the Upper and Lower Bakken Member also have disputed lithological descriptions. Meissner (1984) described the decreasing organic content of the Lower

Bakken Member; however Sonnenberg and Pramudito (2009) described the Lower

Bakken being as more organic rich than the Upper Bakken, except for the lithofacies that

contains more siltstone away from the center of the basin. Sonnenberg and Pramudito

(2009) also described the Lower Bakken Silstone as commonly having brachiopod fossils

with frequent bioturbation. Smith and Bustin (1995) described the Upper and Lower

Bakken Member as black clay and silt, with quartz silt grains, and amorphous organic

material. Secondary structures included within the shale members could include calcite

laminations, abundant pyrite laminations, nodules and concretions, few calcite

concretions, and few lag deposits containing pyrite grains. Both the Upper and Lower

Bakken Members have been labeled as the most prolific hydrocarbon source rocks in the

Williston Basin; the first publication to discuss the immense size and hydrocarbon

potential of the Bakken Formation was by Dow (1974).

　　　Although the Middle Member of the Bakken Formation is widely acknowledged

in the literature, the composition and lithology is greatly disputed.   Meissner (1984)

provided only a singular lithological description of the Middle Bakken, defining it as a

middle siltstone member composed of sandstone, light to gray-brown, very-fine grained,

calcareous, and interbedded with minor amounts of gray-brown limestone. Thrasher

(1987) described the Middle Bakken Member as having three units: units one and three

contain massive, fossiliferous siltstone or silty limestone, and unit 2 is a thick,

unfossiliferous sequence of thin beds of shale, siltstone, and sandstone. Sonnenberg and

Pramudito (2009) described two different units with the entirety of a dolostone: an upper

unit composed of a sandy dolostone (bioturbation at the top, followed by parallel

lamination, fllowed by ripple lamination), followed by a lower unit composed of

bioturbated dolostone. The three previous authors described three or fewer distinct

lithofacies within the Middle Bakken Member. Other authors described as many as eight

lithofacies: Smith and Bustin (1995) described eight distinct lithofacies within the Middle

Bakken Member. The lowest lithofacies of the Middle Bakken, labeled Lo, is less than

one meter thick, contains light gray, oolitic limestone, variable concentrations of quartz

sand grains, and few brachiopod shell fragments. The second lowest lithofacies of the

Middle Bakken, labeled Msm, is less than ten meters thick with grey to greenish grey

mudstone. The Msm member contains massive and poorly defined horizontal intervals.

This description seems to match the descriptions of Sonnenberg and Pramudito (2009)

who described bioturbated lamination in the bottom portion of the Middle Bakken. The

third lithofacies within the Middle Bakken, labeled Msh, is less than seven meters thick

and contains green to dark grey mudstone with rare calcite cementation. This unit also

has poorly defined horizontal lamination. The fourth lithofacies within the Middle

Bakken, labeled as MSI, is less than four meters thick and contains predominantly green

to dark grey mudstone with quartz silt grains and lesser amounts of fine quartz sandstone.

The fifth lithofacies within the Middle Bakken, labeled Sw, is less than nine meters thick

and contains very fine and subangular gray quartz sandstone with wavy bedding. The

sixth lithofacies within the Middle Bakken, labeled, Sf, is less than nine meters thick and

contains very fine, subangular to angular, grey quartz sandstone with lesser amounts of

quartz grains. The seventh lithofacies within the Middle Bakken, labeled Sr, is less than

five meters thick and contains well sorted and grey quart sandstone with rare inclusions

of green mudstone. Finally the eighth and uppermost lithofacies in the Middle Bakken,

labeled St, is grey with fine to medium, well sorted, and moderately spherical quartz

sandstone. The Smith and Bustin (1995) analysis of the Middle Bakken Formation differed substantially from Meissner (1984), Sonnenberg and Pramudito (2009), and Thrasher (1987) descriptions regarding the Middle Bakken Member. The most apparent problem with the Smith and Bustin (1995) Middle Bakken description is the lack of dolostone and the over-abundance of sandstone throughout their descriptions.

The Middle Bakken Member lithological interpretation that seems to find a middle ground between the barren lithofacies descriptions of Meissner (1984), Sonnenberg and Pramudito (2009), Thrasher (1987), and the overabundant lithofacies descriptions of Smith and Bustin (1995) appeared to be (LeFever et al., 1991), which described seven lithofacies within the Middle Member of the Bakken Formation. Lithofacies one, located at the bottom of the Middle Bakken, is composed of massive, dense, and very calcareous siltstone. Lithofacies one is composed of highly fossiliferouy and gray-green siltstone and disseminated pyrite. Lithofacies two, located above lithofacies one, is composed of parallel interbreeds of dark-gray shale and silty sandstone. This unit also has disseminated pyrite, is fossiliferous, and has a lower gradational contact with lithofacies one. Lithofacies three and four are composed of sandstone, with a central division of wavy and flaser bedded silty sandstone. The predominant minerals are mainly quartzite with minor feldspar and heavy minerals. Lithofacies five and six are composed of parallel interbeds of dark-gray shale and buff silty sandstone. Disseminated pyrite exists in lithofacies five and six, and the unit generally coarsens upward. Lithofacies seven, the uppermost member of the Middle Bakken Member, is composed of siltstone that is massive, gray-green, and fossiliferous. Pyrite is disseminated throughout, and the contact with the Upper Bakken Member is sharp. The LeFever et al. (1991) and

Smith and Bustin (1995) descriptions of the Middle Bakken Member were both in-depth descriptions of the Middle Bakken Member; the LeFever et al. (1991) description is more agreeable with other published literature and provided more descriptions of calcareous micro-lithofacies within the larger macro-lithofacies.

Perhaps discrepancies experienced between the different Middle Bakken researchers stems from the fact that the Middle Bakken Formation thickens from the south to the center of the Williston Basin. Near the South of the Basin the Upper Shale is present as a two-foot interval, followed by approximately two feet of Middle Bakken inorganic silica rich mudstone, followed by two feet of thin alternating beds of wackestone and sandstone. It is also interesting to note that in the southern part of the basin, the Lower Bakken Member is absent in the core section (Egenhoff, 2011). In the center of the basin, the Middle Bakken formation becomes more than forty feet thick. The Upper Shale is present as organic-rich black shale, and is underlain by siltstone. The siltstone is underlain by massive and horizontal cross-bedded sandstone or quartz sandstone with ooids. Horizontally laminted siltstone and macaronichnus siltstone follow this unit that is then underlain by a thicker layer unit of horizontally laminated siltstone. This pattern generally continues until a thick layer of siltstone before again encountering the underlying organic-rich Lower Bakken Member. This interpretation by Egenhoff (2011) seems to accurately show the thickening of the Bakken Formation and the presence of the Bakken Shale from the South of the Basin into the center section of the Basin, and the lithological descriptions do seem to generally match the descriptions of (LeFever et al., 1991). For instance both LeFever et al. (1991) and Egenhoff (2011) mentioned a carbonaceous unit sitting directly above the Lower Bakken Member in the

thickest portions of the Basin. Perhaps the lithological descriptions only including three

units within the Middle Bakken Member by Meissner (1984), Sonnenberg and Pramudito

(2009), and Thrasher (2010) involved core sections away from the Middle of the Basin,

and they based their descriptions of the Middle Bakken on sections that were not

stratigraphically complete. Perhaps Smith and Bustin (1995, 1996) did have a complete

section from towards the center of the basin but were overzealous with their lithological

descriptions, trying to see more in the core than was present. It is also interesting to note

than in the Smith and Bustin (1996) paper they based their paleoenvironment analysis on

the lithological descriptions of LeFever et al. (1991) rather than their own Smith and

Bustin (1995) descriptions. For instance, rather than the eight lithological descriptions

they included in their 1995 paper, their 1996 paper separated the Middle Bakken Member

into six formations.

The depositional history of the Upper and Lower Bakken Member is the most

controversial aspect of all Bakken-Three Forks oil pool research. Numerous researchers

have listed the formation environment as a deep-water column with anoxic bottom

conditions. Smith and Bustin (1996) listed the formation environment of the Upper and

Lower Bakken Members as a distal deep water (greater than two-hundred meters) marine

environment with stagnant bottom conditions. They also noted than the bottom waters

were periodically disturbed by slow moving currents, a slow rate of clastic sedimentation,

and a substrate with highly anoxic conditions. Smith and Bustin (1996) listed six different

depositional environments for the Middle Bakken Formation; starting with an offshore

environment, regressing to a lower shore face, transgressing slightly to a upper shore

face, continuing to transgress into an offshore environment, regressing again into an

upper shore face, then transgressing into an offshore environment, finally with a large-scale transgression that allowed for the distal deep marine waters needed for the Upper Bakken Member. Although this interpretation makes sense in terms of the regressive and transgressive pattern, the value of two-hundred meters of sea-level needed for Bakken Shale production appears to arbitrary and misguided. The interpretation that the Upper and Lower Bakken Members formed in anoxic conditions compared to the Three Forks, Middle Bakken Member, and Lodgepole Formations accounts for the differing lithology and organic content seen in each formation; the value of two-hundred meters of sea-level movement and constant regression, transgression, and movement over the short period from the Late Devonian-Early Mississippian makes much less sense.

A deep-water marine environment is not the only interpretation for the formation of the Bakken Shale; other researchers believe that the Upper and Lower Members were deposited in an offshore marine environment during periods of sea-level rise (Webster, 1984; LeFever et al., 1991; Lineback and Davidson, 1982). These interpretations also suggested that the middle member was deposited in a coastal regime following a rapid-sea level drop. All of the academic arguments agree that the Bakken Shale was deposited in a water column much deeper than the column that deposited the Middle Bakken Member; the strongest disagreement is the overall water column depth needed for the highly anoxic conditions that would prevent sulfate and oxygen destruction of kerogen. Many arguments from the respective authors state that pyrite had precipitated from the Three Forks into the Bakken; it is important to analyze the sequence of electron acceptors and donors to analyze whether this iron truly precipitated from the Three Forks or if it was a product of iron in the water column.

26

Table 4. Middle Bakken Member Lithology. Based upon the lithological descriptions of (Meissner, 1984; LeFever, 1991; and Smith and Bustin, 1995). Note the presence of shale in Lithofacies 5 and 6 within the Middle Bakken Member.

Middle Bakken Member Lithology	
Lithofacies 7	Silstone, massive, dense, dolomitic, disseminated pyrite, slighly bioturbated.
Lithofacies 5&6	Parallel interbeds of dark gray shale and silty sandstone, disseminated pyrite, overall coarsening upward, gradational lower contact.
Lithofacies 3&4	Sandstone, mainly quartzite with minor feldspar and heavy minerals, few brachiopods, disseminated pyrite, calcareous, no bioturbation.
Lithofacies 2	Parallel interbeds of dark gray shale and silty sandstone, disseminated pyrite, overall coarsening upward, gradational lower contact, dolomitic.
Lithofacies 1	Silstone, massive, dense, very calcareous, gray-green, highly fossiliferous.

An important thought to consider is the following: in modern day Spontaneous Potential (SP) borehole geophysical logs a baseline shift to negative SP will usually occur when less saline drilling mud comes into contact with more saline connate water (whether the anion is magnesium, sodium, or potassium). Shale will typically have a positive (non-negative) SP value, whereas highly porous sandstones or carbonates will show a baseline deflection. This baseline deflection is usually caused by sodium and chloride. This fact is important because it tells us that in shale: light, polar, ions will not diffuse or diffuse extremely slowly through the material in a horizontal direction. Now if we imagine that the original ions in the Three Forks Formation are iron, such as pyrite (FeS_2), which has a larger atomic mass than chloride, the iron would have had to diffuse off of the sulfide and precipitate into the overlying Bakken shale in a vertical direction. Because the sea-water was likely saline, the iron could have immediately bonded with chloride to form iron (II) chloride, or $FeCl_2$. Most of the authors consistently listed pyrite

(FeS_2) as common throughout the Bakken-Three Forks Formations (Smith and Bustin, 1995; LeFever et al., 1991). Due to the limited diffusion ability of shale and the high atomic weight of iron, it seems difficult to figure out how diffusion occurred from the Three Forks into the Lower and Middle Bakken Members. Another large problem to consider is that if the pyrite did dissociate in the Three Forks, depositing H_2S into the Lower Bakken Member, the reduction needs a heat of 500°C, and will also produce FeO, Fe_3O_4, Fe_2O_3, and SO_4 (Schwab and Philinis, 1947). This chemical interpretation creates problems with the interpretations that have been made; ignoring the heat of reaction needed to react iron with hydrogen, the byproducts would destroy kerogen. The Bakken is widely regarded as a prolific source rock. How would kerogen remain organic if sulfate and oxygen were both also seeping into the source rock (along with the H_2S)? A better interpretation may involve water-depths and oxygen conditions as a function of the electron acceptor and donor sequences established for water systems. As water becomes more anoxic it allows for the species of iron and then H_2S to dominate in a water environment. This could reconcile the problems with pyrite dissolution and explain why pyrite is present throughout the Lower Shale and the Middle Bakken. Questions of this magnitude need to be answered using greater precision analytical equipment; as the human race continues to be part of the technological revolution we can answer geologic questions with certainty rather than with well-educated generalizations. This thesis used x-ray fluorescence data to answer these questions.

The Pronghorn Member of the Bakken Formation is described as highly bioturbated with rare to no primary sedimentary structures. The Pronghorn Member ranges from six to eight feet in thickness, is laterally discontinuous, and quartz-rich. The

28

Pronghorn Member is primarily located in areas of the Williston Basin where the Bakken Formation is thicker; the Pronghorn Member is completely absent in the South Dakota portion of the Williston Basin. The Pronghorn Member has been described differently by several geologists, and was historically labeled as the "Sanish Sandstone." This interval refers to a sandy and silty member between the Three Forks and Bakken Formations. The 1954 North Dakota Geological Society description of the Sanish Sand included it as the lowermost portion of the Bakken Formation, Berwick (2008) described the Sanish Member as the topmost portion of the Three Forks Formation, and finally LeFever, et al. (2011) renamed the Sanish Sand as the Pronghorn Member as the lowermost unit within the Bakken Formation. The Pronghorn Member will always rest between the overlying Bakken Formation and the underlying Three Forks Formation. Typically the Pronghorn Member erosionally truncates the Three Forks Formation in the northeast, western, and northwestern parts of the Williston Basin. Figure 5 shows the approximate location of the Pronghorn Member as a function of a north-south transect in the Williston Basin.

In the northern part of the Williston Basin the Pronghorn Member is predominantly shale, typically mixed with sandstone and siltstone. The entire Pronghorn Member interval is a series of medium gray-green to dark-green shale beds (Bottjer et al., 2011). The depositional environment of the Pronghorn Member is considered to be a marine environment with alternating oxidizing and poorly oxygenated conditions. The Pronghorn Member is considered to be a transitional period of deposition between the underlying shallow marine limestone of the Three Forks Formation and the overlying deep water marine deposition of the Lower Bakken Member (Bottjer et al., 2011). This interpretation becomes interesting because it would theoretically match the

interpretations that the Upper and Lower Bakken Members were formed in an anoxic, deep marine, offshore environment. The Pronghorn shows a mixture of shale and siltstone, showing what could be interpreted as a transition from a shallow-marine environment into a deep-water marine environment.

Stratigraphy of the Devonian Three Forks Formation

The Devonian Three Forks Formation was explained through the works of Nicolas (2006) and LeFever & Nordeng (2011). The former publication discussed the Three Forks Formation in the Canadian Province of Manitoba; the latter publication discussed the Three Forks Formation in the State of North Dakota. Generally the Three Forks Formation is considered to overly the Devonian Birdbear Formation and underlay the Mississippian Bakken Formation. The Three Forks Formation is widely considered to be a mixture of grey-green dolomitic shale, alternating cycles of siltstone clasts, and massive oxidized silty shale. Although the Three Forks Formation was historically ignored for Williston Basin Production, recent advancements in horizontal drilling have allowed the Three Forks Formation to become a prolific hydrocarbon producer, especially in the State of North Dakota. The Three Forks Formation is present throughout the Williston Basin, and is sometimes referred to as the Torquay formation in Saskatchewan. In 2011 Continental Resources Inc. drilled the Charlotte 1-22H, 2-22H, 3-22H, and 4-22H to investigate the performance of the Middle Bakken Formation and three reservoirs within the Three Forks Formation. The primary reservoirs in the Three Forks Formation are the uppermost unit and the middle unit; LeFever et al. (2011) listed these units as Unit Six and Unit Four, Nicolas (2006) listed these units as Unit Four and Unit Two-C.

LeFever et al. (2011) identified six different lithological units within the Three Forks Formation of North Dakota. Unit Six, the uppermost unit of the Three Forks, is composed of a basal thin, massive, tight grey-green dolomitic shale to silty shale sequence. Unit five is composed of rusty brown dolomitic shale with faint psuedomorphs of rotted, angular, and fine grained siltstone. Unit four is composed of randomly alternating cycles of light brown to tan doloarenitic clasts in a shale matrix, alternating laminated siltstone and shale, and massive grey-green shale as laminae. Unit three is massive oxidized silty shale. Unit Two is composed of concentrated breccia with rotted dolomite fragments in a brown mudstone matrix. Unit one, the lowermost unit of the Three Forks, is composed of a red brown to light brown dolarenite with grey green shale. Anhydrite occurs throughout the unit as white or resinous blebs.

Nicolas (2006) identified four primary lithologic units with the Three Forks Formation of Manitoba. Unit One, the lowermost unit, of the Three Forks is the most weathered member, is dominantly red-brown, and contains light brown to tan brecciated dolarenite with a grey-green shale to silty matrix. Porosity in Unit One is approximately 10-15%, and anhydrite occurs throughout this unit as a brown "bleb." Unit Two consists of interbedded siltstone and shale with occasional massive shale; this unit has also been split into four sub-units. Unit Two-A consists of massive oxidized silty shale, Unit Two-B consists of alternating cycles of brecciated dolarenitic siltstone and massive to silty shale. Unit Two-B also contains oxidized siltstones, disseminated pyrite, and rare anhydrite. Unit Two-C contains light brown to tan dolarenitic siltstone with grey-green shale as laminae, interbeds, and matrix. Unit Two-C contains oxidized pyrite that often alters to hematite. Finally, Unit Two-D consists of thin, massive, and tight green

dolomitic shale. Unit Three consists of rusty-brown dolomitic shale with massive

bedding. Unit Three has a high gamma-ray signature compared to the overlying and

underlying units; this signature decreases in the middle of the unit. Unit Four contains

three subunits, but generally consists of interbedded siltstone and shale with thick units of

highly brecciated siltstone beds. Unit Four-A consists of thin, grey-green dolomitic

shale, lithologically identical to Unit Two-D. Unit Four-B consists of light brown to tan

doloarenitic siltstone clasts within a grey-green shale to silt matrix. Finally, Unit Four-C,

the uppermost unit, of the Three Forks Formation is composed of light brown to tan

dolarentic sandstone with common gray-green shale laminated with interbeds and a

matrix. Pyrite is common in the shale bedding planes, and anhydrite is also common.

Unit Four-C is the primary reservoir rock in the Manitoba Sinclair Oil Field.

Overall the descriptions of LeFever et al. (2009) and (Nicolas, 2006) were almost

equivalent when discussing the overall stratigraphy of the Three Forks Formation. The

most interesting aspect of the Nicolas (2006) descriptions were of the pyrite oxidizing

into hematite in Unit-2C. The depositional environment for Unit-2C was considered to be

a shallow-marine environment thinning towards the east with aerial exposure. Although

this interpretation would describe the reason for oxidized hematite in the Three Forks

Formation in Manitoba, and explain the lack of oxidized hematite from pyrite in other

localities within the Three Forks Formation, perhaps the interpretation is incorrect. This

part of Manitoba was not aerially exposed for long periods of time; pyrite likely

dissociated into hydrogen sulfide and hematite byproducts. Perhaps the shallow

conditions allowed for more oxygen that helped lower the heat of reaction between pyrite

and water (Schwab and Philinis, 1947).

CHAPTER III

X-RAY FLUORESCENCE SPECTROSCOPY

Spectroscopy is the identification of unique interactions between matter and radiated energy. Numerous types of analytical spectroscopy have been discovered throughout the annals of scientific history, this thesis focuses solely on x-ray fluorescence spectroscopy. X-ray fluorescence spectroscopy is a branch within the study of emission spectroscopy. Emission is the process in which matter is excited by high energy electromagnetic radiation; the matter will then emit photons to return to a lower state of energy (Kubo, 1978). The difference between the excitation energy and the emission energy is equal to the energy carried by the photon. The energy level needed to create emission will depend on the size of the matter. Ultraviolet light has enough energy to create emission in molecules, x-ray radiation has enough energy to create emission in atoms, and gamma ray radiation has enough energy to create emission in the atomic nuclei. Emission spectroscopy is important for chemical and analytical analysis because each unique elemental atom will release a different amount of energy regardless of excitation energy (Croudace and Rothwell, 2006). This relationship was first quantified and published by the German theoretical physicist Max Planck in 1901. The Planck Relation describes the proportionally constant relationship between the energy of a charged photon (E), the frequency of the photon wave (v), and an empirically derived constant known as Planck's Constant (h):

Planck's Relation: (3−1)

$$E = h\upsilon$$

where: E   = Energy of a photon (Joules)

       h = Planck's Constant (6.626×10^{-34} Joule·Seconds)

       υ = Frequency of the photon (Hertz)

Max Planck and Albert Einstein later related Planck's constant with the wavelength of a photon using the Planck-Einstein Equation; the energy of a charged photon (E) is equal to the ratio between the multiplication of Planck's Constant (h) and the speed of light (c) and the wavelength of the photon (h):

Planck-Einstein Equation: (3-2)

$$E = \frac{hc}{\lambda}$$

where: E   = Energy of a photon (joules)

       h = Planck's Constant (6.626×10^{-34} joule·seconds)

       λ =Wavelength of the photon (meters)

       c =Speed of light in a vacuum (2.998×10^8 meters/ second)

The importance of Planck's Relation and the Planck-Einstein Equation for emission spectroscopy is that both equations allow for relations between the energy of an electromagnetic wave and an autonomous property of that wave (either wavelength of frequency). In the case of x-ray fluorescence analysis, the energy of the electromagnetic x-ray radiation is converted into

wavelength; because each chemical element will emit unique wavelengths of x-ray radiation, the wavelength will then be converted into elemental counts.

Physics of X-Ray Fluorescence Analysis

Electromagnetic radiation is a form of radiant energy guided by the intensity of a combined electric and magnetic field; all electromagnetic radiation will propagate at the speed of light in a vacuum. All forms of electromagnetic radiation will propagate in a sinusoidal wave motion at the speed of light; different forms of electromagnetic radiation occur because of changes in wavelength and frequency. As a function of wavelength the electromagnetic spectrum can be listed as follows (increasing to decreasing wavelength): long radio waves (10^4 to 10^8 meters), frequency modulation (FM) and amplitude modulation (AM) radio waves (10^0 to 10^2 meters), infrared radiation (10^{-4} to 10^{-6} meters), the visible light spectrum (10^{-7} meters), ultraviolet light (10^{-7} to 10^{-8} meters), x-ray radiation (10^{-9} to 10^{-11} meters), and gamma ray radiation (10^{-11} to 10^{-16} meters). This thesis will only directly analyze the physics behind active x-ray radiation; gamma ray radiation will be used as passive radiation and will not be discussed.

X-ray radiation is a form of electromagnetic radiation that exhibits wave-like behavior as it propagates; the wavelength will be in the range of 10^{-9} to 10^{-11} meters and the frequency will be approximately 10^{18} hertz. X-ray fluorescence is the natural emission of high-energy electromagnetic radiation that occurs when charged particles bombard with target atoms. If the photon is carrying sufficient ionizing energy (x-rays at higher than 1 keV), electrons in the inner-shells of the target atom will vibrate and eject from their orbitals. The vacancy in the shell is then filled by an electron from a higher orbital

shell. X-ray fluorescence spectroscopy involves measuring the photon energy created by electron ejection and replacement and categorizing the elemental composition by photon wavelength. This physical process will take less than 10^{-9} seconds for the electron to move orbital shells.

X-ray fluorescence uses x-ray notation to describe electron orbitals; this is in stark contrast to the more commonly used atomic notation. This is important to discuss because of the multidisciplinary nature of this research. X-ray notation labels electron orbitals in the following manner: The K-shell is the innermost electron orbital shell, the L-shell is the secondary electron orbital shell, the M-shell is the third orbital shell, and finally the N-shell is the outermost electron orbital. The more commonly used atomic notation describes orbital shells in a numeric-alphabetic classification system: the first orbital is known as the 1s shell, the second orbital is known as the 2s shell, the third orbital is known as the 2p shell, the fourth orbital is known as the 3s shell, etc. The K-shell in x-ray notation corresponds to the 1s1 and 1s2 atomic notations, the L-shell corresponds to the 2s1, 2s2, 2p1, 2p2, and 3p2 atomic notations, and finally the M-shell corresponds to the 3s shell.

Four different types of x-ray fluorescence commonly occur: Kα, Kβ, Lα, and Lβ fluorescence. Kα fluorescence occurs when a dislodged electron the K-shell orbital is filled by an electron from the L-shell orbital. Kβ fluorescence occurs when a dislodged electron from the K-shell orbital is filled by an electron from the M-shell orbital. Lα fluorescence occurs when a dislodged electron from the L-shell orbital is filled by an electron from the M-shell orbital. Finally, Lβ fluorescence occurs when a dislodged electron from the L-shell is filled by an electron from the N-shell.

The first scientist to discover x-ray fluorescence spectroscopy was H.G. Moseley in 1912. He found that plotting one divided by the square root of the wavelength of an x-ray versus the atomic number of an element yielded a perfect correlation. Combing the finding of Mosely with Planck's Relation (Equation 3-1) a definitive identification can be made between the energy of a photon, the wavelength of a photon, the frequency of a photon, and the chemical composition of the element releasing the photon. This means that the chemical composition of any x-ray produced from emission can be identified and categorized.

Coupling Planck's Relation (Equation 3-2) with the empirical finding of Moseley allows for estimations of the energies needed to create atomic fluorescence using x-ray radiation. The energy needed for fluorescence can be calculated knowing only the atomic number of an element:

$$E_{L\alpha} = -(Z-1)^2 \frac{13.6eV}{4}$$

$$(3\text{--}3)$$

$$E_{K\alpha} = -Z^2(13.6eV)$$

$$(3\text{--}4)$$

where: $E_{K\alpha}$ = Energy needed for Ka fluorescence to occur (eV)

      $E_{L\alpha}$ = Energy needed for Lα fluorescence to occur (eV)

      Z   =Atomic number of an element

When equations (3-3) and (3-4) are calculated for the periodic table, we find that the energy needed to create Kα fluorescence is, although dependent on the exact chemical element, four to five times greater than the energy needed to create Lα fluorescence. (Table 5) shows the atomic symbol, atomic number, wavelength, Kα, and Lα for each element used in the study.

Due to the energy requirement for Kα fluorescence is greater than Lα fluorescence, it becomes impossible to distinguish the two fluorescence types between each other, especially with a Bruker Tracer IV-SD handheld XRF. For instance, Kα iron fluorescence requires 9.190 keV of excitation voltage whereas Lα iron fluorescence requires approximately 2.125 keV of excitation voltage. Therefore, if Iron Lα fluorescence is occurring it can be mistaken for either Kα Aluminum fluorescence, which requires 2.300 keV of excitation voltage, or magnesium fluorescence, that requires 1.960 keV of excitation voltage. The Bruker Tracer IV series technology uses Silicon Drift Detection (SDD) that is based on energy dispersive x-ray fluorescence. This means that photons are categorized based on their energy rather than their wavelength or frequency; the internal calculation then uses Planck's Relation (3-2) to convert
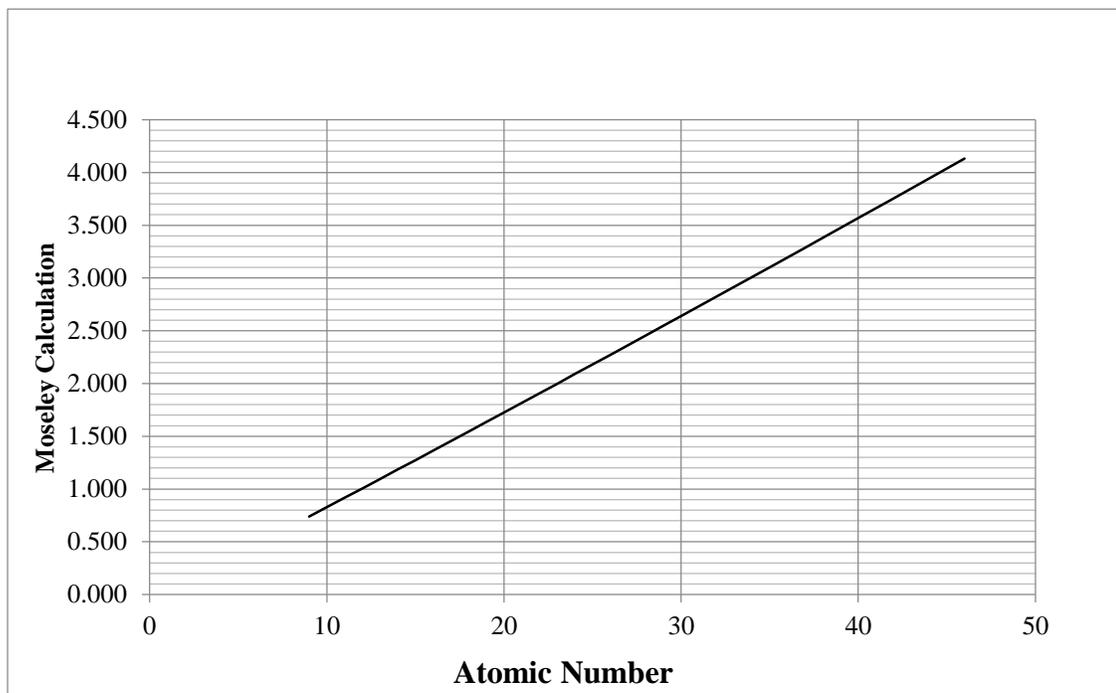
Figure 2. Moseley Plot of Atomic Number versus X-Ray Wavelength. This figure is a graphical representation showing the atomic number of a chemical element (*Z*) versus the Moseley Calculation (Equation 3-3). The results show a perfect correlation; the foundation of x-ray fluorescence spectroscopy.

to wavelength; once wavelength is obtained the chemical element can be distinguished using Moseley's empirical findings.

During the preliminary data collection of this thesis, it was often a puzzle understanding why spectral peaks were created between elements such as magnesium and aluminum. Understanding Equation (3-2) and calculating the energies needed for Lα and Kα fluorescence explain why peaks occur between x-ray that should all have uniform wavelength and energy. For the above reasoning, only Kα fluorescence should be used during x-ray fluorescence analysis of cuttings, core, and all other geologic samples. Another point that should be noted is the fact that scanning a sample with higher keV intensity x-ray will also excite lower energy elements; exceeding the energy requirement does not prevent fluorescence. The Bruker Tracer IV series handheld XRF can produce a keV intensity in the range from 5keV to 45keV; it is illogical to use anything less than the highest setting because regardless of the range Lα and Kα fluorescence radiation will be indistinguishable. To keep analysis as uniform as possible it is necessary to use uniform scanning times, uniform excitation energy, and uniform data analysis.

Table 5. Moseley Calculation for Fluorescence Kα Excitation Energy. All twenty-seven thesis elements were included in this plot. The results show that all study elements are within the excitation voltage of the Bruker Tracer IV handheld XRF. Note the high energy ratio between the excitation voltages needed for Kα and Lα fluorescence.

Element Symbol	Atomic Number	Wavelength	Moseley Equation $\sqrt{(1/\lambda)}$	Excitation Energy (Kα)	Excitation Energy (Lα)	Ratio of Kα:Lα Energy Requirement
		(nm)	(nm)	(keV)	(keV)	-
F	9	1.832	0.739	1.100	0.218	5.055
Na	11	1.191	0.916	1.650	0.340	4.853
Mg	12	0.989	1.006	1.960	0.411	4.764
Al	13	0.834	1.095	2.300	0.490	4.698
Si	14	0.713	1.185	2.670	0.575	4.647
P	15	0.616	1.274	3.060	0.666	4.592

Table 5 Continued.

S	16	0.537	1.364	3.480	0.765	4.549
Cl	17	0.473	1.454	3.930	0.870	4.515
Ar	18	0.419	1.544	4.410	0.983	4.488
K	19	0.374	1.635	4.910	1.102	4.457
Ca	20	0.336	1.725	5.440	1.227	4.432
Ti	22	0.275	1.907	6.580	1.499	4.388
V	23	0.250	1.998	7.190	1.646	4.369
Cr	24	0.229	2.090	7.830	1.799	4.353
Mn	25	0.210	2.181	8.500	1.958	4.340
Fe	26	0.194	2.273	9.190	2.125	4.325
Ni	28	0.166	2.456	10.660	2.479	4.301
Cu	29	0.154	2.547	11.440	2.666	4.292
Zn	30	0.144	2.640	12.240	2.859	4.281
As	33	0.118	2.916	14.810	3.482	4.254
Br	35	0.104	3.101	16.660	3.930	4.239
Rb	37	0.093	3.287	18.620	4.406	4.226
Sr	38	0.088	3.380	19.640	4.655	4.219
Zr	40	0.079	3.567	21.760	5.171	4.208
Mo	42	0.071	3.755	23.990	5.715	4.197
Pd	46	0.059	4.131	28.780	6.885	4.180
Sn	50	0.048	4.564	34.000	8.163	4.165

Four standardized electromagnetic equations dictate the propagation of electromagnetic energy in a combined electric and magnetic field, these equations are often listed as the four Maxwell Equations:

Gauss's Law: (3-5)

$$\Phi E = \frac{Q}{\epsilon}$$

Gauss's Law for Magnetism: (3-6)

$$\nabla \cdot B = 0$$

Faraday's Law: (3−7)

$$\nabla \times E = -\frac{\partial B}{\partial t}$$

Ampere-Maxwell Law: (3-8)

$$\nabla \times B = \frac{1}{c^2}\frac{\partial E}{\partial t}$$

where: ΦE = Electric Flux (volt·meters)

Q = Total Charge of the photon (coulombs)

c = Speed of light in a Vacuum (2.998×10^8 meters/second)

E   =Electric Field Intensity (volts/meter or newtons/coulomb)

B =Magnetic Field Intensity (teslas or newton·seconds/coulomb·meters)

The four generalized electromagnetic equations are of the utmost importance to understand before conducting x-ray fluorescence analysis; they predict that any number of analytical variables can affect the precision of results. Gauss's Law for Magnetism (Equation 3-6) predicts that the net magnetic flux through a closed surface will be zero; meaning regardless of chemical composition, all matter can carry an electric charge-even if incredibly resistive-all geologic samples regardless of water or hydrocarbon saturation can be examined using XRF. Faraday's Law (Equation 3-7) predicts that the convergence of an electric field intensity (E) will be with respect to the ratio of the partial derivative of the magnetic field intensity (B) and time. This means that changing the time of sample x-ray scanning can change the electric field intensity, causing a sample to show a higher count rate. Faraday's Equation shows that all samples should be analyzed with uniform scanning times. The Ampere-Maxwell Law (Equation 3-8) predicts that the convergence of a magnetic field intensity (B) will be with respect to the ratio of the partial derivate of

41

the electric field intensity (E) and time. This means that changing the ratio of the intensity of the electric field to the time scanned can alter the intensity of the magnetic field, which will once again cause alteration of the overall electric intensity of the analysis. These equations show that all scanning should occur with a uniform scan time and a uniform x-ray intensity. For the sake of this thesis all samples were scanned for a total of 30 seconds, electric intensities of 30keV and 45keV were collected and only the 45keV intensity scans were used.

The four Maxwell Equations (Equations 3-5, 3-6, 3-7, and 3-8) also predict that the chemical composition of a geologic sample can be edited by the mineralogical composition of the parent material. Minerals containing samarium, cobalt, neodymium, and magnetized irons will have display ferromagnetic properties; when scanning these elements with induced electromagnetic x-ray radiation Faraday's Law (Equation 3-7) predicts that the resulting electric field intensity will increase due to the already higher intensity of the magnetic field. This theory was tested by scanning magnetized ferromagnetic iron oxide (magnetite-Fe_3O_4) samples versus antiferromagnetic iron oxide (hematite-Fe_2O_3). The magnetite magnet weighed 35.347 grams and consequentially 35.347 grams of hematite power was used. The molar mass of magnetite is 231.53 grams per mole; the molar mass of hematite is 159.69 grams per mole. The mass percentage of iron in magnetite is 72.34%, the mass percentage of iron in hematite is 69.94%. Assuming both samples were pure mineralogical composition, the magnetite contained 25.58 grams of iron whereas the hematite contained 24.72 grams of iron. Each sample was scanned for thirty seconds and the total counts were used for data analysis.

The first equation applied was the Planck-Einstein Equation (Equation 3-2) that showed enabled the calculation of the frequency from only the wavelength of iron. The wavelength of iron is 1.936×10^{-9} meters. The photons/second were calculated just to show that the magnetite produced more photons per second. Planck's Relation (Equation 3-1) was then used to calculate the energy in joules of each photon. The hematite and magnetite should both have equivalent wavelengths, frequencies, and photon energies. The joules produced was then calculated by multiplying the photons counted by the Planck's photon energy. The results show that the magnetized magnetite iron released an average of 1.0383×10^{-14} joules of fluoresced energy whereas the non-magnetized hematite iron released an average of 3.7341×10^{-15} joules of fluorescence energy. This means that the amount of fluorescence energy released by the magnetite was 2.78 times greater than the amount of fluorescence energy released by the hematite. The amount of iron in the magnetite, assuming 100% purity was 25.578 grams; the amount of iron in the hematite, assuming 100% purity was 24.723 grams. The ratio of iron in the magnetite sample to the hematite sample should have been 1.03:1.

Table 6. Hematite and Magnetite Kα Fluorescence. Performing x-ray fluorescence on ferromagnetic Magnetite will produce a higher count rate than performing x-ray fluorescence on antiferromagnetic Hematite.

Sample Type	KeV Applied	Sample Weight	% of Iron	Time of Scan	Iron Photon Counts
Magnetite	45	35.347 grams	72.34%	30.10	990,556.05
Magnetite	45	35.347 grams	72.34%	30.10	1,004,622.13
Magnetite	45	35.347 grams	72.34%	31.00	1,029,169.97
Magnetite	45	35.347 grams	72.34%	30.96	1,058,775.82
Magnetite	45	35.347 grams	72.34%	31.13	976,483.36
Sample Type	Wavelength	Photons/Second	Frequency	Planck's Relation Energy (Joules)	Joules Produced
Magnetite	1.936E-09	32,908.84	1.54851E+17	1.02605E-20	1.0164E-14
Magnetite	1.936E-09	33,376.15	1.54851E+17	1.02605E-20	1.0308E-14

Table 6 Continued.

Sample Type	KeV Applied	Sample Weight	% of Iron	Time of Scan	Iron Photon Counts
Magnetite	1.936E-09	33,199.03	1.54851E+17	1.02605E-20	1.0560E-14
Magnetite	1.936E-09	34,198.19	1.54851E+17	1.02605E-20	1.0864E-14
Magnetite	1.936E-09	31,367.92	1.54851E+17	1.02605E-20	1.0019E-14
Hematite	45	35.347 grams	69.94%	30.86	360,120.67
Hematite	45	35.347 grams	69.94%	30.82	391,125.92
Hematite	45	35.347 grams	69.94%	31.75	419,865.44
Hematite	45	35.347 grams	69.94%	29.93	337,071.49
Hematite	45	35.347 grams	69.94%	30.92	311,473.82

Sample Type	Wavelength	Photons/Second	Frequency	Planck's Relation Energy (Joules)	Joules Produced
Hematite	1.936E-09	11,669.50	1.54851E+17	1.02605E-20	3.6950E-15
Hematite	1.936E-09	12,690.65	1.54851E+17	1.02605E-20	4.0131E-15
Hematite	1.936E-09	13,224.11	1.54851E+17	1.02605E-20	4.3080E-15
Hematite	1.936E-09	11,261.99	1.54851E+17	1.02605E-20	3.4585E-15
Hematite	1.936E-09	10,073.54	1.54851E+17	1.02605E-20	3.1959E-15

The results from the hematite and magnetite fluorescence analysis clearly showed that magnetic strength plays a greater role in energy dispersive x-ray analysis than chemical composition. Obviously both samples showed a strong presence of iron, but it is clear that a standard linear or exponential based calibration curve would not be adequate for analyzing core and cuttings samples. For this reason the idea of using calibration curves was completely abandoned in this thesis. The use of calibration curves will be greatly affected in geologic analysis due to the mixed presence of ferromagnetic, paramagnetic, and antiferromagnetic metallic species. Furthermore, over geologic time as samples are buried with temperature and pressure, high heating rates can alter magnetism once temperatures pass the metal species Curie temperature. For this reason, constructing a calibration curve similar to the types used in Flame Atomic Adsorption Spectroscopy (FAAS) or ion chromatography is inadequate for accurate chemostratigraphic analysis-

magnetization does not display a linear trend with respect to chemical composition, only to electrical field intensity.

Previous Use of X-Ray Fluorescence in the Earth Sciences

The earliest literature describing the use of x-ray fluorescence in the earth sciences was completed as early as 1963 when the technology first became available for research interests (Rose et al., 1963). Before x-ray fluorescence became available to the academic sector chemical digestion was commonly used to distinguish the composition of shale, sandstone, and carbonate samples (Rose, et al., 1963). Composition analysis could take up to ten hours depending on the composition of the sample; precision was relatively abundant but still limited to larger mineralogical groups such as carbonates, silicates, phosphates, and evaporites. After the ground-breaking work in 1963, the literature exploded with x-ray fluorescence analysis in the 1970's: in 1972 x-ray fluorescence was used for geochemical studies of uranium, molybdenum, and vanadium in the Swedish Alum Shale (Armands, 1972); in 1973 x-ray fluorescence was used to examine the ion exchange rates for nickel and cobalt in various shales (Blount, 1973); in 1979 x-ray fluorescence was used to create synthetic standard references for oil samples (Giauque, et al., 1979). One interesting research paper from 1979 discusses the use of rubidium-strontium ratios for the determination of shale horizons in the Late Pre-Cambrian shale of Northern Norway (Pringle, 1979). The geologic academia lexicon involving x-ray fluorescence literature slowed throughout the 1980's and re-emerged in the 1990's and 2000's with numerous additions to the literature.

X-ray fluorescence analysis was first used for petroleum, lignite, and fuels-based research in the early 1970's. In 1978 ground breaking research found that x-ray fluorescence could identify the differences between mineral oil, shale oil, and N-Bromosuccinimide (NBS) reagents used as a chemical reagent in oil refining. Mineral oils were rich with chromium and rhodium, shale oils were concentrated with iron, nickel, zinc, and arsenic, and oils that had been refined using NBS were rich with vanadium, iron, nickel, and molybdenum (Kubo et al., 1978). Further research was completed in 1994 with the discovery that x-ray absorption spectroscopy could determine the levels of oxidation in bitumen and asphaltene samples (Kasria et al.., 1994).

Following the previous discussions (Chapter III-Section "Physics of X-Ray Fluorescence Analysis"), the absolute chemical concentrations cannot be adequately calculated using counts or calibration curves alone. After initial data processing it was apparent that no identifiable trend could be found across the Bakken-Three Forks Formation contact using fluorescence Kα data alone. Analytical chemistry methods such as ion chromatography (IC) and flame atomic adsorption spectrometry (FAAS) rely on linear calibration curves created from samples of known chemical concentrations before unknown concentrations can be determined. During energy dispersive x-ray fluorescence analysis, the magnetic and electric fields of the unknown samples (in this case the core sections) cannot be replicated in a laboratory setting. Simply creating calibration samples with chemical concentrations of 10%, 50%, and 100% concentration will not adequately represent the degree of magnetization within the core sample. The intensity of both the electric and magnetic field within the core sample are unknown; comparing the fluorescence values of the calibration samples will not account for the electric and

magnetic properties of the core. Perhaps the most important previously completed

research on x-ray fluorescence analysis in the earth sciences was completed in 2006 by

Dr. Ian Croudace and Dr. Guy Rothwell; using an ITRAX scanner they disseminated the

problems associated with using x-ray counts alone for chemical composition analysis.

Large analytical errors may arise due to poor peak discrimination in the x-ray spectra,

compaction of the grain size, and when the x-ray scanner is not positioned in the center of

the sample being analyzed (Croudace and Rothwell, 2006). X-ray fluorescence data

integrity will be most vulnerable during the analysis of low atomic weight elements at

low x-ray energies. Another fundamental consideration during all analysis is whether or

not the sample being analyzed was previously saturated; brines can leave behind sodium,

magnesium, chloride, and potassium. Hydrocarbons deposition and subsequent

evaporation can deposit nickel, molybdenum, and iron into core samples (Kubo, 1978).

Croudace and Rothwell (2006) proposed that the sole use of x-ray counts is inadequate

for definitive analytical determinations of chemical concentrations. The use of count

ratios has empirically proven to provide higher accuracy during chemical x-ray

fluorescence analysis than counts alone.

Table 7. Geologic and Diagenetic Interpretations using Fluorescence Ratios. Table created based of the results present by (Croudace and Rothwell, 2006).

XRF Ratio	Geologic and Diagenetic Interpretations Using Fluorescence Ratios
Ca:Fe	Indicative of detrital clay: biogenic carbonate ratio. Also can distinguish shell rich layers.
Ca:Fe	Good proxy for grain size relationships.
Sr:Ca	Higher Strontium can indicate the presence of Aragonite, indicating relative sea level fall or shallow water source.
Sr:Ca	Value may increase when sediment porosity increases, grain size also effects value.
K:Rb	Potassium is commonly associated with detrital clay, enhanced in turbidite muds.
Zr:Rb	Zirconium concentration is higher in heavy resistant minerals, enhanced in turbidite muds.

Table 7 Continued.

Ti:Rb	Titanium concentration is higher in heavy resistate minerals, enhanced in turbidite muds.
Si	May be useful as a sediment-source/provenance indicator.
Fe:Rb	Iron mobilized during redox-related deposition and diagenesis.
Fe:Ti	Iron mobilized during redox-related deposition and diagenesis.
Mn:Ti	Good indicator of redox-related diagenesis.
Br:Cl	High ratios of Bromine can indicate organic-rich layers. (Bromine and Sulfur are rich in organic sediments).
S:Cl	High ratios of Sulfur can indicate organic-rich layers. (Bromine and Sulfur are rich in organic sediments).
Cu:Rb	Sharp copper peaks are indicative of diagenesis.

Although x-ray fluorescence spectroscopy has been used extensively in the geologic sciences and chemical related fuel studies, few researchers have completed research regarding the potential use of x-ray fluorescence as a well-logging method. No published academic research currently exists outlining the potential benefits or feasibility of using XRF or XRFWL for detailed stratigraphic analysis of Williston Basin stratigraphic intervals. X-ray fluorescence was used to record the regional weathering profile at the Paleocene-Eocene boundary in the Williston Basin, but the stratigraphic location was above any recoverable hydrocarbon deposits (Clechenko, 2007). X-ray fluorescence was also used to measure the geochemical variation of inorganic constituents in North Dakota Lignite (Karner, 1984). No researchers have combined x-ray fluorescence analysis with the Lodgepole, Bakken, or Three Forks Formations in the literature. The goal of this thesis was to lay a foundation for x-ray fluorescence analysis of hydrocarbon bearing strata in the Williston Basin of North Dakota.

CHAPTER IV

WELL-LOGGING IN HYDROCARBON BEARING FORMATIONS

This thesis analyzed whether LWD or wireline formation evaluation is more beneficial in the Bakken-Three Forks oil pool of North Dakota. Understanding the benefits and consequences of Logging-While-Drilling and wireline logging lead to determinations of whether X-Ray Fluorescence Well-Logging (XRFWL) should be incorporated into an MWD package, incorporated into a wireline package, or used strictly in association with drill and mud cuttings. Although borehole geophysical characterization, or well-logging, has been used in nearly every geological drilling application, this thesis will focus solely on shale, sandstone, and carbonate unconventional hydrocarbon environments.

Gamma ray, sonic, acoustic, photoelectric, resistivity, neutron porosity, density, and nuclear magnetic resonance (NMR) techniques are commonly available well-logging tools provided by well-service companies such as Schlumberger and Baker-Hughes (Kundert and Mullen, 2009). Each log will provide individual benefits, but some of the common benefits discussed by the literature for shale logging include: gamma ray values are often used for geosteering and determinations of kerogen content; sonic measurements are used for fracture zone selection, wellbore stability, and perforation locations; photoelectric logs help identify lithology as long as barite mud is not being used; resistivity logs will typically include measurements from the flushed zone,

49

transition zone, and uninvaded zone and can be used to identify zones of high gas

porosity and an implicit indication of permeability; neutron porosity logs will help

identify clay and mineral bound water saturation, along with kerogen deposition; and

finally density logs can be used in combination with NMR logs to help calculate the total

porosity in the region of interest. Readily available wireline logs include gamma ray,

sonic, photoelectric, laterolog resistivity, density, and NMR logs. Logs that are typically

unavailable in wireline packages include propagation resistivity and azimuthal gamma

and resistivity tools. Readily available LWD logs include gamma ray, monopole sonic,

and azimuthal resistivity tools. Logging tools that are far less common during LWD

operations include photoelectric, neutron porosity, density, and NMR logs (Ramakrishna

et al., 2010; and Prammer et al., 2007).

One fundamental consideration to remember during unconventional shale logging

is whether the log can be effective on a cased borehole. If the log is only effective on an

uncased hole and borehole collapse is occurring, vertical to horizontal correlations will

become truncated and precision will be affected. Gamma ray and sonic are typically the

only measurements that can be performed after the well bore has been cased. Even sonic

logs have difficulty in cased holes; cement jobs with loose (as opposed to dense)

compaction will absorb a considerable amount of the sonic wave, transit times will be

decreased, and lithology will be misrepresented (Market and Canady, 2010).

Photoelectric, resistivity, neutron porosity, density, and NMR logs all cannot be recorded

after the well bore has been cased.

Another discussion that should be mentioned is the use of mud-logging for

stratigraphic identification. Mud-logging is technically a LWD technique in that drill-

cuttings will only be sent to the surface during drilling operations. Mud-logging is a fundamental practice used in industry, and will reveal the mineralogy and geochemistry of the drilling zone. Mud-logs will hopefully reveal the grain size, lithology, percentage of carbonate in the sample, and porosity of the interval being drilled. The physical inspection of the formation provides several benefits that no well-log can provide: 1) sonic and acoustic interval transit times rely on matrix assumptions, these assumptions must be made in combination with other logs 2) neutron porosity and density porosity determinations depend on reference porosities (such as limestone), these assumptions also must be made in combination with other logs and 3) drill-cuttings in combination with an experienced mud logger can provide immediate identification of the lithology and present formation. Drill cutting analysis from LWD drilling operation will allow macro-scale changes to the direction of drilling (e.g. a mud-logger would be able to tell you that your horizontal well had transitioned from the Middle Bakken into the Upper Bakken Member after seeing distinctly black and fine-grained shale cuttings as opposed to the Middle Bakken siltstone/carbonate mixture).

Unconventional Hydrocarbon Resource versus Conventional Resource

The Bakken-Three Forks oil pool of North Dakota represents an "Unconventional Resource Play," a term applied to in-situ oil and gas trapped within layers of impermeable metamorphosed clay or shale without structural control. Unconventional and conventional resource play terminology should not be confused with unconventional and conventional oils. Unconventional oils are typically considered to be heavily dense, sulfur-rich, and carbon-laden including bitumen, coke, and kerogen (Gordon, 2012). Conventional oils are considered to be hydrogen rich with short carbon chains (ranging

between C1 and C60) and typically have a higher API gravity (Gordon, 2012). The oil produced from the Bakken-Three Forks oil pool from the Williston Basin is affectionately referred to as "The Bakken Sweet Crude," and is a conventional type oil based on the (Gordon, 2012) descriptions. Despite the oil being conventional, the formation environment and production techniques are not conventional, rather they are unconventional.

Conventional oil resource plays have historically been the most productive units in the world. Several geological features are necessary for a conventional resource type: a fine-grained source rock that prevents sulfate and oxygen destruction of kerogen in anoxic conditions, a permeable layer that allows hydrocarbons to flow from the source rock into the reservoir, a porous and permeable reservoir, and a structural trap that is contained with layers of impermeable clay, shale, or mudstone and contains the hydrocarbon accumulation. Without a structural trap (such as an anticline or an aquitard with hydrodynamic influence) to contain the hydrocarbon, economic production can become impossible.

Unconventional oil resource plays, such as the Bakken-Three Forks oil pool, are quickly headed towards becoming prolific world producers. Rather than hydrocarbon production being a function of generation, migration, and accumulation as seen in a conventional resource, unconventional resources only rely on a source rock and an impermeable rock with high porosity. The impermeable host rock is then drilled, either horizontally or vertically, as an attempt to draw hydrocarbons to the bore hole. Horizontal drilling is common in unconventional resource types; hydraulic-fracturing is often performed after drilling is completed to induce fractures in the host rock and

increase effective permeability (Market et al., 2010). Other secondary recovery
techniques can include fire flooding to increase well pressure, carbon dioxide injection to
decrease oil-wet saturation and increase well pressure, and acid injection to react with
carbonate lithology and increase permeability; in all cases the goal of enhanced oil
recovery in an unconventional resource type is to increase the effective permeability and
move carbons from the formation to the borehole. Four main stages exist in the
exploitation of unconventional resources: exploration, evaluation, delineation, and
development (Haskett and Brown, 2005).

Table 8. Summary of Well-Log Measurements Available in the Williston Basin. This table was
modified from the results of (Market, 2010).

Measurement	Use in Shale	Available LWD?	Available WL?	Cased Hole?
Gamma Ray	Geo-steering (LWD), Kerogen Content	Yes (Azimuthal Common)	Yes	Yes
Sonic	Fracture Zone Selection, Wellbore Stability, Perforation Locations	Yes (Monopole Tools Common)	Yes	Yes-Cement Variable
Photoelectric	Mineralogy (Only in Barite-Free Mud)	Yes	Yes	No
Propagation Resistivity	Locate Zones of Gas Porosity	Yes	No	No
Laterolog Resistivity	Geo-steering (LWD)	Yes	Yes	No
Chemostratigraphy	Mineralogy	Yes-Mud Logging	No	No
Nuetron Porosity	Gas, Clay, Kerogen Determinations	Yes	Yes	Approximated
Density	Effective Porosity	Yes	Yes	Approximated
NMR	Total Porosity	Yes	Yes	No

Unconventional shale lithology has historically been evaluated using wireline logging tools (Market et al., 2010). Recent technological advancements allow for horizontal and directional drilling, but new challenges have become common during formation evaluation. Wellbore stability considerations, zones of high initial pressure, and the need for real-time data while drilling can make LDW measurements more desirable than their wireline counterparts. The history of wireline logging has primarily been a matter of acquiring open hole logs on the vertical well, selecting the region of interest, and drilling the horizontal well into that zone. Obviously this method has drawbacks including not precisely knowing what structural changes occur as the distance from the borehole increases. Due to higher pressure when turning lateral, the horizontal leg of the well is rarely left open; also rare is the collection of cased hole logs after production casing is placed.

Wireline Logging

Wireline logging involves the use of a small, light, and typically delicate tool that will provide good borehole contact, high data speeds, and easy communication (Market, 2010). Readily available wireline logs include gamma ray, sonic, photoelectric, laterolog resistivity, density, and NMR techniques. Logs that are typically unavailable in wireline packages include propagation resistivity and azimuthal gamma and resistivity tools; otherwise wireline logging will typically have more options than LWD. Wireline logging also offers a distinct advantage that LWD cannot; areas where data was not recorded or where data was destroyed can be measured over. Perhaps the best way to analyze the benefits of wireline logging is to view what they are marketed for. In Schlumberger (2011), the benefits of using a wireline tool include: reservoir delineation, hydrocarbon

saturation determinations, moveable hydrocarbon determination, locations of porous and permeable zones, gas detection, porosity analysis, and well-to-well correlation. Other noted benefits include better-quality logs with higher resolution revealing hard-to-find pay zones, fifty percent reduction in time logging, and more reliable performance. Despite the enthusiasm of Schlumberger, LWD drilling will always provide results faster than wireline logs due to the access of real time data. Fortunately for the sake of this paper, the wireline logging for the Continental Resources, Inc. Charlotte 1-22H well was performed using a Schlumberger Platform Express wireline tool.

Logging-While-Drilling (LWD/MWD)

Perhaps the most beneficial feature of Logging-While-Drilling (LWD) is the ability to collect real-time data. LWD sensor data is typically transmitted to the surface in the mud column through a continuous mud wave transmission, which is then detected by pressure transducers for data analysis (Hassan and Amar, 1998). Multiple pieces of data can be transmitted in real-time to the drilling engineer or surface geologist including weight-on-bit, gamma ray, and resistivity curves. The most immediate impact of LWD is the minimum exposure of the wellbore to drilling mud; during wireline logging operations additional mud is added to the borehole to condition the hole. As the formation exposure time to the drilling mud increases, the clay hydration also increases. Clay hydration can lead to numerous problems such as wellbore deterioration, stuck drill pipes and wireline tools, side-tracks due to wellbore collapse, and holdup of wireline tools (Hassan and Amar, 1998). Readily available LWD logs include gamma ray, monopole sonic, and azimuthal resistivity tools. Logging tools that are far less common during LWD operations include photoelectric, neutron porosity, density, and NMR logs.

(Ramakrishna et al., 2010; and Prammer et al., 2007). The LWD tool (figure three) will typically measure resistivity at the bit of the tool, with shallow resistivity being at the top of the drill stem and deep resistivity being further down towards the bottom.

In many circumstances LWD logs have complemented, rather than replaced wireline measurements (Sutiyono, 1992). Physical advantages to LWD logs include several circumstantial but commonly occurring events: in washed out boreholes, LWD logs will be recorded prior to the wash-out and preserve better data; in sandstones with high gas saturation, LWD logs will be recorded prior to gas invasion; in shale the high dielectric contrast LWD shallow resistivity values will often be lower than the deep resistivity regardless of formation fluid due to the high dielectric constant in the shale; and finally in intervals with high resistivity contrast, LWD readings will commonly see these values with greater precision because solution mixing occurs subsequently to drilling. Perhaps the future of well-logging in the Bakken-Three Forks oil pool will involve the use of wireline and LWD logs in tandem. For instance, LWD logs can be used to determine the resistivity of the formation, but they commonly are not able to determine the resistivity of the invaded zone. However, with the used of the wireline resistivity logs (inversion based resistivity), determinations of hydrocarbon saturation can be completed through the following steps: estimate formation resistivity using R deep-induction LWD data, estimate flushed zone resistivity using Rxo wireline data, and then determine the hydrocarbon saturation in the saturated zone by subtracting the deep LWD data from the flushed wireline data. (Based on the model of Frenkel, et al., 2004). The theory presented by (Frenkel et al., 2004) is an application combining resistivity LWD and wireline log data, but the theory can also be applied to other tools:

Gamma Ray values can be recorded by the LWD tool during drilling, and measure (depending on the tool) 8–10 feet into the formation (Rider, 2011), the wireline measurement can then be recorded and a rough inference of the formation porosity can be established. In circumstances where the gamma value was higher on the wireline than the LWD log at an equivalent depth, potassium rich saline solution likely flowed from the formation into the flushed zone. Gamma ray LWD values should be recorded during the drilling of the vertical section. Before the vertical section is cased, wireline values can also be recorded for correlation between the two tools. This would answer whether discrepancies exist between the values, if highly accurate data exists down the vertical extent of the well, the gamma signature from the formation of interest can be followed during horizontal drilling.

LWD caliper measurements can record the borehole diameter during drilling, then wireline caliper measurements can record the borehole diameter after drilling. The differences between the values can give an indication of whether or not borehole collapse has occurred in the formation. It would also be interesting to know whether or not the borehole collapsed during drilling or after exposure to the open hole. LWD sonic measurements can be recorded as a background or calibration recording for the lithology/lithology formation fluid transit time. The wireline log can then record new values to assess the quality of the cement job. (Market, 2010). These values could also be useful if you find a poor or loose cement job in the cased region of the area of interest; perforation charges could be more effective. LWD neutron porosity and neutron density values can be measured during the initial drilling stage of the well, subsequent wireline neutron porosity and neutron density values can be measured during the wireline analysis

57

of the well. In a formation saturated with gas the differences between the density-porosity crossovers can give a rough indication of porosity with respect to time. Furthermore, other hydrogen rich fluids such as oil can be discovered using the same methodology.

CHAPTER V

METHODOLOGY

Study Location

This thesis was broken into two autonomous sections from this point forward.

The first section involved analysis of nine different core sections representing the Bakken

and Three Forks Formation contact in the Williston Basin of North Dakota. The second

section involved analysis of the stratigraphic interval spanning the top of the

Mississippian Lodgepole Formation through the bottom of the Devonian Three Forks

Formation (this stratigraphic interval includes the Lodgepole Formation, Upper Bakken

Member, Middle Bakken Member, Lower Bakken Member, Pronghorn Member, and

Three Forks Formation).

Figure 3. Geographical Location of Cored Wells used for XRF Analysis. The blue triangles represent wells examined at the Bakken-Three Forks contact. The red triangle represents the Charlotte 1-22H core section representing the stratigraphic interval from the top of the Lodgepole Formation to the bottom of the Three Forks Formation.

Ten total core sections from independent wells were analyzed for this thesis. The first group of nine wells represented the Bakken-Three Forks contact and contained the following wells: Nordstog 14-98H, Rosenvold 1-30H, Muller 1-21-16H, Sara G. Barstad 6-44H, Rink 12-4ESH, Martin Weber 1-18, Johnson 43-27, Rasmussen 1-21H, and Washburn 44-36H.
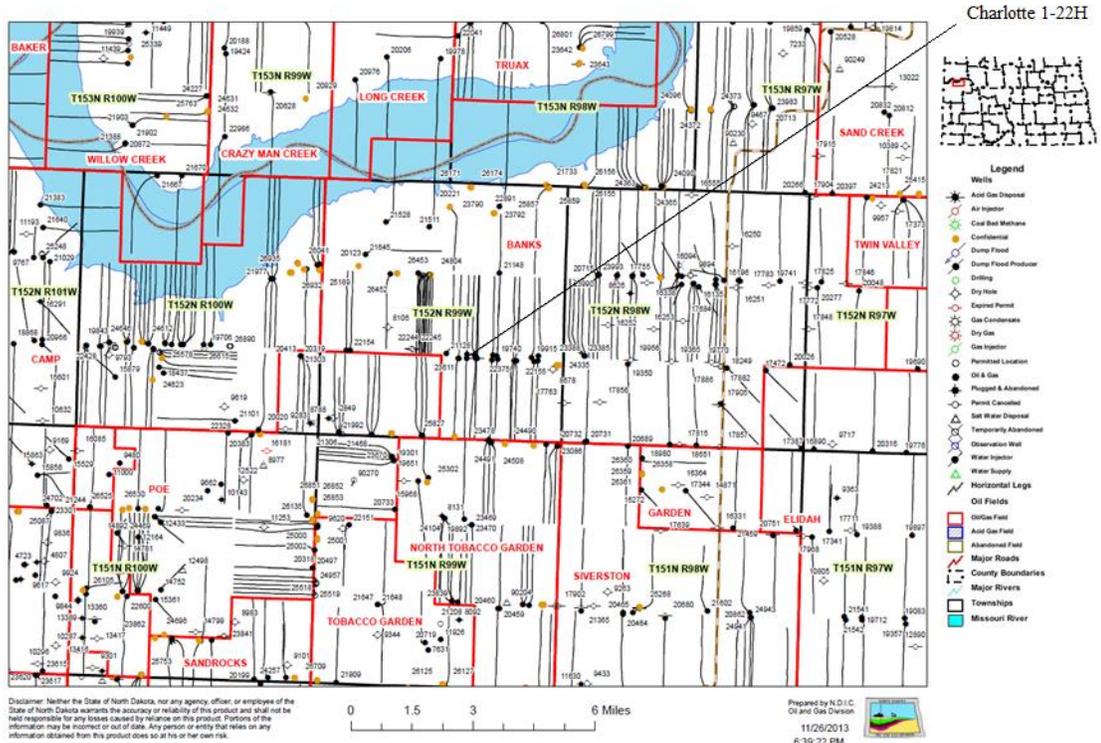
Figure 4. Horizontal Wells in McKenzie County, North Dakota. This map was created using the North Dakota Industrial Commission (NDIC) ArcGIS software; Charlotte 1-22H is located in the center of the map. Each linear black feature shows a horizontal leg at depth.

The reason this thesis analysis was split into two autonomous sections was for proof of concept and additional research objectives. The first nine wells were selected to study whether or not XRF can adequately pinpoint a sharp and conformable geologic contact. The Lower Bakken-Three Forks Formation contact is widely regarded as a sharp and conformable contact of shale and mixed dolomite, shale, and alternating bands of

pyrite. Theoretically this sharp contact should provide a sharp and definitive contact based on the fact that the lithology is transitioning from a detrital shale to a carbonate. Charlotte 1-22H was selected based on the fact that it would expand the thesis study to four contacts rather than one contact. Instead of just the Lower Bakken-Three Forks contact being analyzed, the Lodgepole-Upper Bakken Member, Upper Bakken Member-Middle Bakken Member, Middle Bakken Member-Lower Bakken Member, and Lower Bakken-Three Forks contact would be established. Additional benefits to including Charlotte 1-22H in the thesis research included being able to precisely analyze chemostratigraphic alterations within the middle of a thicker formation.

Table 9. Summary of Core Sections Scanned using X-Ray Fluorescence.

Well Name	Charlotte 1-22H	Nordstog 14-98H	Rosenvold 1-30H	Muller 1-21-16H	Sara G. Barstad 6-44H
NDIC#	19918	16089	19709	20552	15889
API#	33-053-03358	33-023-00489	33-023-00658	33-105-02157	33-061-00490
Operator	Continental Resources	Baytex Energy	Continental Resources	HRC Operating	Hess
County	McKenzie	Divide	Divide	Williams	Mountrail
Latitude	47.964578	48.764564	48.661666	48.489876	48.183932
Longitude	-103.333939	-103.357934	-103.132496	-104.009671	-102.825858
Oil (Bbls)	185,535	40,822	56,314	60,205	26,447
Formation	LP-TF	BK-TF	BK-TF	BK-TF	BK-TF
Depth	11,210-11,572	8,704-8,718	9,303-9,317	9,660-9,667	10,471-10,485
Data Points	362	14	14	14	14
Intensity	45KeV	15KeV&45KeV	15KeV&45KeV	15KeV&45KeV	15KeV&45KeV
Sample	Core Section (4"diameter)	Core Section (4"diameter)	Core Section (4"diameter)	Core Section (4"diameter)	Core Section (4"diameter)
Well Name	Rink 12-4ESH	Martin Weber 1-18	Johnson 43-27	Rasmussen 1-21H	Washburn 44-36H
NDIC#	21786	6082	21424	20844	17309
API#	33-053-03843	33-025-00067	33-025-014353	33-105-02204	33-053-02894
Operator	XTO Energy	Petro-Hunt	XTO Energy	HRC Operating	Burlington Oil

Table 9 Continued.

County	McKenzie	Dunn	Dunn	Williams	McKenzie
Latitude	47.930117	47.3808	47.34751	48.402809	48.027304
Longitude	-103.239484	-103.091538	-102.761725	-103.876436	-102.828902
Oil (Bbls)	78,429	919,159	58,329	84,883	81,595
Formation	BK-TF	BK-TF	BK-TF	BK-TF	BK-TF
Depth	11,180-11,195	10,971-10,985	10,870-10,884	10,264-10,278	10,541-10,554
Data Points	14	14	14	14	14
Intensity	15KeV&45KeV	15KeV&45KeV	15KeV&45KeV	15KeV&45KeV	15KeV&45KeV
Sample Type	Core Section (4"diameter)	Core Section (4"diameter)	Core Section (4"diameter)	Core Section (4"diameter)	Core Section (4"diameter)

The first group of nine wells was also selected based on the presence of a Bakken

and Three Forks Formation Contact. Furthermore, core sections were selected based on

isopach thickness of the Bakken Formation; localities where the Bakken Formation was

thicker were selected. This area typically represents the geographical locations of Burke,

Divide, Dunn, McKenzie, Mountrail, and Williams County, North Dakota. Specific

isopach thickness maps were obtained from Nordeng (2010). The thickness of the

Bakken Formation is a topic that has been thoroughly established in the geologic

literature (Meissner, 1984; LeFever, 1991; Nordeng, 2010; Pollastro et al., 2013). The

Charlotte 1-22H well section was selected based on the providence that it contained all

the necessary factors for thorough analytical dissemination: the geographical location of

the well was located in the thickest section of the Bakken, the Wilson B. Laird Core and

Sample Library at the University of North Dakota had the entire core section available

during the time of research, the North Dakota Industrial Commission had wireline and

LWD well-log files available, and finally the interval cored contained the entire section

from the top of the Lodgepole formation through the bottom of the Three Forks Formation.

All data collection was completed at the Wilson B. Laird Core and Sample Library at the University of North Dakota in Grand Forks, North Dakota. The Wilson B. Laird Core and Sample Library contains approximately 70 miles of cores and 34,000 boxes of drill cuttings. The cores represent approximately 75 percent of the cores cut in the North Dakota portion of the Williston Basin. It also must be noted that, despite the best efforts to choose core sections based on the aforementioned criteria, core sections were also chosen based on availability in the core and sample library. Furthermore, on curator specimens were chosen in the core and sample library to provide a uniform sample for analysis. Curator samples are created using the following methodology: a 4″ diameter core is drilled in an in-situ geologic environment, the cores are cleaned, cut in thirds, and placed in uniform 3′ boxes. The cores are relatively flat (exceedingly so in terms of core samples) and provide superior uniformity to drill cutting samples.

Continental Resources Charlotte 1-22H

The Continental Resources, Inc. Charlotte 1-22H well is located in McKenzie County, North Dakota in the Banks Oil Field. The American Petroleum Institute (API) number for this well is API# 33-053-01349. The Charlotte 1-22H, 2-22H, 3-22H, and 6-22H2 wells were completed by Continental Resources Inc. to test the performance of four autonomous reservoir benches in the Bakken-Three Forks oil pool. Charlotte 1-22H was intended to produce from the Middle Bakken Formation. One of the reasons the Charlotte H series wells have been so important to Continental Resources, Inc. is because the Banks Oil Field has become a tremendous producer of hydrocarbons. Production in
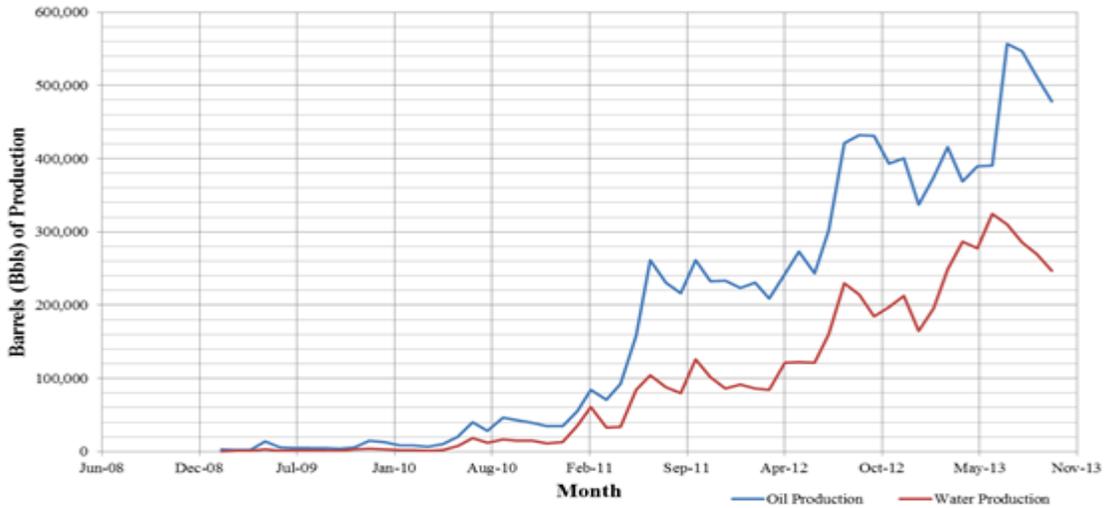
Figure 5. Banks Field Oil and Water Production, 2008-2013. The Charlotte 1-22H core section was drilled from Banks Field in McKenzie County, North Dakota. Note the high amount of water production since 2011.Production data is courtesy of the North Dakota Industrial Commission (2013).
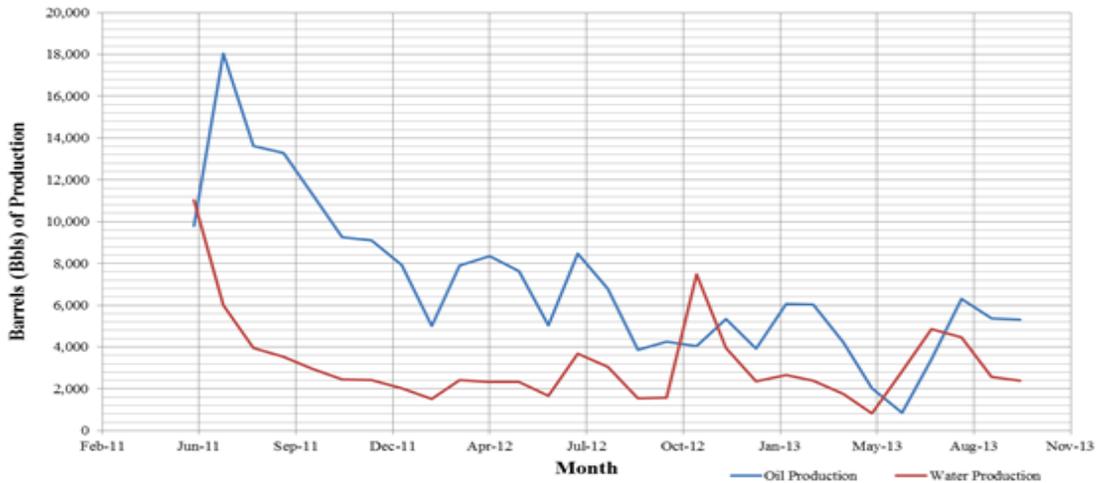
Figure 6. Charlotte 1-22H Oil and Water Production, 2008-2013. The Charlotte 1-22H well from Continental Resources, Inc. is producing from the Middle Member of the Bakken Formation. Production data is courtesy of the North Dakota Industrial Commission (2013).

Banks Field was non-existent until May, 2009. Over the last four years, the average monthly production in Banks Field has increased exponentially; during July, 2013 the average monthly production was 550,000 barrels of oil. Along with the extravagant oil

64

production, Banks Field has also become a prolific producer of water. During July, 2013

Banks Field produced more than 300,000 barrels of water.
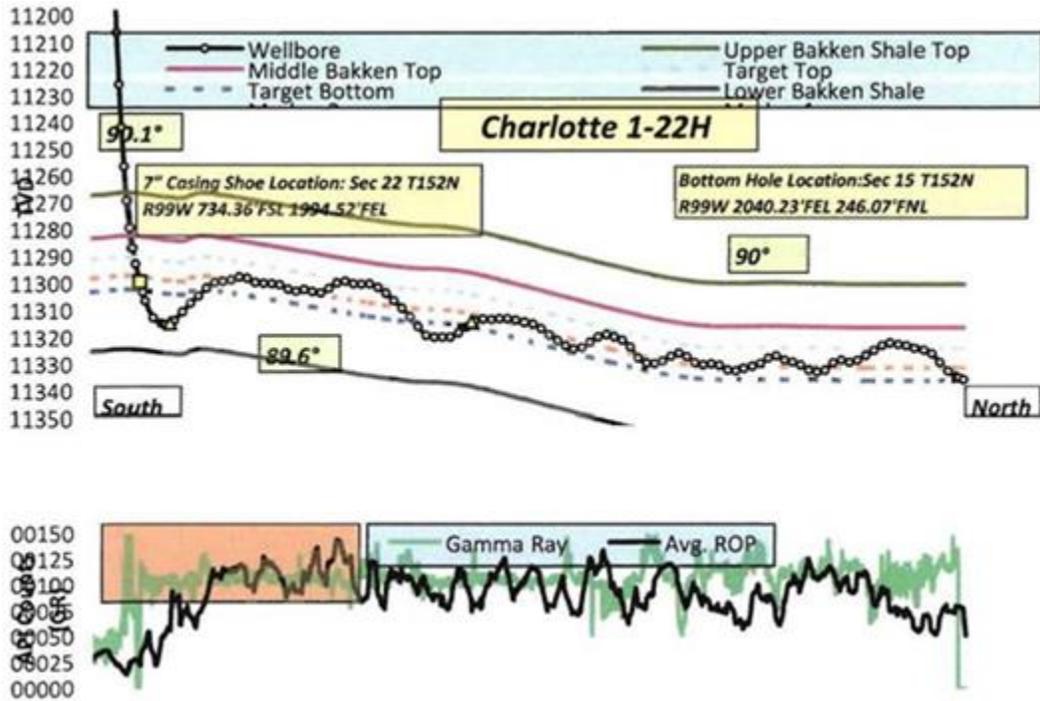
Figure 7. Charlotte 1-22H Horizontal Drilling Path. The Charlotte 1-22H well was cored to the bottom of the Three Forks Formation. The horizontal leg was then completed into the Middle Bakken Formation; geosteering was completed using LWD gamma ray. This photo is courtesy of the North Dakota Industrial Commission (NDIC).

The chronological logging of Charlotte 1-22H went as follows: at 00:31:00 on

March 14th, 2011 LWD logs were created based on the drilling for the interval of 2,245

feet to 11,686 feet (from the bottom of the well pad). At 22:28:00 on March 14th, 2011 a

wireline log was completed representing the same interval. In total two logs are present

showing the formation properties during drilling and 22 hours after drilling (it should be

noted that the actual time between drilling each interval and the wireline log created is

probably greater than 22 hours, hopefully allowing for fluids to move from the uninvaded

zone into the invaded zone. For the sake of this Charlotte 1-22H analysis, LWD and

wireline properties were compared from the top of the Lodgepole formation (11,210 ft) to

the bottom of the first zone of the Three Forks Formation (11,410 ft). This interval was

chosen to limit the total amount of data processing (consistent wireline and LWD data

was available for an interval of 9,250ft-11,500ft) and to represent the major formation

units in the Bakken-Three Forks oil pool. The top zone of the Three Forks (referred to as

Unit 4 by Nicolas, 2006 and 2007) is conventionally known as the reservoir unit of the

Three Forks Formation. The Lodgepole, Upper Bakken Member, Middle Bakken

Member, Lower Bakken Member, and Three Forks Formation were included in the

overall analysis.
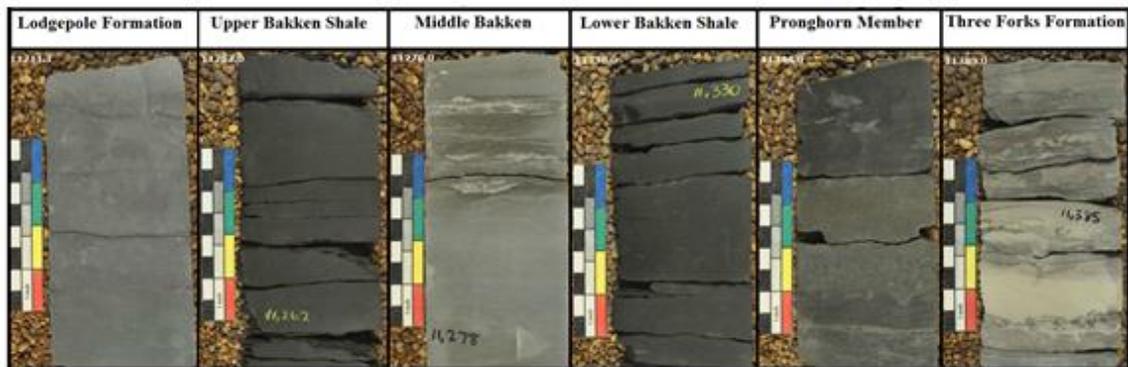
Figure 8. Charlotte 1-22H Core Photographs. In these pictures the Upper and Lower Bakken
Members display their notoriously black color. The Bakken Shale is easily distinguishable from
the underlying and overlying units. (Images courtesy of the North Dakota Industrial Commission)

Analytical Testing Procedures

The Wilson B. Laird and Sample Library catalogs core sections based on gamma-

ray data from well-logs provided by the industrial driller. Current well-logs do not

pinpoint lithological changes, formation contacts were manually identified before

analysis. Lower Bakken-Three Forks Formation contacts are easily identifiable using

visual cues; the Lower Bakken Formation is entirely dark black with a dull luster, fine-

grained, and displays no identifiable bedding. Alternatively, the Three Forks Formation

is dull green in anoxic zones, rusty red in oxidized zones, and displays numerous sections

of thin beds.

After the contacts were manually identified x-ray counts were collected using a

Bruker Tracer IV-SD Handheld XRF instrument. This technology uses Silicon Drift

Detection (SDD) for dramatically improved speed and sensitivity. The advent of the

SDD technology allows for accurate light element analysis; previous XRF analysis relied

on vacuum and helium flushing. The technology is based on energy dispersive x-ray

fluorescence and uses an x-ray tube as its excitation source. Operation acceleration

voltages range from 10 to 45 keV and anode currents range from 0.05 to 60 µA. The

Bruker Tracer IV-SD XRF instrument is fully field portable and can be used in

combination with S1PXRF software for bench-top analysis. For the purpose of this

thesis, the Bruker Tracer IV-SD was configured into a vertical stand and core sections

were placed on top of the instrument. Each core section was exposed to ionizing x-rays

at excitations of 15 and 45 keV for thirty seconds. Backscatter x-ray energies were

detected and quantified as an anode current to create an elemental spectrum. Initially all

samples were scanned at 15 keV and 45keV; after data analysis and a literature review of

x-ray fluorescence technology showed that scanning at 15 keV versus 45 keV yielded no

significant differences, samples were only scanned at 45 keV.

For both the nine well Bakken-Three Forks contact group of cores and the

Charlotte 1-22H core, samples were scanned using the following procedure: each core

section was placed on top of the bench top configuration stand, the x-ray source was

turned on and allowed to collect data for 30 seconds, and finally the x-ray source was

shut off and the core sample was placed back into its receptacle. For the nine well

Bakken-Three Forks contact group of cores, scans were completed at seven, five, two,

and one feet above the contact, at the contact, and at one, two, five, and seven feet below

the contact. This process was repeated at energy intensities of 15keV and 45keV. In

total, 15 data points were collected for each Bakken-Three Forks contact. For the

Charlotte 1-22H well, scans were completed at every foot for the entire depth of the

Lodgepole-Three Forks interval. In total this interval spanned 353 feet; scans were

collected at an intensity of 45keV.

For selected core sections in the first group and the entire Charlotte 1-22H core

section; spectral gamma ray analysis was also completed using an OFITE-SGR 740 core

gamma ray logger. The SGR-740 measures the natural electromagnetic gamma emission

from the decay of potassium, uranium, and thorium. The major difference between all x-

ray fluorescence analysis and core gamma analysis is the fact that x-ray fluorescence is

active electromagnetic radiation; gamma ray analysis is entirely passive. For x-ray

fluorescence spectroscopy an x-ray is produced from a source, for spectral gamma ray

analysis no source is produced- in both circumstances an electromagnetic signal is

detected and classified based on the energy of the received photon. After allowing the

equipment to collect a 15-minute background concentration the core samples are scanned

at a rate of 0.2 feet per minute, or 5 minutes per foot. For a one hundred foot section of

core, this process will take a substantial amount of time. Using a rate of 0.2ft/min, the

Charlotte 1-22H core section took a total of 29.42 hours to complete analysis that

corresponds to about a week of laboratory work. Out of the first group of nine core

sections, spectral gamma ray analysis was completed on the Nordstog 14-98H,

Rosenvold 1-30H, and Muller 1-21-16H core sections over the entire 15 foot Bakken-

Three Forks contact interval.

Data Processing

Bruker Tracer IV Handheld XRF equipment is operated using S1PXRF software.

This software was created using Microsoft Visual Basic and must be used on a personal

computer using Windows 7. The OFITE Spectral Gamma Ray logger is also powered

with a personal computer using Windows 7; the spectral gamma ray logger data

acquisition is powered using LabVIEW from National Instruments. All data from

S1PXRF and LabVIEW was processed using only Microsoft Excel. MS Excel is capable

of calculating all necessary well-log equations; MS Excel is often labeled as an inferior

software for graphical solutions-it may not be user friendly but it is definitely effective

when used correctly. MS Excel also offers the added benefit of wide scale availability on

nearly all computer systems using MS Office: industry, academia, and personal

computing applications utilize Microsoft Software.

For this thesis research twenty-seven unique elements were used for

chemostratigraphic analysis: fluorine, sodium, magnesium, aluminum, silica, phosphorus,

sulfur, chlorine, argon, potassium, calcium, titanium, vanadium, chromium, manganese,

iron, nickel, copper, zinc, arsenic, bromine, rubidium, strontium, zirconium,

molybdenum, and palladium. These elements were chosen because their excitation

voltages were all below the 45 keV excitation limit of the Bruker Tracer IV series XRF

(Equation 3-3 and 3-4). In the S1PXRF software, the user automatically selects the

element they wanted to study: count rates at elemental photon energy voltage (based on

Equation 3-2) are listed within the S1PXRF software. This data can then be copied into any software designed for data analysis, preferably MS Excel.

Well-Log Equations and Calculations

Well-logging equations and calculations are included in this thesis to assess the advantages of MWD/LWD drilling versus wireline drilling in the unconventional Bakken Formation. After this analysis was completed, both results were compared to XRFWL results. XRFWL well-logging applications cannot and will not replace all well-logging tools currently used in industry. This technology is currently limited to core and drill-cuttings; if this technology is incorporated into a MWD/LWD package new data will have to be collected and processed to assess the accuracy of the system. However, it should be noted that this thesis attempts to provide theory for future downhole XRFWL.

The first well-logging analysis completed in this thesis will involve shale volume calculations. Shale volume calculations are commonly used to determine the amount of shale in a lithostratigrahic unit from the LWD or wireline log. Shale is well established as a hydrocarbon source rock in the Williston Basin, it is known to be a poor reservoir rock due to lower permeability and effective porosity within the Bakken. Shale volume calculations from wireline and LWD data will then be compared with shale volume calculations from XRF data. The most commonly used shale volume calculations include the Clavier Method, the Steiber Method, and the Larionov Method (Paleozoic).

Clavier Vsh: (5-1)

$$= 1.7 - [3.38 - (IGR + .7)^2]^{1/2}$$

Steiber Vsh: (5-2)

$$= \frac{IGR}{3 - (2 \times IGR)}$$

Larionov Vsh (Paleozoic): (5–3)

$$= .33 \times \left(2^{(2IGR)} - 1.0\right)$$

IGR: (5-4)

$$= \frac{GRlog - GRclean}{GRshale - GRclean}$$

XRF Vsh: (5-5)

$$= \frac{\frac{NiK\alpha}{MnK\alpha}log - \frac{NiK\alpha}{MnK\alpha}Carbonate}{\frac{NiK\alpha}{MnK\alpha}Shale - \frac{NiK\alpha}{MnK\alpha}Carbonate}$$

where: GR = Gamma ray value of the geologic unit (API)

$\frac{NiK\alpha}{MnK\alpha}$ = The ratio of Kα nickel fluorescence to Kα manganese fluorescence

IGR = Shale indicator (API)

The XRF Vsh Equation (Equation 5-9) can be used to calculate the volume of sedimentary and metamorphic carbonates, sandstones, shales, and evaporites. The equation would simply replace the shale fluorescence indicator with other chemostratigraphic indicator units in the Williston Basin or other unconventional shale logging environments. For instance the XRF Sandstone Volume (Vss) Equation would take the fluorescence ratio of silica to

calcium to show highlight the high silica compositions in orthoclase, plagioclase, microcline, and quartz arenite (Equation 5-10). XRF Carbonate Volumes (Vca) can be calculated using the ratio of Kα calcium fluorescence to Kα magnesium fluorescence.

XRF Vss: (5-6)

$$= \frac{\frac{SiK\alpha}{CaK\alpha}log - \frac{SiK\alpha}{CaK\alpha}Carbonate}{\frac{SiK\alpha}{CaK\alpha}Sandstone - \frac{SiK\alpha}{CaK\alpha}Carbonate}$$

where: $\frac{SiK\alpha}{CaK\alpha}$ = The ratio of Kα Silica fluorescence to Kα Calcium fluorescence

XRF Vca: (5-7)

$$= \frac{\frac{CaK\alpha}{MgK\alpha}log - \frac{CaK\alpha}{MgK\alpha}Sandstone}{\frac{CaK\alpha}{MgK\alpha}Carbonate - \frac{CaK\alpha}{MgK\alpha}Sandstone}$$

where: $\frac{CaK\alpha}{MgK\alpha}$ = The ratio of Kα Calcium fluorescence to Kα Iron fluorescence

The XRF volume equations can be applied to numerous types of lithologic and mineralogical volume calculations. These applications will not be limited to only the petroleum industry, the mining industry will also benefit from the use of these ratios. For instance the equations can be applied for halite exploration by using the ratio of Kα sodium fluorescence to Kα Chlorine fluorescence. Gypsum ($CaSO_4$) and other sulfate minerals such as barite ($BaSO_4$), hanksite ($NaKSO_4$), and anhydrite ($CaSO_4$) can be identified by using the ratio of Kα sulfur

fluorescence to Kα silica fluorescence. The sulfide group of minerals such as bornite (Cu_5FeS_4),

galena (PbS), sphalerite (ZnS), chalcopyrite ($CuFeS_2$), pyrrhotite (FeS), cinnabar (HgS), realgar

(As_4S_4), orpiment (As_2S_3), stibnite (Sb_2S_3), pyrite (FeS_2), marcasite (FeS_2), and molybdenite

(MoS_2) can also all be identified with the use of the Kα sulfur fluorescence to Kα silica

fluorescence ratio. Because Silica is not present in sulfate or sulfide minerals, fluorescence

values represent the high level of sulfur in comparison to silica.

Water saturation is perhaps one of the most important equations for oil and gas

identification and production within the Williston Basin. Using any porosity log (whether

acoustic, sonic, or NMR) and typically deep induction resistivity logs, the percentage of water

saturation can be determine. The most commonly used method for the determinations of water

or hydrocarbon saturation is Archie's Equation, that takes into account formation porosity (φ),

formation water resistivity (R_w), observed bulk formation resistivity (R_t) , a constant (a), a

cementation factor (m), and a saturation exponent (n):

The Archie Equation: (5-8)

$$Sw = \left[\left(\frac{a}{\varphi^m}\right)\left(\frac{Rw}{Rt}\right)\right]^{1/n}$$

where: Sw = Bulk water saturation (%)

       a = Formation constant (usually 1)

      Rw = Formation water resistivity (ohm·meters)
      Rt =Formation saturated water resistivity (ohm·meters)
      m =Cementation factor (usually 1.8-2.0 for sandstones, carbonates, and shale)
      n =Saturation exponent (usually close to 2.0)
      φ =Rock matrix porosity (%)

After Archie's Equation has been applied to a geologic formation the relative percentage of hydrocarbon saturation can easily be determined using the simply equation:

Hydrocarbon Saturation Equation: (5-9)

$$So = 1 - Sw$$

where: Sw = Bulk water saturation (%)

      So = Bulk hydrocarbon saturation (%)

To incorporate Archie's Equation into x-ray fluorescence core analysis, it is essential to be able apply a Kα fluorescence ratio into the Archie's Equation values for porosity (φ) and formation resistivity (Rt). Water resistivity (Rw) could theoretically be assumed for water, fresh water, and brine water; however the calculation would at then best be a speculation and multiple calculations would have to take place and then combined with lithology. Water resistivities, in general, are based upon numerous variables and give only a rough calculation of water saturation. Because of changes in resistivity due to grain compaction, degree of diagenesis, and formation temperature the bulk formation resistivity and the formation water resistivity values are not always precise. Although Archie's Equation is the industry standard for determining water saturation and hydrocarbon saturation, it would be far more convenient to scan formation lithology and chemically analyze whether or not the stratigraphy is hydrocarbon bearing. (Kubo, 1978). Archie's equation is calculated for the Charlotte 1-22H core section and then will be compared with XRF ratios to examine possible relationships between the data. During hydrocarbon exploration during drilling operations, it would be pleasantly convenient to scan lithology using XRFWL and identify nickel, vanadium,

74

molybdenum, and sulfur. These elements represent the common hydrocarbon trace metals identified by (Kubo, 1978). Then instead of logging the entire subsurface lithology from the top of the Kelly Bushing to the bottom of the hole, common well logs such as porosity and resistivity could then be performed in the areas that XRFWL already proved contained hydrocarbon presence. Archie's Equation (Equation 5-11) could then be used to assess the water saturation versus hydrocarbon saturation to assess the economic feasibility of producing the zone.

Another important water-saturation calculation involves the determinations of apparent water resistivity (Rwa). The determination of Rwa can give an indication of whether or not strata is hydrocarbon bearing. Empirical evidence has proven that hydrocarbon bearing zones will contain an apparent water resistivity (Rwa) higher than the formation water resistivity (Rw). Both formation water resistivity and apparent water resistivity can be calculated using many of the same parameters as Archie's Equation (Equation 5-12).

Apparent Water Resistivity: (5-10)

$$Rwa = \frac{Rt \times \varphi^m}{a}$$

Formation Water Resistivity:

$$Rw = \frac{Ro \times \varphi^m}{a}$$

where: Rwa = Apparent water resistivity (ohm·meters)

a = Formation constant (usually 1)

Rw = Formation water resistivity (ohm·meters)
Rt = Formation saturated water resistivity (ohm·meters)
m = Cementation factor (usually 1.8-2.0 for sandstones, carbonates, and shale)
Ro = Invaded zone resistivity (ohm·meters)
φ = Rock matrix porosity (%)

75

Following the methodology of Croudace and Rothwell (2006) all x-ray fluorescence ratios were calculated using Microsoft Excel. These calculations were completed for all twenty-seven study elements: in total 702 ratios were calculated for each data point collected. For each Bakken-Three Forks contact well 9,828 ratios were calculated. The total amount of ratios calculated for the Bakken-Three Forks contact group of wells was 88,452. A similar methodology was used for the Charlotte 1-22H well. The total number of ratios calculated for Charlotte 1-22H was 247,806. The total number of ratios calculated for this thesis was 336,258 ratios. The relative simplicity of the calculation is in large-part due to the ease of the calculation; the elemental fluorescence ratio calculation can best be described as simple division:

Elemental-Fluorescence Ratio: (5-11)

$$= \frac{XK\alpha}{YK\alpha} \ or \ \frac{XL\alpha}{YL\alpha} \ or \ \frac{XL_\beta}{YL_\beta}$$

where: X = The collected counts of the first element

Y = The collected counts of the second element

$K\alpha$ = $K\alpha$, $L\alpha$, or L_β fluorescence counts

Croudace and Rothwell (2006) suggest that fluorescence ratio of Sr:Ca is an effective indicator of relative porosity. To compare x-ray fluorescence porosity results with well-log porosity, this thesis will use density logs from Charlotte 1-22H. The bulk density (ρ_b) is considered to be the sum of the fluid density (ρ_f) times its volume (φ), plus the density of the rock matrix (ρ_{ma}) times its relative volume (1-φ). The value for the matrix density of quartz is

considered to be 2.65g/cc, the value for the matrix density of calcite is considered to be 2.71 g/cc, the value for the matrix density of dolomite is considered to be 2.87g/cc, and the density of anhydrite is considered to be 2.96g/cc (Myers, 2007). The equation for density-porosity:

Density-Porosity: (5-12)

$$\varphi = \frac{\rho_{ma} - \rho_b}{\rho_{ma} - \rho_f}$$

where: φ = Porosity of the matrix (%)

ρ_{ma} = Density of the rock matrix (g/cc)

ρ_b = Density measured from the well-log (g/cc)
ρ_f = Density of the fluid (g/cc)

For the sake of this thesis, the Sr:Ca Kα fluorescence raito will replace the rock-matrix density parameter (ρ_{ma}) from the Density-Porosity Equation. Because this thesis is examining core sections that are c dry, it is not necessary to include the fluid density parameter (ρ_f). This equation for x-ray Kα fluorescence Sr:Ca fluorescence will simplify to:

Sr:Ca Kα Fluorescence Porosity: (5-12)

$$\varphi = \frac{\frac{Sr}{Ca_{ma}} - \frac{Sr}{Ca_b}}{\frac{Sr}{Ca_{ma}}}$$

where: φ = Porosity of the matrix (%)

$\frac{Sr}{Ca_{ma}}$ = Average Sr:Ca Kα fluorescence ratio of the rock matrix (counts)

$\frac{Sr}{Ca_b}$ = Sr:Ca Kα fluorescence measured at depth (counts)

For the Sr:Ca fluorescence porosity problem to become experimentally viable, it is necessary to establish average Sr:Ca count values for siliclastic, calcite, dolomite, shale, and anhydrite lithology. During the course of this research, it was not possible to get standardized lithologic samples during the time x-ray fluorescence analytical equipment was available for use. For this reason Sr:Ca standard values will be averaged from the Lodgepole, Upper and Lower Bakken, Middle Bakken, and Three Forks Formation. The average Sr:Ca ratio in the Lodgepole was 0.19, in the Bakken Shale it was 1.55, in the Middle Bakken it was 0.45, and in the Three Forks it was 0.37. Based on these averages, this thesis will assume that shale contains a $\frac{Sr}{Ca}_{\text{ma}}$ of 1.55, calcite contains a $\frac{Sr}{Ca}_{\text{ma}}$ of 0.19, and dolomite has a $\frac{Sr}{Ca}_{\text{ma}}$ of 0.37.

CHAPTER VI

RESULTS

Elemental Fluorescence Ratios

For the Bakken-Three Forks Formation contact group of wells, the ratios of all nine wells across the contact were averaged. Decreasing and increasing ratio trends were observed throughout the study ratios. The ratios of Fe:S, Fe:Ca, Fe:Mn, Ni:Mn, Ni:Zr, Br:Cl, and S:Cl all recorded maximums within the Bakken Formation and minimums within the Three Forks Formation. The ratios of Ca:Mg, Ca:S, Ca:Ti, Ca:Zn, all recorded lows within the Bakken Formation and increased into the Three Forks Formation. The implication that the Three Forks Formation is a calcium bearing formation is widely supported by the literature (Nicolas 2006, 2007). Based on the initial results, it is obvious that the Bakken and Three Forks contact can be distinguished through the use of x-ray fluorescence ratios. For instance, without even looking at the core sections the contact of the Lower Bakken-Three Forks could easily be determined through the ratios of Fe:S, Fe:Ca, Fe:Mn, Ca:Mg, Ca:S, etc. Future x-ray fluorescence core analysis could be coupled with software such as LabVIEW into a user-friendly system that already has common contact ratio data; scans could be completed and the software could easily identify the formation for the user. The feasibility of using x-ray fluorescence for formation contacts is demonstrated with the following data.

79

Table 10. Nine Well Fluorescence Ratios for Bakken-Three Forks Contact. Ratio values were obtained from fluorescence analysis on cores listed in Table 9. Ratios were selected based on the diagenetic and geologic interpretations summarized by (Croudace and Rothwell, 2006).

Bakken-Three Forks Contact Selected Ratio Averages									
Unit	Depth, ft	Fe:S	Fe:Ca	Fe:Mn	Fe:Rb	Ni:Mn	Ni:Zr	Ni:Mo	Br:Cl
Bakken	7	68.34	31.08	103.69	36.63	2.39	0.34	0.67	1.54
Bakken	2	56.6	24.81	91.68	10.32	1.8	0.15	0.13	1.12
Bakken	1	56.14	23.29	86.83	12.53	1.31	0.15	0.12	1.17
Contact	0	32.21	8.01	48.49	7.62	0.9	0.07	0.09	0.75
Three Forks	-1	35.77	3.53	37.41	7.44	0.34	0.03	0.07	0.94
Three Forks	-2	34.19	3.2	37.49	13.89	0.27	0.04	0.08	0.75
Three Forks	-7	25.29	2.16	27.89	7.2	0.34	0.04	0.09	0.8
Unit	Depth, ft	S:Cl	K:Rb	Ca:Mg	Ca:S	Ca:Ti	Ca:Zn	Ca:Rb	Ti:Rb
Bakken	7	1.36	2.16	3.47	4.25	4.17	10.6	8.54	0.73
Bakken	2	0.85	0.68	3.16	3.19	3.59	10	1.59	0.31
Bakken	1	1.06	0.77	2.82	2.71	3.01	9.45	1.31	0.35
Contact	0	0.69	0.7	5.56	6.14	5.54	21.18	2.14	0.37
Three Forks	-1	0.49	0.64	11.27	13.08	9.99	34.97	2.94	0.3
Three Forks	-2	0.65	0.88	15.28	18.04	16.71	53.31	5.78	0.41
Three Forks	-7	0.68	1.03	17	18.51	18.1	62.19	7.45	0.48

Table 11. Fluorescence Ratios for Charlotte 1-22H Core. Ratios were selected based on the diagenetic and geologic interpretations summarized by (Croudace and Rothwell, 2006).

Charlotte 1-22H Selected Ratio Averages						
Ratio	Lodgepole	Upper Bakken	Middle Bakken	Lower Bakken	Pronghorn	Three Forks
Mg:Si	0.93	0.76	0.76	0.77	0.78	0.83
S:Cl	0.93	1.31	1.04	1.36	1.95	0.87
K:Rb	0.95	0.53	0.66	0.57	0.65	0.69
Ca:Mg	88.17	5.06	26.61	5.64	6.16	22.66
Ca:S	82.35	4.96	28.37	3.97	4.26	21.19
Ca:Ti	170.38	3.43	23.85	4.65	3.05	22.25
Ca:Zn	312.01	7.82	78.43	3.39	6.54	67.63
Ca:Rb	32.25	1.12	7.28	1.35	1.80	6.01

Table 11 Continued.

Ti:Rb	0.21	0.29	0.34	0.30	0.38	0.29
Fe:S	19.83	69.53	34.02	75.96	63.84	37.75
Fe:Ca	0.60	18.12	2.69	29.86	18.14	1.99
Fe:Mn	20.14	97.97	34.00	115.97	96.46	32.21
Fe:Rb	5.05	14.99	6.88	17.74	57.45	7.59
Ni:Mn	0.30	3.04	0.39	3.07	0.53	0.28
Ni:Zr	0.05	0.31	0.03	0.32	0.09	0.04
Ni:Mo	0.07	0.16	0.06	0.12	0.11	0.06
Br:Cl	1.08	2.12	1.82	1.98	1.56	1.62

When examining the average ratios obtained from analysis of the Charlotte 1-22H core, it becomes obvious that large scale formation identification is feasible using x-ray fluorescence. The ratios of Ca:Ti and Ca:Zn clearly identified the Lodgepole Formation and separate the Lodgepole Formation from any other formation in the stratigraphic interval. The value obtained in the Lodgepole for Ca:Ti was 170.38 compared to 3.43 in the Upper Bakken Member. The value obtained in the Lodgepole Formation for Ca:Zn was 313.01 compared to a low value of 7.82 in the Upper Bakken Member. Ratios that could be used to identify the Lodgepole Formation (through relative local highs) include Ca:Rb, Ca:Zn, and Ca:Ti, and Ca:Mg. Fluorescence ratios that outline the Upper and Lower Bakken Members include Fe:Mn, Fe:Rb, Fe:Mn, Ni:Mn, Fe:S and Ni:Mo. The Pronghorn Member is also identified through the previous ratios. Ratios that highlight the Three Forks Formation include Ca:Mg and Ca:Zn. Some may criticize that the same ratios that define the Lodgepole define the Three Forks Formation, but this will prove to not be a serious issue because additional ratios can separate the Three Forks and Lodgepole Formations. For instance, a primary Ca:Mg or Ca:Zn ratio can first identify the fact that the formation is carbonate rich; then a secondary Fe:S ratio of can be applied

to the lithologic analysis and show that the Three Forks Formation has a much higher

Fe:S ratio than the Lodgepole Formation.

Comparing the x-ray fluorescence data with the diagenetic implications listed by

Croudace and Rothwell (2006) important geologic interpretations become available. The

ratio of Fe:Ca is reported to be indicative of detrital clay and a good proxy for grain size

relationships. This diagenetic characterization is supported in this effort with the average

Bakken Fe:Ca ratio was calculated to be 31.08, and the average Three Forks Fe:Ca ratio

was 2.16. The Bakken Formation is a fine-grained shale whereas the Three Forks

Formation is a mixture of carbonate, sandstone, and thin member shale (Smith and

Bustin, 1995). The Sr:Ca ratio indicates the presence of aragonite carbonate, that is

indicative of a relative sea level drop. The Sr:Ca ratio is also suggestive of porosity,

higher values will have higher porosity. The average Sr:Ca ratio in the Bakken was

recorded at 1.074, the average Sr:Ca ratio in the Three Forks was recorded at 3.421. This

indicates that Three Forks deposition occurred in a shallow marine environment; a

relative sea level rise occurred between Three Forks and Bakken deposition. Whether the

Bakken is interpreted as a deep water marine environment or a de-oxygenated shallow

marine environment, all literature agrees that Bakken deposition occurred in a deeper

water column than Three Forks deposition (LeFever et al., 1991; Smith and Bustin, 1995;

Nicolas, 2006). The Sr:Ca ratios also outline the higher porosity values in the Three

Forks than the Bakken. The K:Rb ratio is similar to the Fe:Ca ratios for the

determination of detrital clay, once again the Bakken recorded an average K:Rb value

2.164 compared with the Three Forks Formation that contained a ratio of 0.642. Both the

Ti:Rb and Zr:Rb ratio highlights the notion that highly resistive minerals will commonly

be found in association with heavier elements such as Iron, Nickel, Molybdenum, etc.

The Zr:Rb ratio shows a value of 1.581 in the Bakken and a value of 3.419 in the Three

Forks. These values do not appear to correlate with the fact that the Bakken Formation

has a higher concentration of metallic minerals than the Three Forks Formation

(Meissner, 1984). However, both the Ti:Rb and Zr:Rb ratios are based on turbidite muds;

if the Bakken Formation was truly deposited in a 200 meter standing water column

(Smith and Bustin, 1996), turbidite flow would have been impossible during Bakken

deposition.

Table 12. Geologic Fluorescence Interpretations-Bakken and Three Forks Contact. Interpretations are based on the fluorescence ratio empirical analysis conducted in previous geologic core analysis (Croudace and Rothwell, 2006).

Diagenetic and Geologic Interpretations-Bakken and Three Forks Contact Wells			
XRF Ratio	Geologic and Diagenetic Interpretations (Croudace, 2006)	Bakken	Three Forks
Fe:Ca	Indicative of detrital clay: biogenic carbonate ratio.	31.08	2.16
Fe:Ca	Good proxy for grain size relationships.	-	-
Sr:Ca	Higher Strontium can indicate the presence of Aragonite, indicating relative sea level drop.	1.074	3.421
Sr:Ca	Value may increase when sediment porosity increases, grain size also effects value.	-	-
K:Rb	Potassium is commonly associated with detrital clay, enhanced in turbidite muds.	2.164	0.642
Zr:Rb	Zirconium concentration is higher in heavy resistate minerals, enhanced in turbidite muds.	1.581	3.419
Ti:Rb	Titanium concentration is higher in heavy resistate minerals, enchanced in turbidite muds.	0.729	0.482
Si	May be useful as a sediment-source/provenance indicator.	1377 Kα	420 Kα
Fe:Rb	Iron mobilized during redox-related deposition and diagenesis.	36.629	7.201
Fe:Ti	Iron mobilized during redox-related deposition and diagenesis.	56.775	19.263
Mn:Ti	Good indicator of redox-related diagenesis.	0.536	0.779
Br:Cl	High ratios of Bromine can indicate organic-rich layers. (Br and S are rich in organic sediments).	1.535	0.804
S:Cl	High ratios of Sulfur can indicate organic-rich layers. (Br and S are rich in organic sediments).	1.364	0.686

Silica counts can be useful as a sediment-source and provenance indicator without computing any ratios. The average Silica counts in the Bakken Formation was 1,377. The average silica counts in the Three Forks Formation was 420; this is indicative of sediment source changes. Numerous authors that support shallow water Bakken-deposotion (LeFever et al., 1991) may be able to use the Si count rate to support regional tectonic events associated with the Larimide Orogeny. The ratio of Fe:Rb and Fe:Ti show iron mobilization during redox-related deposition and diagenesis. The Fe:Rb and Fe:Ti ratios in the Bakken were both substantially higher than in the Three Forks Formation; this indication seems to support the hypothesis that the Bakken Formation was deposited in highly oxygenated conditions (Meissner, 1984; Lefever et al., 1991, Smith and Bustin, 1995). Regardless of the water column depth, the Bakken was obviously deposited in conditions with no oxygen. This is further supported using the Ratio of S:Cl, sulfur becomes present in the form of hydrogen sulfide in anoxic conditions; The ratio of S:Cl in the Bakken Formation was recorded at 1.364 whereas the S:Cl ratio in the Three Forks was recorded at 0.686. Because the deposition of the Lower Bakken and Three Forks occurred adjacently in geologic time, the amount of chlorine in sea-water should have been relatively uniform between the Late Devonian and Early Mississippian (Lineback and Davidson, 1982). The fact that the sulfur concentration increased dramatically from the Bakken into the Three Forks tells us that Hydrogen Sulfide deposited within the Bakken formation likely came from anoxic conditions associated with the overall depth of the water column instead of seepage from the underlying Three Forks Formation. Numerous papers such as (Meissner, 1984) suggest that pyrite disassociated in the Bakken and seeped into the Three Forks Formation. One of the huge issues with this

interpretation is the overall heat of reaction needed for pyrite to dissociate into hydrogen

sulfide, H_2S. (Schwab and Philinis, 1947) showed that pyrite disassociation reactions

require a heat of 500C and also produce FeO, Fe3O4, Fe_2O_3, and SO_4. . Sulfate and

oxygen will destroy kerogen and henceforth the oil produced in the Bakken Formation

never would have reached thermal maturity. The fact that the ratio of S:Cl in the Bakken

Formation was higher than the Three Forks Formation supports the hypothesis that

hydrogen sulfide was deposited in the Bakken due to autonomous depositional processes

rather than underlying seepage.

When applying the Croudace and Rothwell (2006) x-ray fluorescence ratios from

the Charlotte 1-22H core section, many of the results from the Bakken-Three Forks

contact wells are verified. The Fe:Ca ratio (indicative of detrital clay) displays low

values in the Lodgepole, Middle Bakken Member, and Three Forks Formations. This

result is expected because the Lodgepole is universally established as a carbonate

formation, the Middle Bakken Member is widely regarded as a mixed siliclastic,

carbonate, and sandstone unit, and the Three Forks Formation is widely interpreted as a

mixed carbonate dolomite formation with intermixed beds of shale. Most interestingly,

the pure carbonate Lodgepole Formation shows the lowest ratio of Fe:Ca. The Sr:Ca ratio

(indicative of relative sea level) was recorded at 0.19 in the Lodgepole Formation, 1.41 in

the Upper Bakken Member, 0.45 in the Middle Bakken Member, 1.69 in the Lower

Bakken Member, 1.41 in the Pronghorn Member, and 0.37 in the Three Forks Formation.

These results are uniform with not only the established geologic literature, but also the

commonly accepted depositional conditions needed for different types of lithology. The

Lodgepole Formation was deposited in a shallow marine environment, the Upper, Lower,

and Pronghorn Members of the Bakken Formation were deposited in a high standing and anoxic water column, and the Three Forks Formation and Middle Bakken Members were deposited in a water column in between the depth of shale and carbonate deposition. These results appear to be uniform with the results from (Meissner, 1984; LeFever et al., 1991; Smith and Bustin, 1995 & 1996, and Nicolas, 2006). The ratio of K:Rb once again is supposed to be a proxy for detrital clay; once again this result appears to be more of an indication of turbidity in the water column rather than detrital clay content. The Lodgepole Formation, Three Forks Formation, and Middle Bakken member averages of K:Rb ratios all showed higher values than the Lower, Upper, and Bakken Members. Once again, the deep water Bakken deposition would not allow for turbidite flow, supporting the results found in this research. The ratios of S:Cl in the stratigraphic interval encompassing the Lodgepole, Bakken, and Three Forks Formations also shows that the Upper and Lower Bakken members contained the highest ratios of S:Cl in the study; this once again leads credence to the fact that the Bakken was deposited in a deep water column that was highly anoxic, allowing for the existence of hydrogen sulfide in the water column. Overall, the results from the elemental fluorescence ratios portion of this thesis clearly show that large scale formations can be identified and separated through the use of elemental fluorescence ratios.

Table 13. Diagenetic and geologic fluorescence interpretations-Charlotte 1-22H. Interpretations are based on the fluorescence ratio empirical analysis conducted in previous geologic core analysis (Croudace and Rothwell, 2006).

Diagenetic and Geologic Intepretations Compared With Charlotte-1-22H								
XRF Ratio	Geologic and Diagenetic Interpretations (Croudace, 2006)	LP	UB	MB	LB	PH	TF	Ratio
Fe:Ca	Indicative of detrital clay: biogenic carbonate ratio.	0.60	18.82	2.08	30.35	14.76	1.97	Fe:Ca

Table 13 Continued.

Fe:Ca	Good proxy for grain size relationships.	-	-	-	-	-	-	Fe:Ca
Sr:Ca	Higher Strontium can indicate the presence of Aragonite, indicating relative sea level drop.	0.19	1.41	0.45	1.69	1.41	0.37	Sr:Ca
Sr:Ca	Value may increase when sediment porosity increases, grain size also effects value.	-	-	-	-	-	-	Sr:Ca
K:Rb	Potassium is commonly associated with detrital clay, enhanced in turbidite muds.	0.95	0.52	0.66	0.56	0.61	0.69	K:Rb
Zr:Rb	Zirconium concentration is higher in heavy resistate minerals, enhanced in turbidite muds.	1.71	1.32	2.95	1.12	1.11	1.99	Zr:Rb
Ti:Rb	Titanium concentration is higher in heavy resistate minerals, enhanced in turbidite muds.	0.21	0.30	0.34	0.30	0.27	0.29	Ti:Rb
Fe:Rb	Iron mobilized during redox-related diagenesis (seen in oxic, or formerly oxic sediment).	5.05	15.31	6.54	17.90	7.48	7.67	Fe:Rb
Fe:Ti	Iron mobilized during redox-related diagenesis (seen in oxic, or formerly oxic sediment).	23	49.07	19.84	60.54	27.76	26.6	Fe:Ti
Mn:Ti	Lower value is good indicator of redox-related diagenesis.	1.97	0.48	0.72	0.49	0.36	1.02	Mn:Ti
Br:Cl	High ratios of Bromine can indicate organic-rich layers. (Br and S are rich in organic sediments).	1.08	2.13	1.81	2.0	1.65	1.6	Br:Cl
S:Cl	High ratios of Sulfur can indicate organic-rich layers. (Br and S are rich in organic sediments.	0.93	1.31	1.04	1.37	0.84	0.87	S:Cl

Well-Log Interpretations

X-ray fluorescence well-logs were created for thirteen Kα fluorescence ratios

(Appendix A) representing the Charlotte 1-22H core section. Although 702 ratios were

calculated over the course of this thesis, only the 13 ratios with significant variability

were chosen for graphical representation. Ratios that highlighted the Upper Bakken

Member, Lower Bakken Member, and Pronghorn Member of the Bakken Formation were

chosen to show that precise XRF can precisely outline thick shale regions. The XRF ratios that highlighted the Bakken Shale Members included Fe:Ca, Fe:Mn, Fe:S, Ni:Mo, Ni:Mn, Sr:Ca, and S:Cl. Ratios that highlighted the Lodgepole Formation, Three Forks Formation, and the Middle Bakken Member were chosen to show that different XRF ratios can be used to highlight other lithological units besides shale. The ratios that highlighted the Lodgepole Formation, Middle Bakken Member and Three Forks Formations included Ca:Ti, Ca:Mg, Ca:Zn, and Ca:Rb.

The ratio of Fe:Mn clearly outlined the Upper and Lower Shale Members of the Bakken Formation. The Lower Bakken Member recorded a higher Fe:Mn value than the Upper Bakken Member; a consistent pattern found throughout the analysis of the Charlotte 1-22H analysis was the fact that the Lower Bakken Member continuously provides higher indications of more organic rich shale. Gamma ray values, x-ray fluorescence values representing organic characteristics, and organic carbon contents were all greater in the Lower Bakken Member.

To answer the question of whether x-ray fluorescence can more accurately predict formation contacts than conventional well-logging methods, the comparisons were made between gamma and the elemental fluorescence ratios of Fe:Mn and Fe:S. The gamma values recorded at the Middle Bakken contact was 541.49 API. The Fe:Mn and Fe:S ratios were 142.99 and 103.16 respectively. One-foot into the Middle Bakken Member, the gamma value recorded was 570.69; the fluorescence ratios dropped to 49.09 (Fe:Mn) and 43.98 (Fe:S). As the depth into the Middle Bakken increases, both fluorescence ratios and the gamma ray values dropped; the gamma value five feet into the Middle Bakken Member increased to 632.60 API. It requires approximately 8 feet of depth into

the Middle Bakken Formation for the gamma values to drop below 100 API; due to the

high gamma values 8 feet into the Middle Bakken Member, it would be easy to mistake

the siliclastic middle Middle Member of the Bakken formation for the Upper Bakken

Member. The Kα fluorescence ratios of Fe:Mn and Fe:S provide superior contact

recognition. After one-foot into the shale the fluorescence ratios dropped and never

exceeded the fluorescence values at the contact. This leads to the interpretation that

fluorescence ratios are more adequate for recognizing large scale formation changes than

gamma methods. When analyzing the Fe:Mn and Fe:S ratios in the Middle Bakken

Formation, it becomes possible to map and identify smaller scale lithofacies.

Table 14. Gamma-Ray and Kα Fluorescence Ratios in the Middle Bakken Member. This table
shows the abrupt change in fluorescence values at the contact between the Upper Bakken
Member and the Middle Bakken Member. Gamma ray has a less abrupt shift.

Depth Above Contact (ft)	Fe:Mn (Kα)	Fe:S (Kα)	Gamma (API)
4	67.31	28.74	388.76
3	92.69	60.88	430.72
2	57.08	24.47	446.26
1	96.15	63.72	497.54
Contact	142.99	103.16	541.49
Depth Below Upper Shale (ft)	Fe:Mn (Kα)	Fe:S (Kα)	Gamma (API)
0	49.09	43.98	570.69
-1	29.75	33.85	486.79
-2	27.52	31.26	410.32
-3	20.37	22.66	443.09
-4	24.02	38.12	525.25
-5	15.99	22.07	632.60
-6	23.15	29.86	370.06
-7	30.40	33.62	140.07
-8	11.93	9.73	86.33
-9	22.00	20.02	65.53
-10	9.90	6.81	71.30
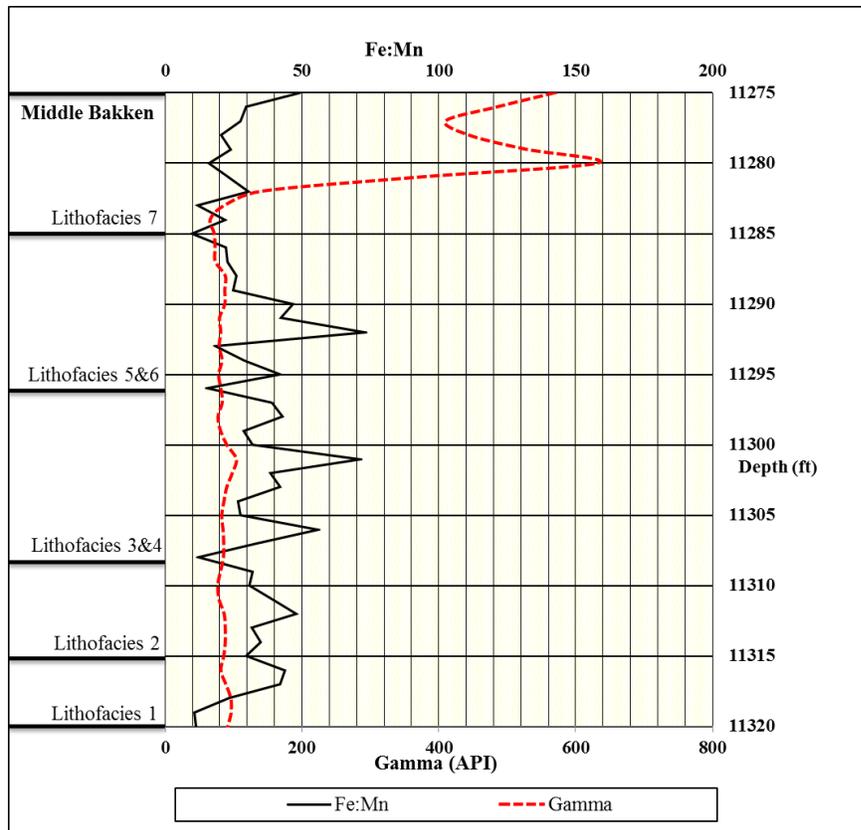
Figure 9. Fe:Mn Kα Fluorescence Ratio in the Middle Bakken Member. Notice that the Gamma ray log still records an API value of 600 five feet out of the Upper Shale.

LeFever et al. (1991) describes lithofacies 7 of the Middle Bakken Member as siltstone, massive, dense, and dolomitic with disseminated pyrite. Based on the Fe:S fluorescence log we see peaks of higher Fe:S ratios, that is likely indicative of the pyrite dissemination. One of the most interesting ratios for examining the Middle Bakken Member is the Fe:Mn ratio in lithofacies 5&6 at a depth of approximately 11,285′ to 11,297′. The Fe:Mn ratio peaks dramatically within lithofacies 5&6, indicating the presence of shale. The LeFever et al. (1991) description for lithofacies 5&6 includes the description of parallel interbeds of dark gray shale. The Fe:Mn ratio in lithofacies 5&6 peaks and parallels the previous geologic descriptions. Observation shows that the

90

Fe:Mn ratio in lithofacies 1,2,3, and 4 remain high on the Fe:Mn log; this could be due to the presence of extensive pyrite. This leads to the conclusion that although certain fluorescence ratios can indicate large scale formation changes, more precise lithofacies analysis may be require the use of multiple logs.
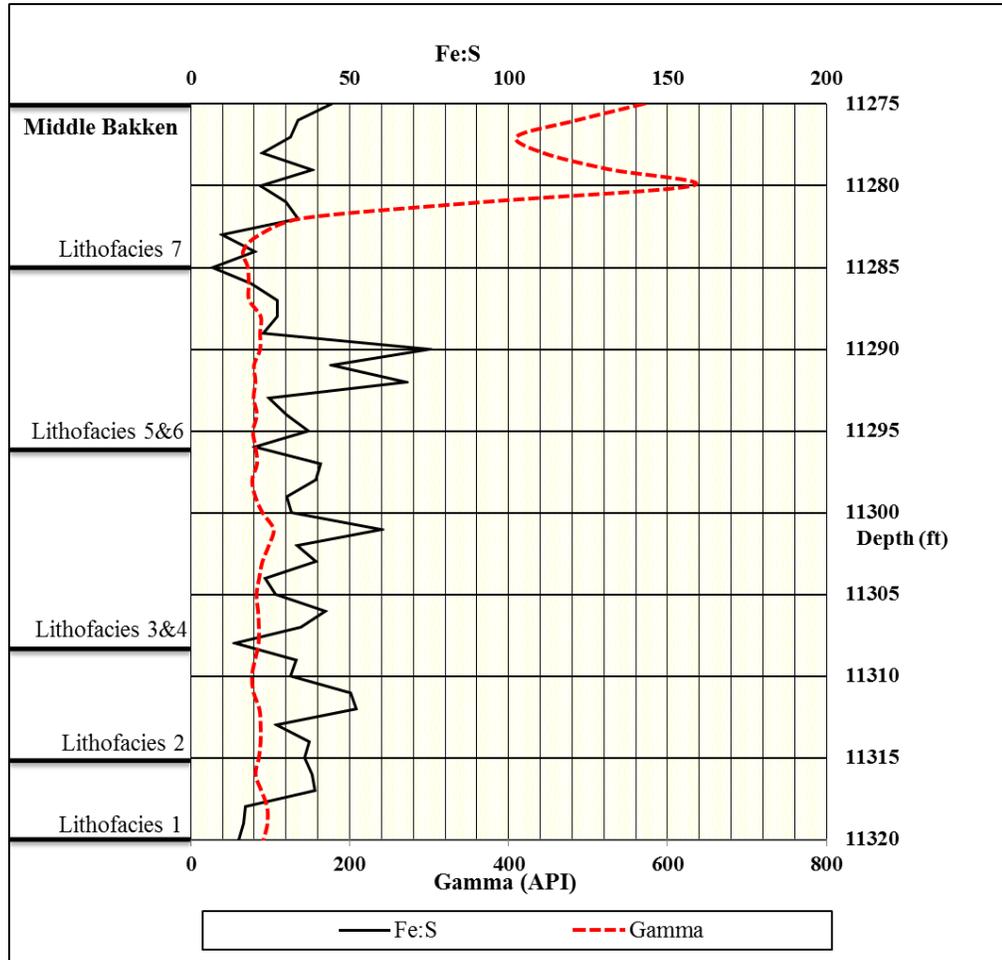
Figure 10. Fe:S Kα Fluorescence Ratio in the Middle Bakken Member. Notice that the Gamma ray log still records an API value of 600 five feet out of the Upper Shale.

The first mathematical analysis completed involved shale volume calculations based on the wireline and LWD gamma logs. Furthermore, shale volume calculations were completed for x-ray fluorescence ratios. Shale volumes for Charlotte 1-22H were

91

calculated using the Clavier Method, the Steiber Method, and finally the Larionov

(Older) Method. The Larionov (Older) Method was selected because the formations in

the study are Mississippian-Devonian aged; this interval dates back to approximately 320

million years before present. Based on Shale Volume calculations produced by Baker

Hughes (2003) the numerical calculation of shale volume should follow the following

trend (smallest to largest volume): Steiber, Clevier, and Larionov. The gamma ray-

values were averaged for each formation in the study area for both the wireline and LWD

logs; then the calculations were performed using the following equations.

Table 15. Charlotte 1-22H LWD Shale Volume Calculations.

3/14/2011 @ 00:31							
Formation/Member	GR	GR Clean	GR Shale	IGR	Clavier	Steiber	Larionov Older
Lodgepole	52.71	43.52	726.89	0.013	0.006	0.005	0.006
Upper Bakken	230.07	43.52	726.89	0.273	0.140	0.111	0.152
Middle Bakken	156.67	43.52	726.89	0.166	0.078	0.062	0.085
Lower Bakken	547.60	43.52	726.89	0.738	0.554	0.484	0.588
Pronghorn	299.81	43.52	726.89	0.375	0.209	0.167	0.225
Three Forks	89.69	43.52	726.89	0.068	0.029	0.024	0.032
3/14/2011 @ 22:28							
Formation/Member	GR	GR Clean	GR Shale	IGR	Clavier	Steiber	Larionov Older
Lodgepole	56.16	46.76	759.23	0.013	0.005	0.004	0.006
Upper Bakken	216.08	46.76	759.23	0.238	0.119	0.094	0.129
Middle Bakken	168.16	46.76	759.23	0.170	0.081	0.064	0.088
Lower Bakken	536.71	46.76	759.23	0.688	0.494	0.423	0.526
Pronghorn	284.12	46.76	759.23	0.499	0.307	0.249	0.329
Three Forks	93.90	46.76	759.23	0.066	0.029	0.023	0.032
GR shale values were averaged from the Lower Bakken, GR clean values were averaged from the Lodgepole Formation							

Based on the results seen in Table 15, all shale volume values calculated show

that the Steiber Method predicted the lowest shale volume, the Clavier Method predicted

the second lowest shale value, and finally the Larionov (older) Method predicted the

highest shale volume. These results were expected based on Baker Hughes (2003). The

calculations showed the highest shale volume in the Lower Bakken and the lowest shale

volume in the Lodgepole Formation. Based on the results from Table 16, LWD gamma

values compared more favorably with core gamma values than the wireline gamma.

Although the LWD value is slightly closer to the core gamma value, the values are still

uniform; neither log would provide a distinct advantage for industrial applications.

Table 16. Charlotte 1-22H Wireline Shale Volume Calculations.

Measurement Rank			Percent Difference Between Wireline and LWD Measurements (%)				
Steiber Rank	Clavier Rank	Larionov Rank	GR	IGR	Clavier	Steiber	Larionov(Older)
Lowest	Middle	Highest	6.14	1.83	1.85	1.85	1.85
Lowest	Middle	Highest	6.48	14.87	18.12	18.18	17.89
Lowest	Middle	Highest	6.83	2.83	3.20	3.18	3.16
Lowest	Middle	Highest	2.03	7.27	12.15	14.30	11.67
Lowest	Middle	Highest	5.52	24.89	31.96	33.18	31.68
Lowest	Middle	Highest	4.48	2.10	2.22	2.20	2.20
Measurement Rank			Percent Difference Between LWD and Wireline Measurements (%)				
Steiber Rank	Clavier Rank	Larionov Rank	GR	IGR	Clavier	Steiber	Larionov(Older)
Lowest	Middle	Highest	6.55	1.80	1.82	1.82	1.82
Lowest	Middle	Highest	6.08	12.94	15.34	15.38	15.17
Lowest	Middle	Highest	7.33	2.91	3.30	3.28	3.26
Lowest	Middle	Highest	1.99	6.77	10.83	12.51	10.45
Lowest	Middle	Highest	5.23	33.13	46.96	49.66	46.37
Lowest	Middle	Highest	4.69	2.06	2.17	2.16	2.16

The XRF shale volume, sandstone volume, and carbonate volume equations were

applied to the entire Charlotte 1-22H core sequence. The Ni:Mn shale parameter was

averaged between the Upper and Lower Bakken Members, the Ni:Mn carbonate

parameter was averaged in the Lodgepole Formation. The Ca:Mg Carbonate parameter

was averaged in the Lodgepole Formation, the Ca:Mg Sandstone parameter was averaged

in the Middle Bakken Formation. The Si:Ca Carbonate parameter was averaged in the

Lodgepole Formation, the Si:Ca Sandstone parameter was averaged in the Middle

Bakken Formation.

Table 17. Charlotte 1-22H Wireline and LWD Gamma-Ray Compared with Core Gamma.

LWD/MWD		Wireline		Core Gamma		% Difference Between Core Gamma and Logging Gamma (API)	
Formation	GR	Formation	GR	Formation	GR	LWD	Wireline 1
Lodgepole	52.71	Lodgepole	56.16	Lodgepole	38.53	36.81	45.76
Upper Bakken	230.07	Upper Bakken	216.08	Upper Bakken	265.80	13.44	18.71
Middle Bakken	156.67	Middle Bakken	168.16	Middle Bakken	136.70	14.61	23.01
Lower Bakken	547.60	Lower Bakken	536.71	Lower Bakken	431.90	26.79	24.27
Pronghorn	299.81	Pronghorn	284.12	Pronghorn	276.70	8.35	2.68
Three Forks	89.69	Three Forks	93.90	Three Forks	58.10	54.38	61.62
LWD Compares More Favorably With Core Gamma				Average		25.73	29.34

The results show that the x-ray fluorescence shale volume calculation accurately

identifies the Upper and Lower Shale as shale rich members; shale volumes in the Three

Forks and Middle Bakken also appear to embody the descriptions of interbedded shale.

The carbonate volume calculations show the Lodgepole Formation as almost entirely

carbonate rich; the value in the Three Forks Formation appears far too low. Perhaps the

carbonate volume equation should be re-labeled as the calcite-carbonate volume

equation; a new ratio may be necessary to highlight dolomite-carbonate. The sandstone

volume equation shows a high level of sandstone within the Middle Bakken and Three

Forks Formation; lower values are seen in the Upper and Lower Bakken Members.

Table 18. X-Ray Fluorescence Shale Volume Calculations.

Formation	Vss (%)	Vca (%)	Vsh(%)	Input Parameters (Kα Counts)			
Lodgepole	0.02	95.51	0.08	Ni:Mn Shale	3.05	Ni:Mn Carbonate	0.30
Upper Bakken	5.35	0.01	98.97				
Middle Bakken	82.78	0.79	1.43	Ca:Mg Sandstone	26.61	Ca:Fe Carbonate	88.17
Lower Bakken	6.04	0.03	99.74				
Pronghorn	41.7	0.04	9.69	Si:Ca Sandstone	0.09	Si:Ca Carbonate	0.02
Three Forks	25.17	0.73	0.91				

When comparing the x-ray fluorescence and gamma shale volume calculations, it becomes apparent that the x-ray fluorescence shale volume calculation can more adequately outline the amount of shale within the Upper and Lower Bakken Members. All three LWD/Wireline shale volume calculations grossly underestimate the amount of shale within the Upper and Lower shale; this underestimation may be because the vertical resolution of the gamma ray log records values at greater depths away from the shale. This would mean that overlying and underlying carbonate formations are included into the shale volume calculation. The data shows that using x-ray fluorescence shale volume calculations is a more precise method of determining the lithology volume composition.

The next comparison between the LWD and wireline logs for Charlotte 1-22H was completed using resistivity measurements. Both the AT90 (two-foot vertical resolution, 90″ diameter into the formation) and the AT10 (two-foot vertical resolution, 10″ diameter into the formation) logs were compared. The goal was to compare the uninvaded resistivity with the invaded zone resistivity. When comparing the resistivity measurements for the LWD and wireline logs, the most interesting aspect to analyze is the large gains in resistivity seen between the LWD and wireline logs on the 10″ diameter invaded zone resistivity (figure 10). This large shift shows that when the well was initially drilled, the resistivity at that value was higher than the mud being used. After

time had passed and the borehole conditions approached equilibrium, the wireline value

increased dramatically in the Upper Bakken Member. The initial interpretation is that

hydrocarbons from the formation fluid (deep resistivity) flowed into the uninvaded zone

and caused a subsequent increase in the total value. This observation was recorded at a

depth of 11, 278′ and can also be seen on the deep induction resistivity log. The deep

resistivity (90″ diameter) showed higher values in the shale, especially in the Upper

Bakken.
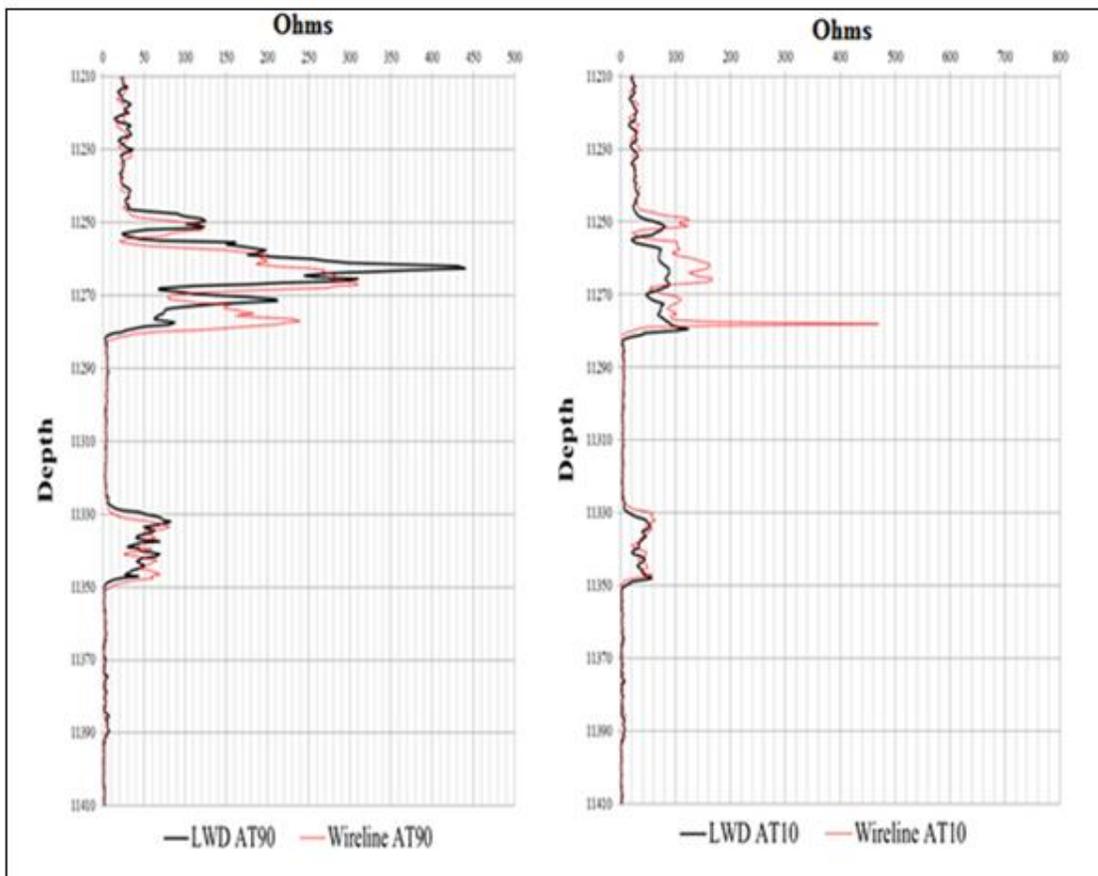
Figure 11. Charlotte 1-22H LWD and Wireline AT90 and AT10 Resistivity.

Additional analysis completed for Charlotte 1-22H included calculations of the

apparent waster resistivity (Rwa) and the water resistivity (Rw) for both the wireline and

the LWD measurements. The theory behind Rwa and Rw calculations is that, when

comparing the values in areas saturated with hydrocarbons, Rwa should be greater

than Rw. To calculate these values the neutron-density average porosity was multiplied

by first the true resistivity of the formation and then by the invaded zone resistivity. The

Rt values were taken from the AF90 log and the Ro values were obtained from the AF10

log. The same methodology was repeated for both the wireline and the LWD logs. For

the resistivity LWD and wireline measurements recorded in the Charlotte 1-22H well,

physics and interpretations should be further discussed. The following discussion is

based on the theory of which fluids should have the greatest resistivity in a geologic

environment. Hydrocarbons should have the highest resistivity and lowest conductivity,

freshwater should have a higher resistivity and lower conductivity than saltwater, and

finally saltwater should have the lowest resistivity and highest conductivity out of the

three most common fluids in a geologic environment. In freshwater muds where the

resistivity of the mud filtrate is greater than the resistivity of the formation water

($Rmf > Rw$), the resistivity of the invaded zone should be highest in the flushed zone,

decrease into the transition/annulus zone, and then decrease into the uninvaded zone. In

saltwater muds where the resistivity of the mud filtrate is equal to or slightly less than the

resistivity of the formation water ($Rmf \sim Rw$), the resistivity of the invaded zone,

transition zone, and uninvaded zone should be approximately equal. For this study, the

following assumptions are used:

 If the entire study area ($11,210' - 11,410'$) is assumed to be only water bearing, and

the drilling mud is assumed to be freshwater, then AF10 and AT10 should be greater than

AF90 and AT90. If the entire study area (11,210′–11,410′) is assumed to be only water bearing, and the drilling mud is assumed to be saltwater, then AF10 and AT10 should be approximately equal to AT10 and AF90. If the entire study area (11,210′–11,410′) is assumed to be hydrocarbon bearing, and the drilling mud is assumed to be fresh water, then AF10 and AT10 should be only slightly greater than AF90 and AT90. If the entire study area (11,210′–11,410′) is assumed to be hydrocarbon bearing, and the drilling mud is assumed to be saltwater, then AF10 and AT10 should be less than AT90 and AF90. In the study area at the depths of 11,210′–11,240′ both the wireline log and the LWD log show about equal values between AT10 and AT90. This leads to the assumption that the study area from 11,210′–11,240′ is water bearing.
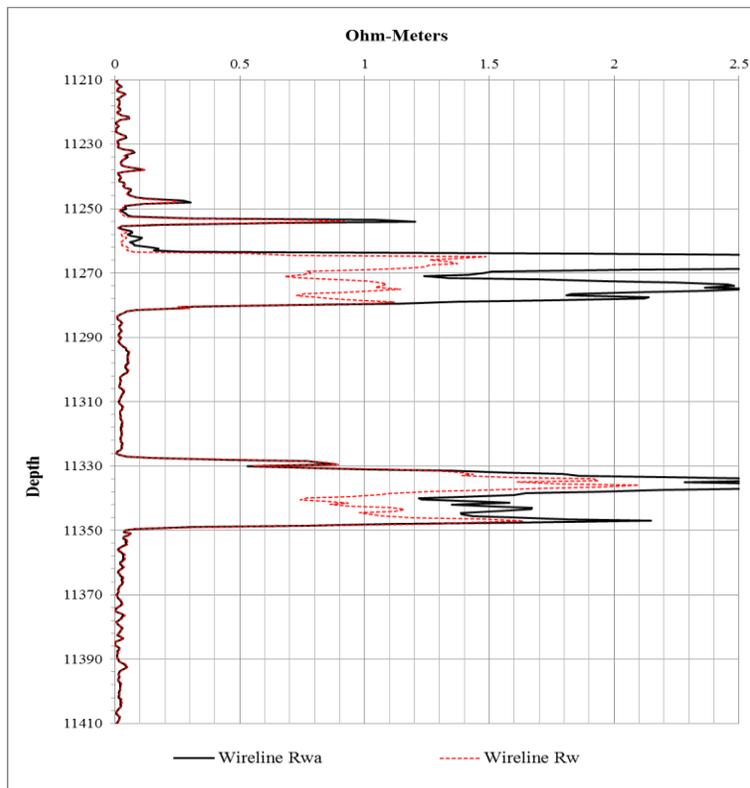
Figure 12. Charlotte 1-22H *Rwa* and *Rw* wireline log water saturation. The Bakken Formation displays *Rwa*>*Rw* value, indicating hydrocarbon saturation.

In the study area at the depths of 11,240′–11,255′ the resistivity of the LWD AT90 is greater than the resistivity of the LWD AT10. On the wireline log, the value of the AT10 and the AT90 are approximately equal. This means that during the LWD logging, the formation would be interpreted as hydrocarbon bearing because AT90>AT10; however during wireline logging these values became approximately equivalent. This could mean that if only the wireline log was used, a potential reservoir could be missed. In the study area at the depths of 11,255′–11,275′ the value of the wireline and LWD AT90 are both much greater than the values of the LWD and Wireline AT10. This would lead to the assumption that this portion of the study area is hydrocarbon bearing. In the study area at the depths of 11,330′–11,350′ the LWD and wireline AT90 values are both greater than the LWD and wireline AT10 values; indicating a hydrocarbon bearing unit. This area on the log corresponds to the Lower Bakken Member, which makes sense because the Upper Bakken Member and the Lower Bakken Member are notoriously recorded as being hydrocarbon saturated.

The Quicklook method is commonly used in industrial well-logging applications to assess the lithology of the formation being drilled. This method was completed on the Charlotte 1-22H core section using LWD data; this process could not be performed on the wireline log because data was not present. On the wireline PE log a consistent value of 10 was recorded the entire length of the formation, leading to the interpretation that the tool was not working while other recording was occurring. To perform the Quicklook calculations using the LWD data, points were measured at each formation contact depth within the stratigraphic interval. The neutron porosity, density porosity, and PE values were recorded to ascertain the lithology.

Table 19. Quicklook Method Charlotte 1-22H LWD. The lithology indicated by each calculation matched the descriptions of (LeFever, 1991).

Formation	Depth	PE	Nphi	Dphi	Lithology
Lodgepole	11230	5.2	.025	.007	Limestone
Upper Bakken	11270	3.4	.313	.253	Shale
Middle Bakken	11310	3.8	.075	.05	Limestone
Lower Bakken	11335	3.6	.316	.238	Shale
Pronghorn	11348	3.8	.281	.234	Shale/Dolomite
Three Forks	11370	3.6	.108	.017	Dolomite
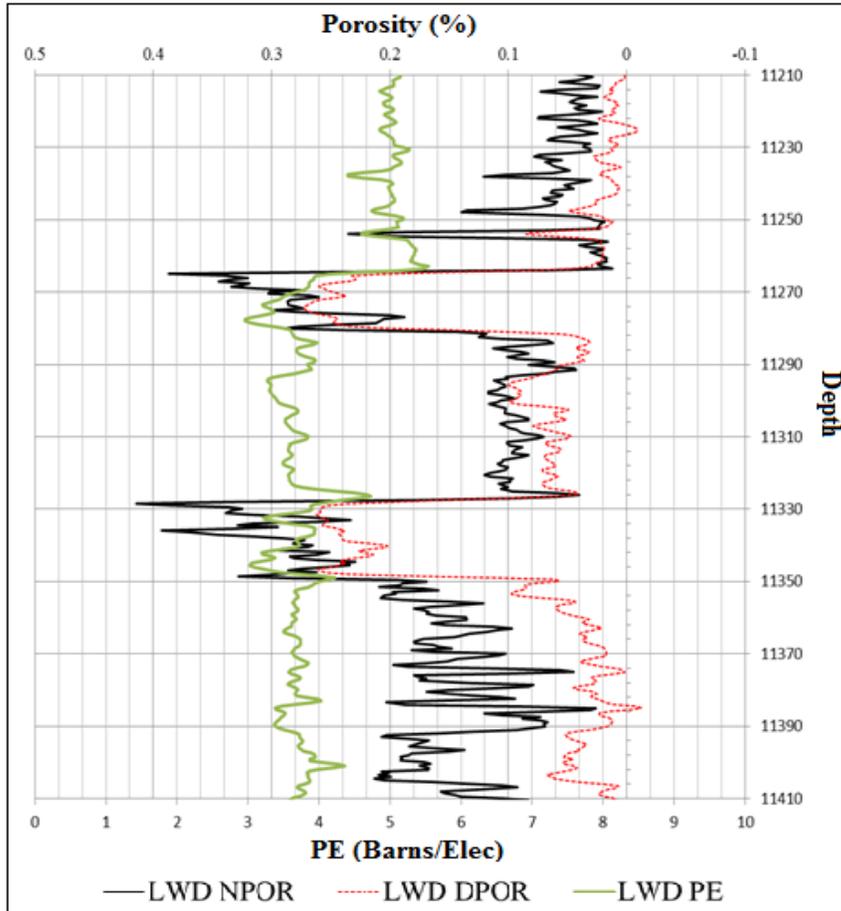
Figure 13. Quicklook Method Charlotte 1-22H LWD. The lithology indicated by each calculation matched the descriptions of (LeFever et al., 1991).

100

Rock Mass Interpretations

Rock Quality Designation (RQD) is a useful index for the description of rock mass fractured state. RQD was initially introduced for tunneling engineering applications; it has since been adopted in mining, engineering geology, and geotechnical engineering. Rock-quality designation (RQD) is the measure of the degree of jointing or fractures within the rock mass. RWD is equal to the sum of the length of core sections greater than 3.93″ divided by the total length of the core run (Wangwe, 2013). This value is measured as a percentage. High-quality rock has an RQD of more than 75%, low quality rock will have an RQD of less than 50%. Lo et al. (2001) describe the strength relationships between silica content, Moh's Hardness Scale, and relative density; higher quartz content leads to choncoidal fracture that requires greater forces for fracture. If silica Kα fluorescence could help determine zones of weaker rock mass, drill cuttings could theoretically be used to determine the rock mass strength down bore. This could lead to improved hydraulic fracturing design; weak rock masses could be identified and fractured.

This thesis analyzed whether silica fluorescence can provide a rock mass correlation with the RQD parameter. For the sake of this thesis RQD was completed for the Lodgepole, Bakken, and Three Forks Formations in the Charlotte 1-22H core sequence. Each core section greater than 3.93″ was measured to the nearest sixteenth of an inch; the lengths were summed and compared with the average silica Kα fluorescence values from each formation. These lengths were then divided by the total core length of the core run; the values were converted to percent and compared with the silica fluorescence values.

101

Using this thesis data, no correlation could be established between Charlotte 1-22H core RQD and silica Kα fluorescence. For instance, the Lower Bakken Member RQD was higher than the Lodgepole Formation RQD (12.79% versus 9.78% respectively), yet the silica Kα counts were higher in the Lodgepole Formation. This is in contrast to the relationship between the Lodgepole and the Upper Bakken RQD and silica Kα values. These results lead to the interpretation that no distinguishable correlation could be established between rock quality designation and silica Kα fluorescence.

The interpretation that no distinguishable correlation can be established between rock quality designation and silica Kα fluorescence was based on data collected in this thesis. One important consideration is that the RQD values were obtained from core that had been drilled, cleaned, transported, and handled frequently in a laboratory setting. Due to the brittleness of the rock mass, it is difficult to determine which fractures have been created naturally and which fractures have been created mechanically. Due to the fact that the Charlotte 1-22H core section has been analyzed for over two years before this thesis research, it is likely that the RQD values are unreliable. For this analysis to be properly conducted, it would be necessary to obtain RQD measurements immediately after the core sections had been drilled.

Table 20. Silica Kα fluorescence versus Rock Quality Designation (RQD). No identifiable correlation could be established between formation silica fluorescence and RQD.

Formation/Member	Total Core Run	∑ RQD Length	∑ RQD Length	RQD	Average SiKα
Units	(feet)	(inches)	(feet)	(%)	(counts)
Lodgepole	48	56.31	4.69	9.78	265.08
Upper Bakken	17	27.38	2.28	13.42	394.12
Middle Bakken	48	67.88	5.66	11.78	295.74
Lower Bakken	23	35.31	2.94	12.79	220.98
Pronghorn	8	8.19	0.68	8.53	281.20
Three Forks	56	45.94	3.83	6.84	274.60

CHAPTER VII

DISCUSSION

Limitations of Data

All data presented in this thesis was collected using core sections from the Wilson B. Laird Core & Sample Library at the University of North Dakota. Core sections are dry and then cut before being placed into curator boxes for later geologic analysis. For this reason alone, the results obtained in this thesis are substantially different than what would be observed in an in-situ geologic environment. In-situ geologic formations would be saturated; the core sections in the Wilson B. Laird Core and Sample Library are dry. For this reason alone, future applications of x-ray fluorescence down bore may not be comparable in the presence of drilling fluid. This thesis does not address how x-ray fluorescence values are affected by the influence of water saturation. It remains unknown how magnesium, sodium, and potassium brine connate waters would affect x-ray fluorescence analysis. Other limitations of data include the fact that core samples, previously exposed to millions of years of saturation, are now dry and obviously total dissolved solids have been deposited within the core sections.

Whether or not the chemostratigraphic results present in this thesis were a product of sediment source, depositional conditions, diagenesis, or hydrodynamic chemical deposition is at best an interpretive estimate. Future XRF analysis could prove to be more

representative of the bulk formation lithology during drill cutting analysis; drilled and mixed samples would be homogenous and represent thicker intervals from the formation. Core section analysis could be unrepresentative of the bulk formation lithology; segregated grains or minerals could be separated from larger scale lithology.

X-Ray Fluorescence Error Analysis

To assess the precision of Bruker Tracer IV Series Handheld XRF analysis, replicate XRF measurements were completed on 13 fly ash samples (Appendix B). The fly ash samples were collected post-combustion from a coal-fired power plant; the samples were collected by University of North Dakota student Dan Madche. The fly ash samples were placed on Whatman 2V filter paper for XRF analysis. Each fly ash sample was scanned five times using both 15KeV and 45KeV excitation voltages. Elemental Kα fluorescence counts were collected for silica, potassium, calcium, manganese, and iron. Elemental Kα fluorescence ratios were calculated for the twenty combinations of the measured elements.

The fly ash XRF data was separated into 26 individual data sets; the mean (μ-Equation 7-1), sample standard deviation (σ-Equation 7-2), and 95% confidence intervals (Equation 7-3) were calculated for each measurement parameter. Only five replicate measurements were completed on each unique sample; after calculating 95% confidence intervals it became apparent that more observations were needed to accurately establish a Gaussian distribution. Using both Kα fluorescence counts and Kα fluorescence ratios, at least one of the five measurements for each parameter did not meet the 95% confidence interval requirement. These results showed that replicate analysis should be completed on

a larger sample size; a 100 sample data set would be ideal for establishing a normally distributed set of fluorescence values.

Arithmetic Mean: (7-1)

$$\bar{X} = (\frac{1}{n}) \sum_{i=1}^{n} Xi$$

where: n = Number of samples in the data
  Xi = Value of the ith observation

Sample Standard Deviation: (7-2)

$$\sigma = \sqrt{(\frac{1}{n-1}) \sum_{i=1}^{n} (X_i - \bar{X})^2}$$

where: n = Number of samples in the data
  Xi = Value of the ith observation
  $\bar{X}$ = Arimethic mean of the data

Confidence Interval for the Mean μ of a Normal Distribution: (7-3)

$$\bar{X} - Z_{\alpha/2} \frac{\sigma}{\sqrt{n}} \leq \mu \leq \bar{X} + Z_{\alpha/2} \frac{\sigma}{\sqrt{n}}$$

where: n = Number of samples in the data
  $Z_{\alpha/2}$ = The confidence interval for the mean μ of a normal distribution
  μ = Mean of a normal distribution

105

$\bar{X}$ = Arithmetic mean of the data
σ = Sample standard deviation

Despite a limited number of measurements for each sample, it was possible to calculate the coefficient of variation for the 26 individual data sets. The Coefficient of Variation (CV-Equation 7-4) is a normalized measure of the variability in relation to the mean of the sample. The CV is mathematically defined as the ratio of the standard deviation (σ) to the mean (μ). This measurement is useful for comparing two data analysis techniques; it is a dimensionless number and allows for comparisons between measurements with different units. To assess whether Kα elemental count or Kα elemental ratio data analysis provided greater analytical precision, the CV measurement was used to describe the variability in relation to the mean of the count data.

Coefficient of Variation: (7-4)

$$C_v = \frac{\sigma}{\mu}$$

where: μ = Mean of a normal distribution
          σ = Sample standard deviation

The CV for the 15KeV measurements were considerably lower for the elemental fluorescence ratio analysis; 12 out of 13 sets of fly ash ratios provided lower variation than when using elemental count data. The average CV for the 15KeV fluorescence ratio analysis was 12.2%; the average CV for the 15KeV fluorescence count analysis was 19.8%. The CV results for the 45KeV measurements were far less convincing; 7 out of 13 sets of fly ash ratios provided lower variation than when using elemental count data. The average CV for the 45KeV fluorescence ratio analysis was 21.47%; the average CV for the 45KeV fluorescence count analysis was 23.75%. The 45KeV fly ash fluorescence

106

ratios that displayed higher variation than fluorescence counts generally contained minor amounts of iron and manganese. Fly ash sample BO-2 displayed a 22.2% coefficient of variation with 45KeV fluorescence counts and a 24.1% coefficient of variation with 45KeV fluorescence ratios. The Fe:Ca ratio in sample BO-2 averaged 1.92 and generally displayed a low iron content. Fly ash sample BO-10 displayed a 26.2% coefficient of variation with 45KeV fluorescence counts and a 19.1% coefficient of variation with 45KeV fluorescence ratios. The Fe:Ca ratio in sample BO-10 was 2.93. Samples with higher concentrations of heavy elements displayed higher coefficients of variation when using 45KeV fluorescence counts; samples with higher concentrations of light elements displayed roughly equal coefficients of variation whether using 45KeV fluorescence ratios or counts. For 15KeV fluorescence analysis, elemental ratios proved to provide lower coefficients of variation. For the 26 sets of data (13 fly ash samples scanned at 15KeV and 45KeV), the use of elemental fluorescence ratios provided lower variation from the mean for 19 out of 26 of the sets of data. Elemental count data provided lower variation from the mean for 7 out of 26 sets of data. For 15KeV fluorescence analysis, the use of elemental ratios provided less variation from the mean for 12 out of 13 samples. For 45KeV fluorescence analysis, the use of elemental ratios provided less variation from the mean for 7 out of 13 samples.

Recommendations for Future X-Ray Fluorescence Analysis:

The results of this thesis showed that XRF spectroscopy should have a definitive role in core analysis, petroleum exploration, and other earth science applications. The area of most intensive XRF use will likely be the academic sector; numerous research questions can be addressed using precise chemostratigraphic analysis. Due to the location

of the Wilson B. Laird Core and Sample Library at the University of North Dakota campus, it appears that numerous graduate students will complete x-ray fluorescence projects over the next several years. Anticipated future uses of x-ray fluorescence in the industrial sector include use as a mud-logging tool; after intensive research and design efforts XRF could also be used as a LWD tool.

Recommendations for Future X-Ray Fluorescence Analysis include:

1. XRF analysis of drill cuttings and core sections should be completed using a voltage of 45KeV for 30 seconds. Elemental counts should be collected and elemental fluorescence ratios should be calculated to determine the lithology of the sample.

2. XRF analysis should be completed using the "bench-top" configuration. Core sections should be placed flat on the bench to provide uniform analysis of core sections. Drill cuttings are preferable to core sections because the samples are homogenously mixed; drill cuttings should be placed on Whatman 2V filter papers and then should be placed flat on the bench to provide uniform analysis of drill cuttings.

3. XRF analysis should be completed on the same drill cutting sample for 100 measurements. Each measurement should take place for 30 seconds; 95% confidence intervals should be calculated for fluorescence ratios and fluorescence counts to determine which method allows for better analytical precision. Initial indications from fly ash data indicate that ratios provide less variation during XRF analysis.

4. XRF analysis should be completed on hydrocarbon saturated drill cuttings from the Middle Bakken Member; water saturated drill cuttings from the Middle Bakken should also be examined. The results could show which fluorescence ratios identify hydrocarbon saturation. The same process could be repeated for the Three Forks Formation.

5. XRF analysis should be completed for every formation in the North Dakota Stratigraphic Column on a one-foot interval. The results could be used to create an XRF stratigraphic column for the State of North Dakota.

   Future industrial questions that could be answered using XRF include:

1. How does XRF core analysis compare with XRF drill cutting analysis? Will drill cuttings display the same fluorescence ratios as the core sections? To answer this question Charlotte 1-22H drill cuttings can be examined using XRF.

2. If the same XRF fluorescence ratios can be used to identify core sections and drill cuttings, can this tool be used in the field to help guide the horizontal drill path? To test this theory drill cuttings should be scanned with XRF during vertical drilling. When the horizontal drilling begins drill cuttings can be examined with XRF to determine if the ratios stay consistent laterally. If the horizontal leg was being drilled into a permeable zone within the Middle Bakken Member, the Fe:Mn and Sr:Ca ratios could be used to keep the lateral path within the permeable zone. If the Fe:Mn ratios peaked while the Sr:Ca ratio dropped, this thesis concludes that the drill path would be within the impermeable Bakken shale.

3. Kubo (1978) discussed the deposition of nickel during the thermal maturation process of organic carbon. Is nickel also present in reservoir rock with ancient hydrocarbon migration? If nickel deposition proves to be characteristic of hydrocarbon fluid deposition, presence in drill cuttings would indicate that the lithology is potentially productive.

4. Can XRF be incorporated into a LWD/MWD package? Although it seems unlikely that x-rays could penetrate thick bentonite drilling mud, could MWD XRF provide information regarding mud content, viscosity, and resistivity?

5. Can XRF be used to determine the formation water resistivity during drill cutting analysis? Would zones with higher resistivity show higher concentrations of chlorine, magnesium, or potassium fluorescence? To test this theory drill cuttings can be compared with wireline or LWD resistivity logs.

Future academic questions that could be answered using XRF include:

1. Can XRF be used for thermal maturity determinations of geologic core? The production of oil is dependent upon time, temperature, and organic carbon content. Kubo (1978) discussed the deposition of nickel during the thermal maturation process of organic carbon. Is the presence of nickel in the Bakken shale a function of hydrocarbon maturation, or is the presence of nickel due to the sediment source of the Late Devonian/Early Mississippian deposition. To test this theory sections of immature Bakken shale can be compared with thermally mature sections of shale (included in this thesis) to determine if nickel deposition is a diagenetic process related to the thermal maturation of organic carbon.

2. Can XRF help determine basin structural history? Gerhard (1982) found that fault movement along the Nesson Anticline changed during both the Permian and Cretaceous Periods. Can these reversals be mapped using XRF? Permian and Cretaceous core sections on both sides of the anticline could be scanned using XRF; ratios could be compared to determine the maximum offset of each faulting event. Mapping the total offset of each faulting event could help determine structural mechanisms; prevailing thought is that the reversal in faulting direction in the Cretaceous was caused by the Laramide Orogeny (Gerhard, 1982).

3. Can XRF be used to map organic horizons within the Bakken Shale? Meissner (1984) claimed that the Upper Bakken Member is more organic rich than the Lower Bakken Member; Pramudito (2009) described the Lower Bakken as more organic rich. If nickel fluorescence is indicative of organic maturation; nickel fluorescence ratios could be used to determine which shale member is more organic rich. If nickel fluorescence presence is not indicative of organic content, S:Cl and Br:Cl ratios could be used to determine the absolute organic content of each shale member.

4. Will the XRF ratio of Sr:Ca prove to be a reliable indicator of effective porosity? To test this theory multiple core sections and drill cuttings should be examined using XRF; the Sr:Ca fluorescence data can be compared with porosity well-logs for correlation. If the Sr:Ca data proves to be a reliable indicator of effective porosity, it could be used on drill cuttings to help guide the horizontal well-path to zones of high permeability.

CHAPTER VIII

CONCLUSIONS

The results published in this thesis provide a new methodology, using analytical XRF chemostratigraphy, for examining Williston Basin core. Through the use of analytical XRF and elemental fluorescence ratios, this thesis completed scientific objectives that further the understanding of using a new analytical tool in core sections from the Bakken-Three Forks oil pool. These objectives have shown that XRF can be used for lithology determinations, hydrocarbon detection, and geologic interpretations. Results presented in this thesis have shown that x-ray fluorescence ratios can uniquely chronicle autonomous lithostratigraphic units with higher efficiency than conventional wireline or logging-while drilling technology.

The first objective of this thesis was to determine whether analytical XRF is capable of chemically distinguishing unique geologic lithology. Elemental Kα fluorescence ratios allowed for autonomous identification of calcite, dolomite, sandstone, and shale lithology. Through the use of calcium Kα fluorescence ratios, calcite and dolomite can be distinguished; these ratios allowed for identification of Lodgepole and Three Forks core. Through the use of iron Kα fluorescence ratios, shale can be distinguished from other lithology; these ratios allow for identification of Upper and Lower Bakken Member core. This method could theoretically be used on drill cuttings in the Williston Basin to determine lithology while drilling.

The second objective of this thesis was to determine whether analytical XRF is capable of distinguishing different geologic formations that consist of the same lithology. Elemenal Kα fluorescence ratios showed that it is possible to chemically distinguish lithology that is visually identical. Although the Upper and Lower Bakken Members both contain characteristic shale lithology that may be visually undistinguishable, iron Kα fluorescence ratios showed that the lower member contains a greater concentration of iron. The iron Kα fluorescence ratios of Fe:S, Fe:Ca, Fe:Mn, and Fe:Rb all proved to contain higher iron fluorescence in the Lower Bakken Member, indicating a higher content of iron. Analytical XRF is capable of first determining lithology type (carbonate, sandstone, or shale) and then genetically separating the same lithology into further subdivisions (same lithology at different depths or depositional conditions). Further research could determine whether this method also allows for genetic mapping of basin-wide diagenetic processes.

The third objective of this thesis was to determine whether analytical XRF is capable of precisely determining formation contacts with greater precision than current geophysical methods. Based on the core XRF, the core gamma ray, and both the wireline and LWD gamma ray values for the Charlotte 1-22H well, XRF provided the best vertical resolution. XRF values will rapidly change at a geologic content. At the Upper Bakken-Middle Bakken Member contact the Fe:Mn and Fe:S Kα fluorescence values immediately dropped within one foot of the contact; the API gamma values take roughly five feet to drop to a lower and distinguishable value. The difference between one foot and five feet of vertical resolution would allow for improved well placement; permeable zones may be overlooked because of the poor vertical resolution in the gamma log.

The fourth objective of this thesis was to determine whether analytical XRF allows comparable well analysis to contemporary geophysical methods. XRF is not capable of determining water saturation or hydrocarbon saturation with the same precision of other porosity logs. Although the Sr:Ca Kα fluorescence value allows a rough estimation of porosity, density measurements still provide higher accuracy for determining hydrocarbon saturation. It is not possible to determine the extent of water versus hydrocarbon saturation using XRF alone. Although XRF may give a rough indication of hydrocarbon saturation through the ratio of Ni:Mn alone, it is not possible to determine the extent of water versus hydrocarbon saturation. Williston Basin wells will not be economical if they produce more water than hydrocarbons; porosity logs will remain essential for well analysis.

The fifth objective of this thesis was to determine whether analytical XRF can be used as a tool to help determine paleoenvironments, sediment source providence, and diagenetic alteration of Williston Basin formations through geologic time. When coupling elemental fluorescence ratios with the diagenetic and geologic interpretations presented by Croudace and Rothwell (2006) the Upper and Lower Bakken Members were deposited in a deep water column that contained highly anoxic conditions. The Kα fluorescence ratios of S:Cl, Br:Cl, Fe:Rb, Fe: Ti, and Mn: Ti all indicate that the Upper and Middle Bakken Members were deposited in abrupt sea level transgression; the Lodgepole, Three Forks, and Middle Bakken Members were deposited in gradual sea level regression. This thesis has shown that geologic analysis and interpretations can be completed using XRF; it is feasible that thermal maturity determinations, basin origin and subsidence, and genetic mapping can be accomplished using XRF.

114

The final objective of this thesis was to answer the question of why increased stratigraphic precision is necessary for future petroleum production in the Williston Basin of North Dakota. The vast majority of horizontal well oil production has been produced from the Middle Bakken and Three Forks Formations. In the history of Williston Basin oil production, Middle Bakken and Three Forks Formation horizontal wells have produced 697.97 million barrels of oil. All other horizontal wells have produced only 32.37 million barrels of oil; it is essential to drill the horizontal wells in permeable reservoir rock surrounded by source rock. Data obtained in this thesis showed that geologic formation contacts are represented as gradual (up to ten foot) transitions on the gamma log. Horizontal well placement is usually determined using the gamma ray log; with a vertical resolution of up to ten feet it is feasible that wells are being drilled into non-porous lithology. This thesis examined core sections using XRF with a one foot vertical resolution; it was possible to determine formation contacts within that one foot interval. It is feasible that XRF could eventually be used on drill cuttings to determine formation contacts; horizontal well placement could then be completed into permeable hydrocarbon bearing units.

APPENDICES
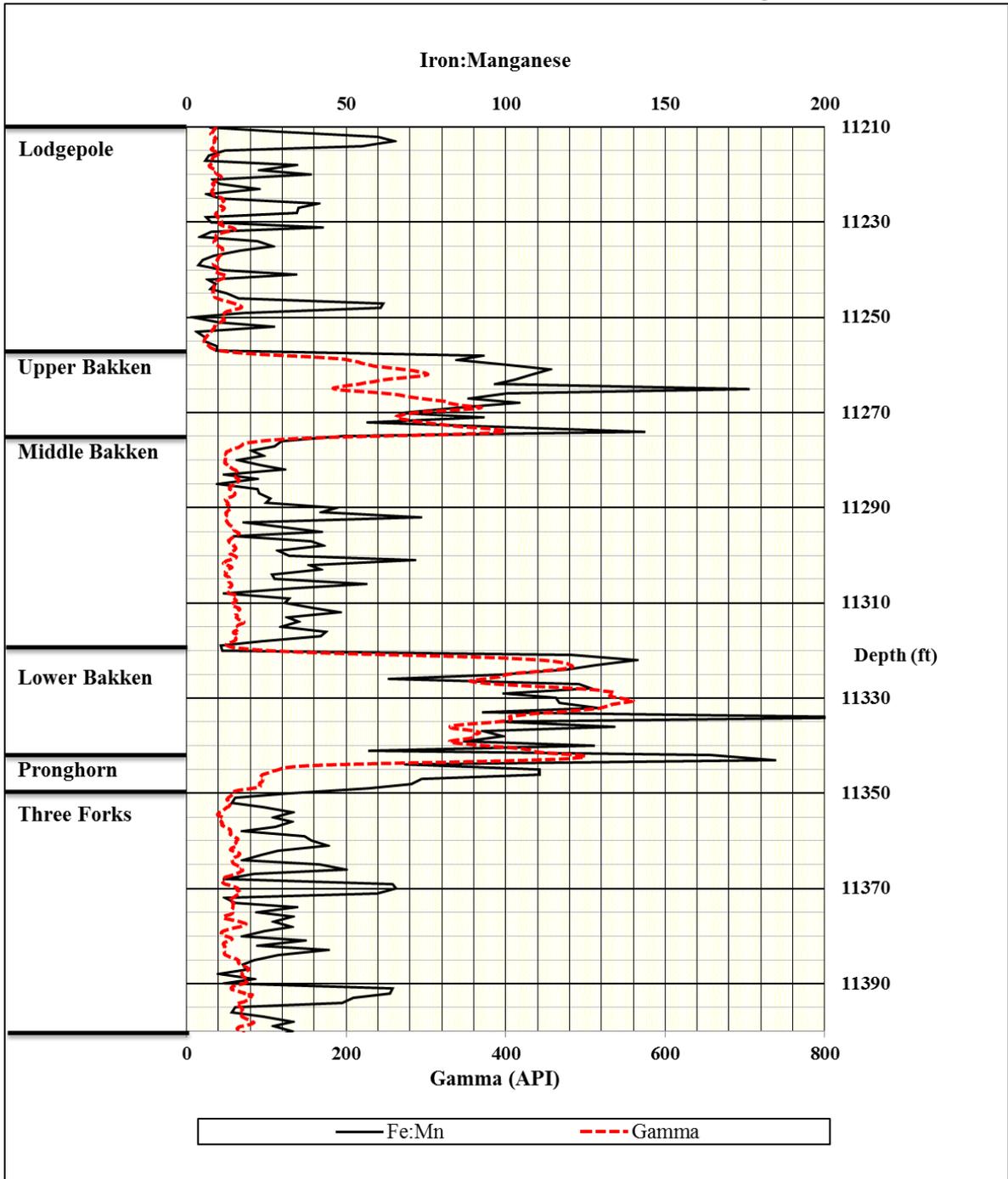
Figure 14. Fe:Mn Kα Fluorescence Log-Charlotte 1-22H.
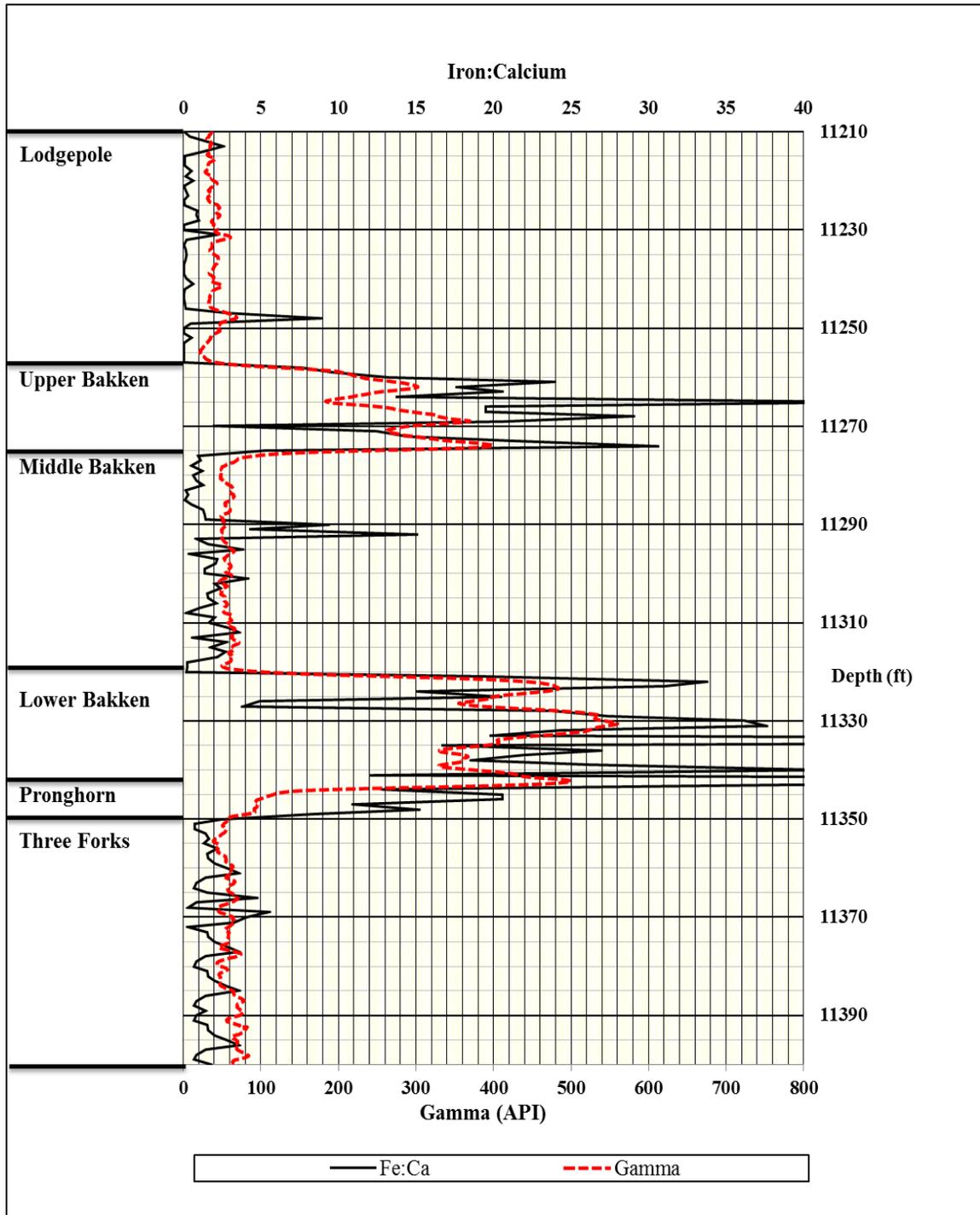
Figure 15. Fe:Ca Kα Fluorescence Log-Charlotte 1-22H.

Appendix A
Charlotte 1-22H Kα Fluorescence Ratio Well-Logs
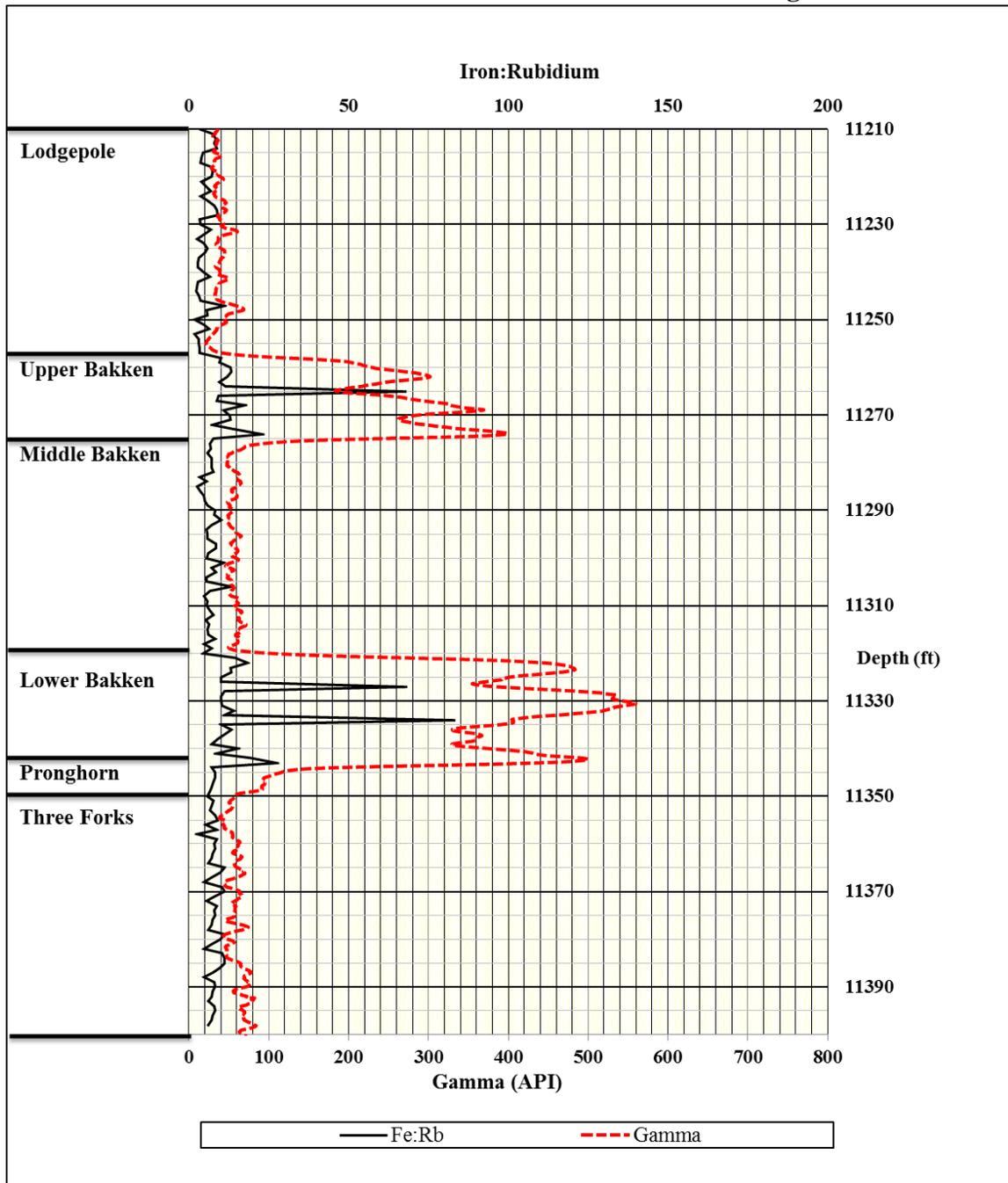
Figure 16. Fe:Rb Kα Fluorescence Log-Charlotte 1-22H.

Appendix A
Charlotte 1-22H Kα Fluorescence Ratio Well-Logs
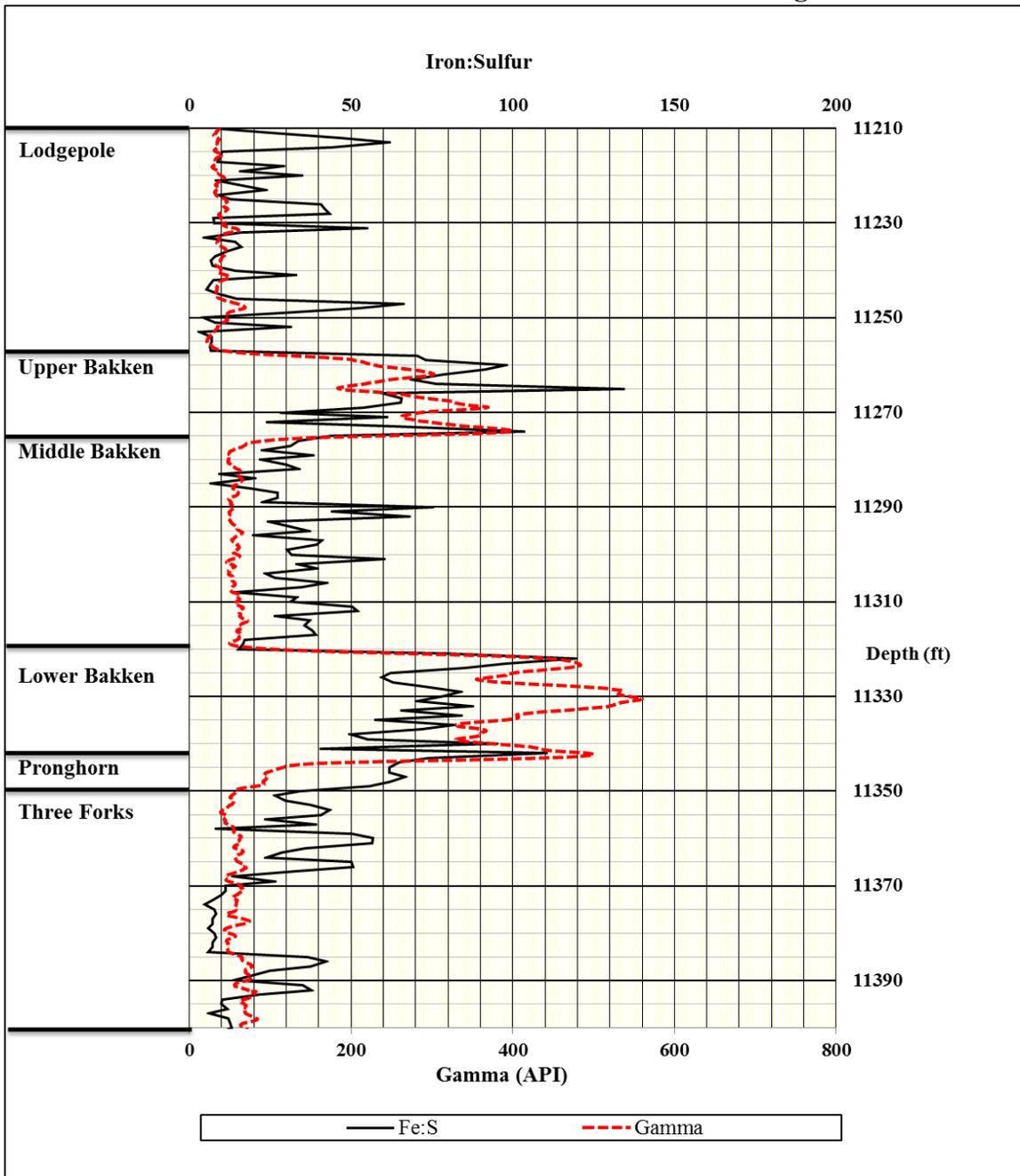
Figure 17. Fe:S Kα Fluorescence Log-Charlotte 1-22H.

Appendix A
Charlotte 1-22H Kα Fluorescence Ratio Well-Logs
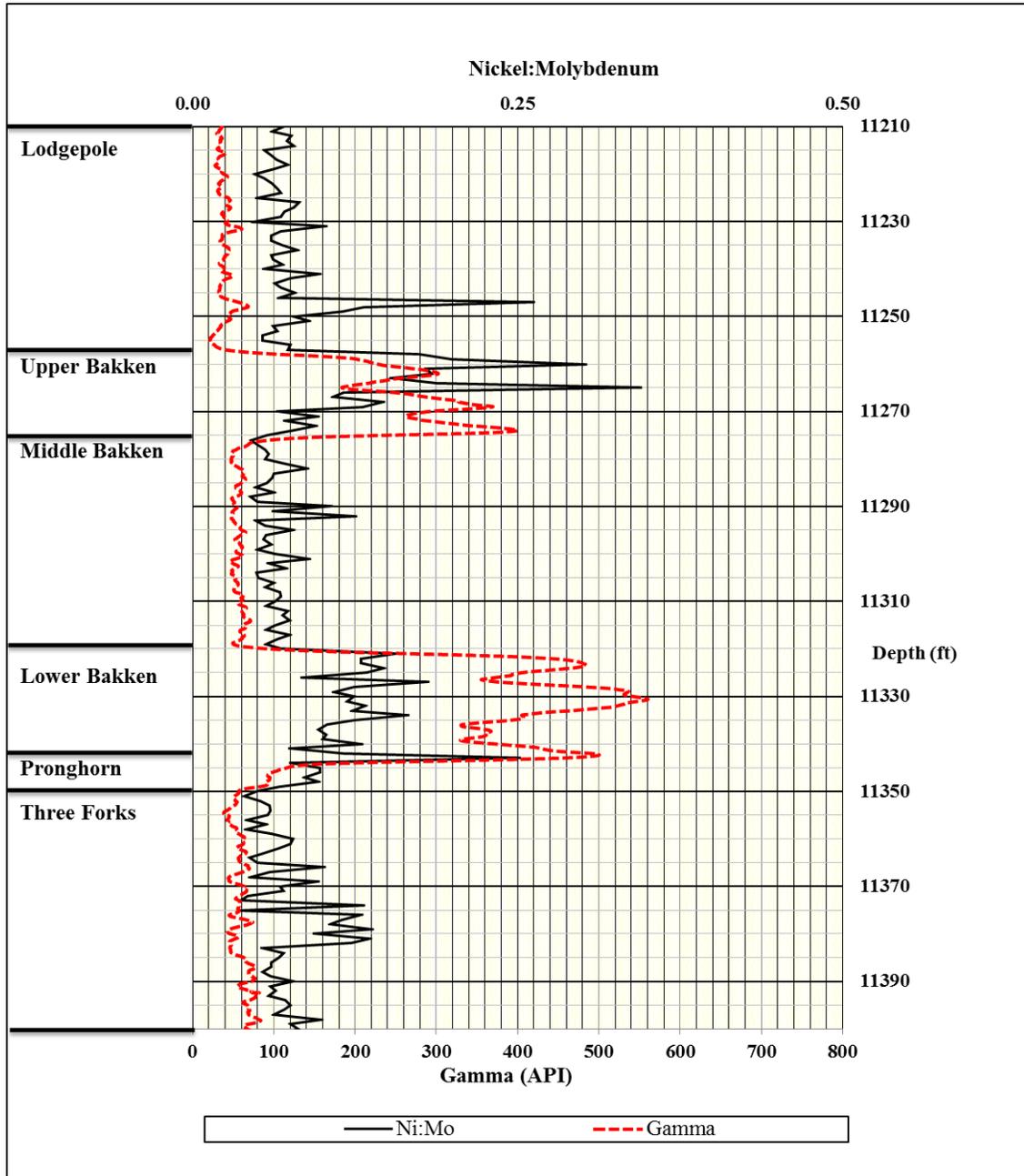
Figure 18. Ni:Mo Kα Fluorescence Log-Charlotte 1-22H.

Appendix A
Charlotte 1-22H Kα Fluorescence Ratio Well-Logs
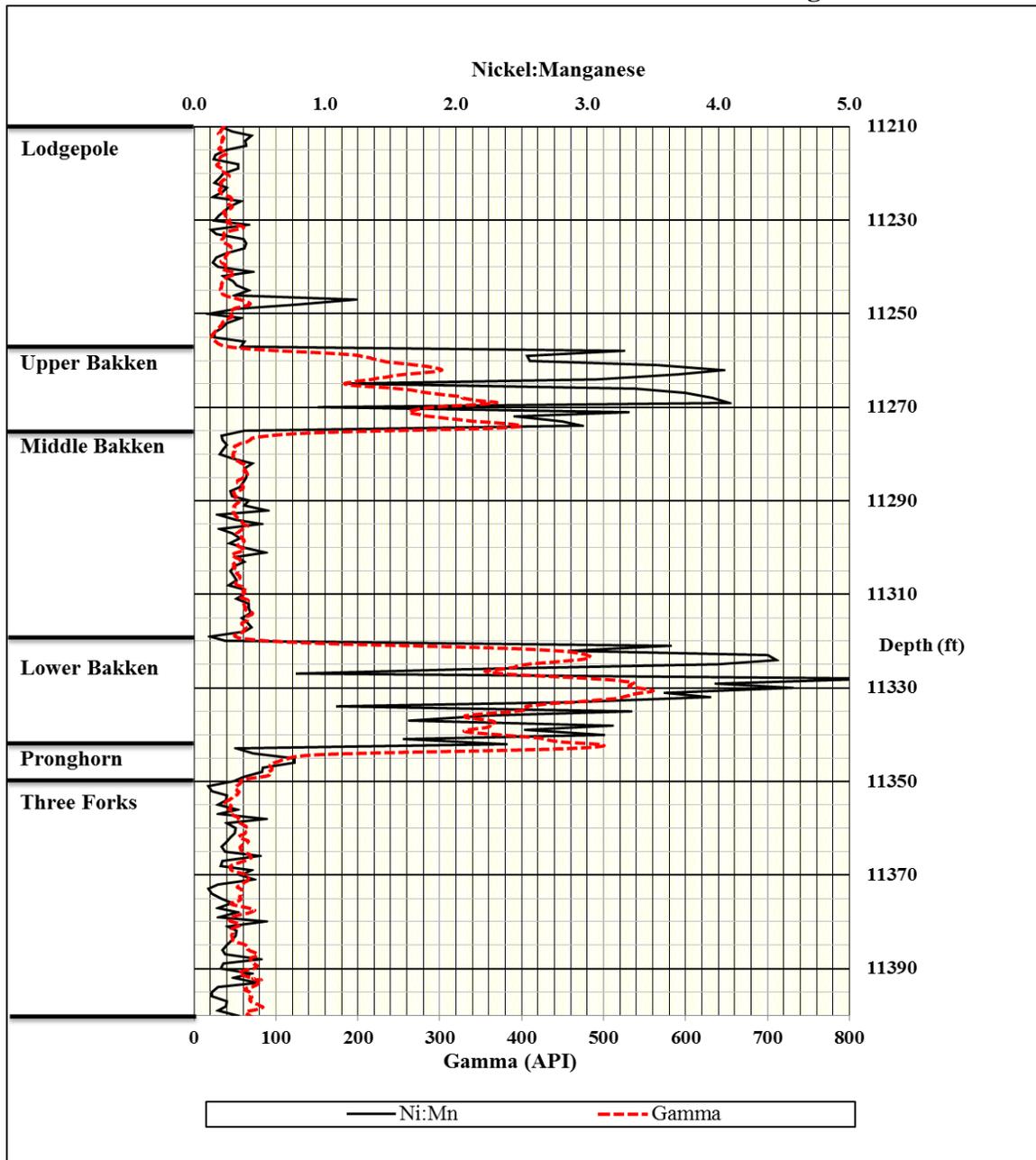
Figure 19. Ni:Mn Kα Fluorescence Log-Charlotte 1-22H.
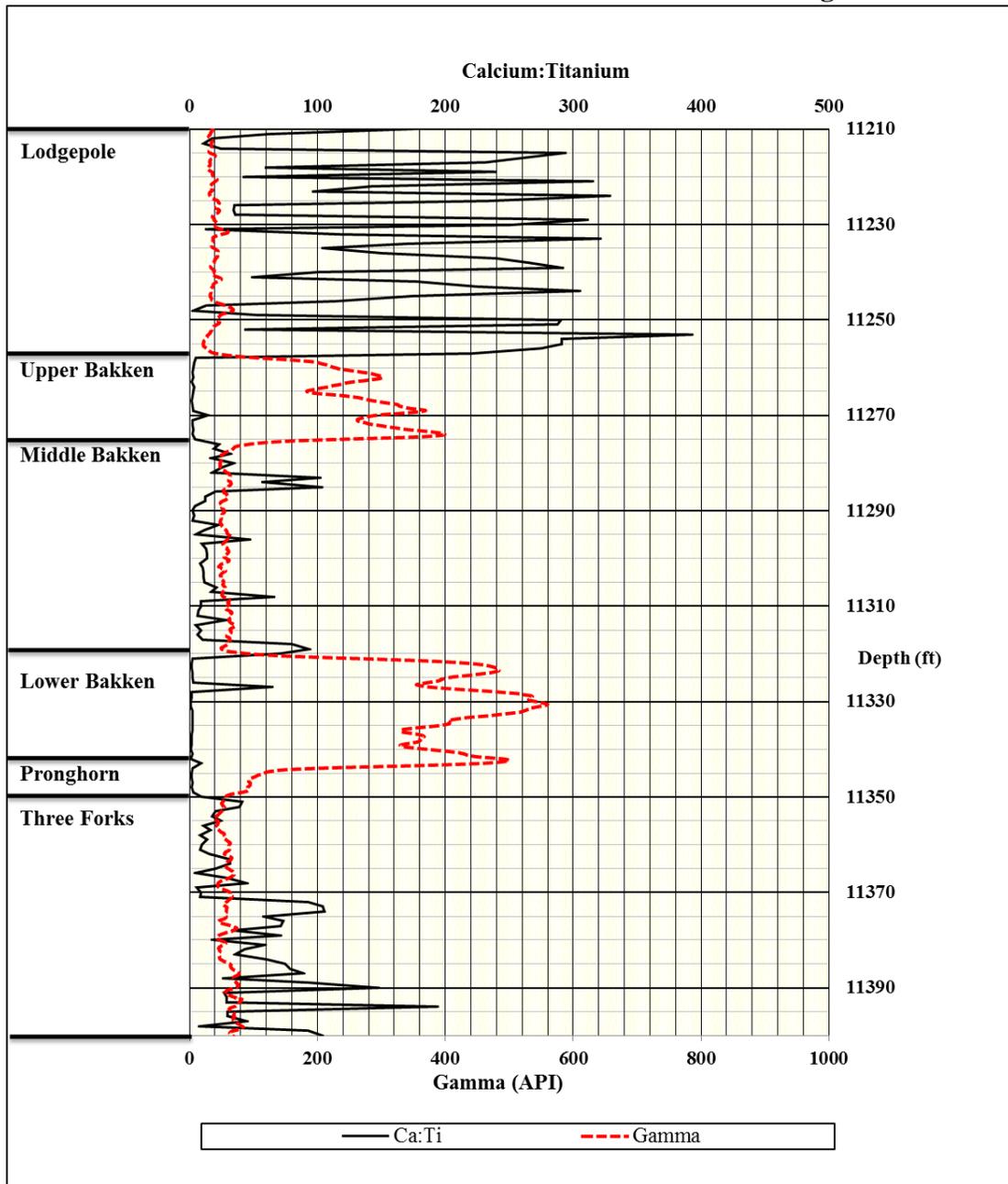
Appendix A
Charlotte 1-22H Kα Fluorescence Ratio Well-Logs

Figure 20. Ca:Ti Kα Fluorescence Log-Charlotte 1-22H.
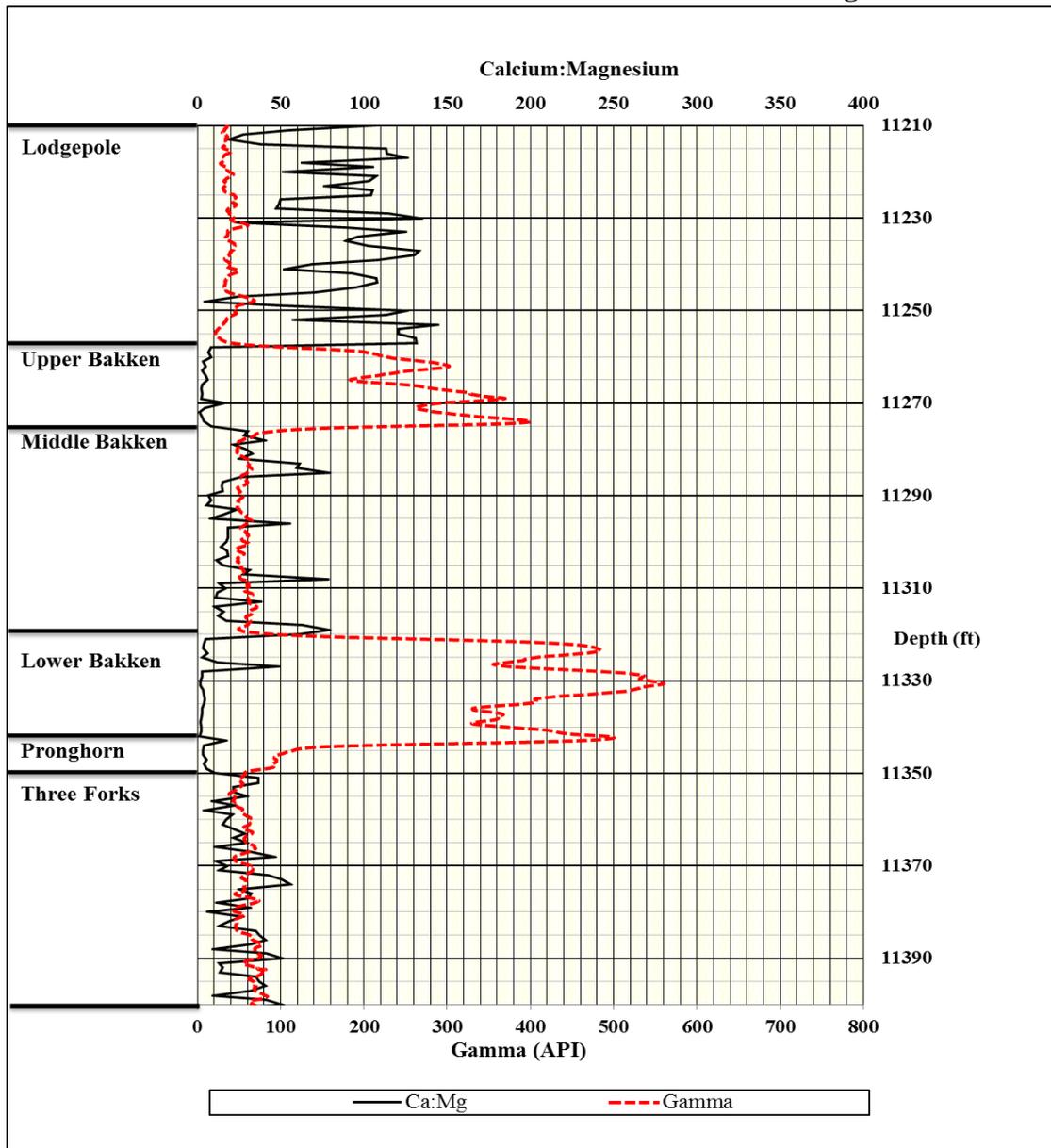
Figure 21. Ca:Mg Kα Fluorescence Log-Charlotte 1-22H.

Appendix A
Charlotte 1-22H Kα Fluorescence Ratio Well-Logs
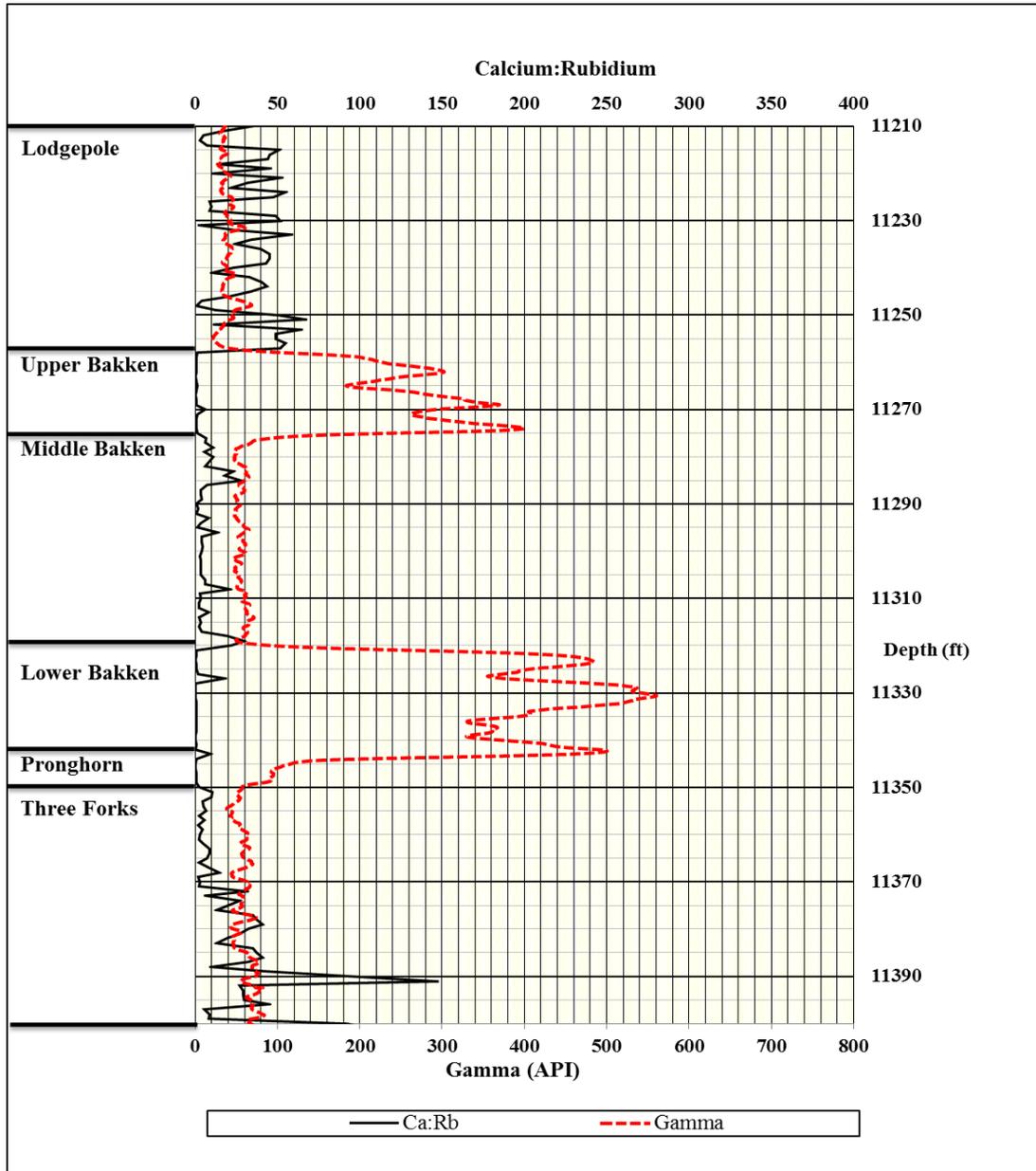
Figure 22. Ca:Rb Kα Fluorescence Log-Charlotte 1-22H.
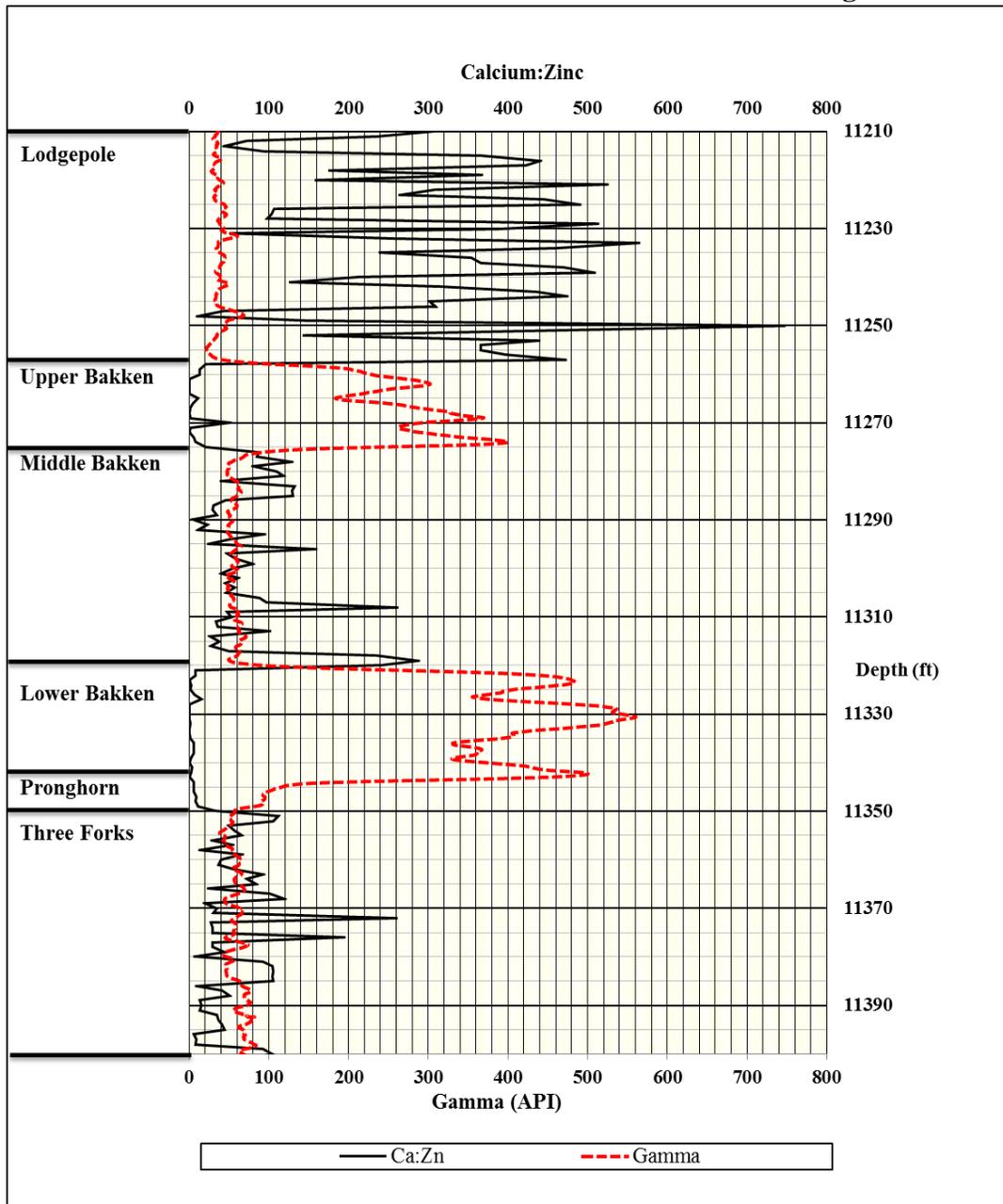
Appendix A
Charlotte 1-22H Kα Fluorescence Ratio Well-Logs

Figure 23. Ca:Zn Kα Fluorescence Log-Charlotte 1-22H.
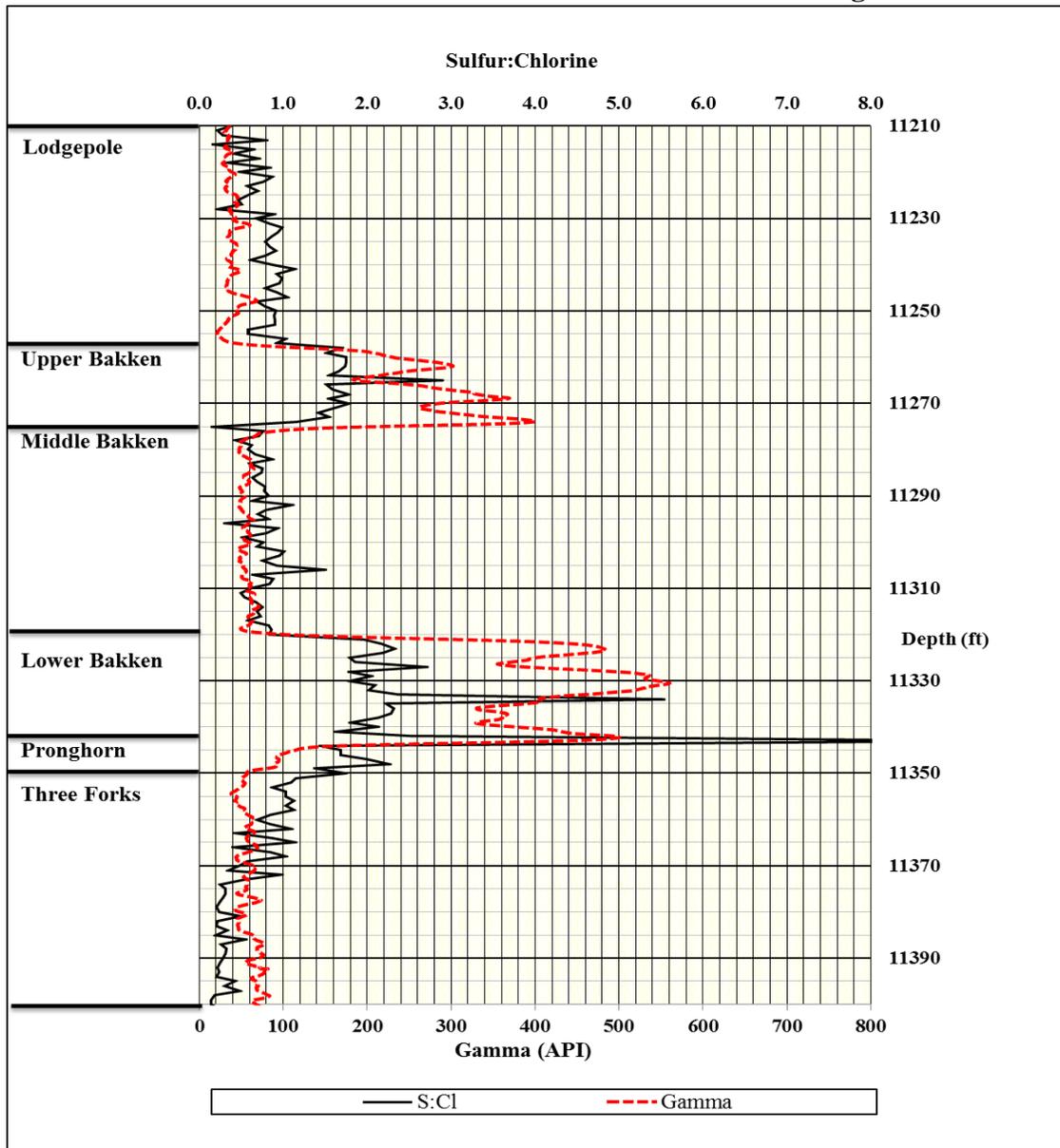
Figure 24. S:Cl Kα Fluorescence Log-Charlotte 1-22H.

Appendix A
Charlotte 1-22H Kα Fluorescence Ratio Well-Logs
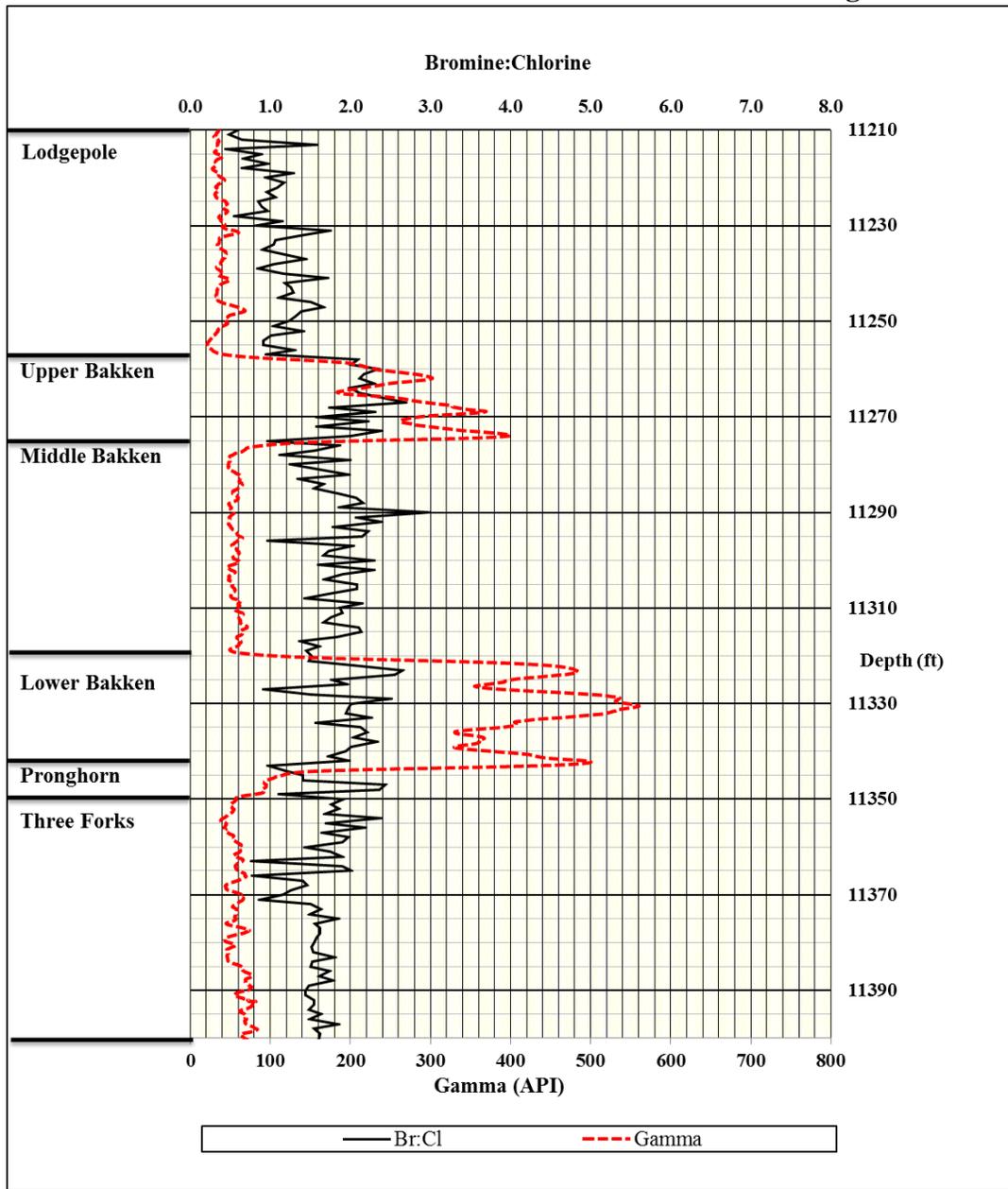
Figure 25. Br:Cl Kα Fluorescence Log-Charlotte 1-22H.

Appendix A
Charlotte 1-22H Kα Fluorescence Ratio Well-Logs
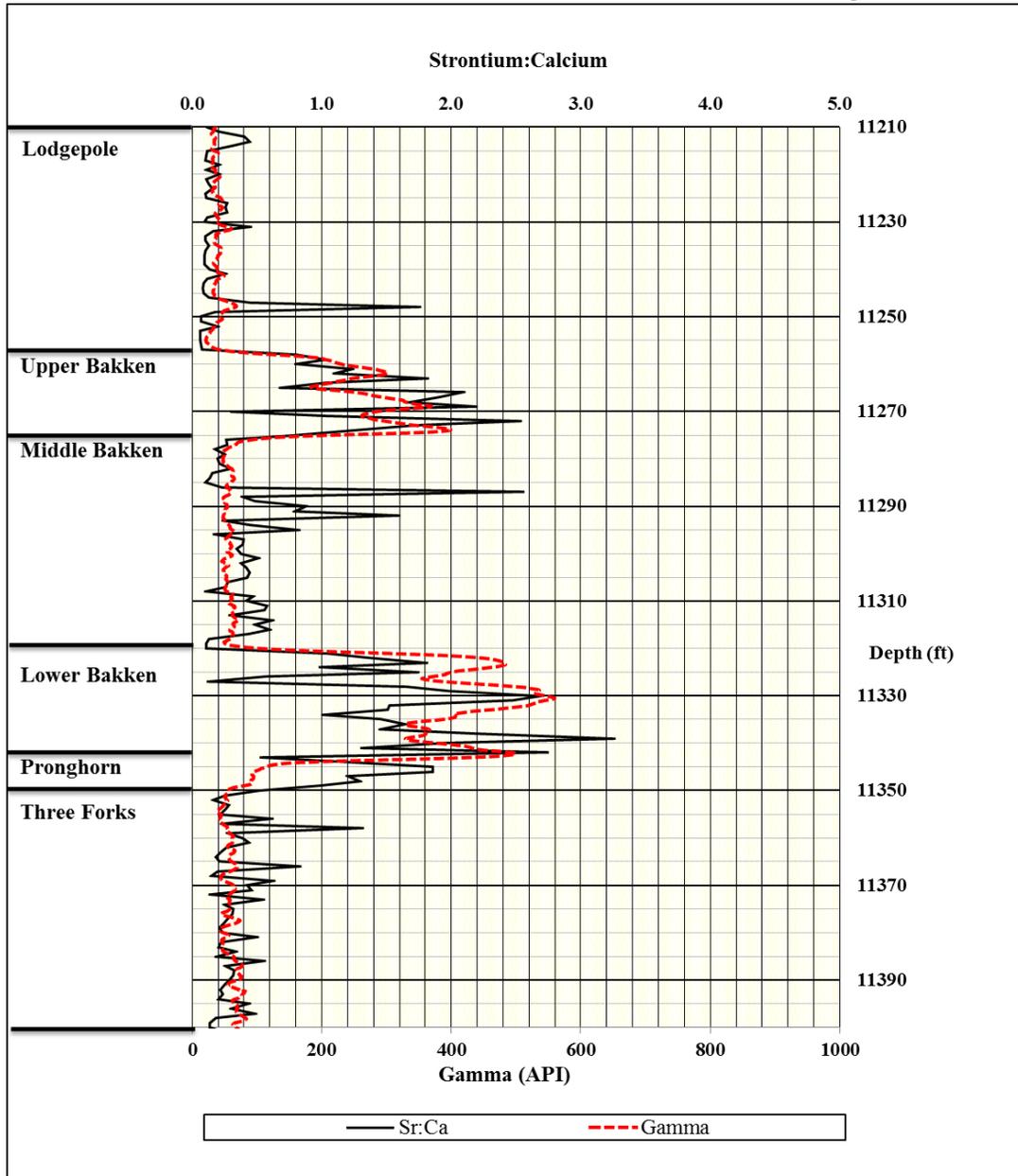
Figure 26. Sr:Ca Kα Fluorescence Log-Charlotte 1-22

Appendix B
Fly Ash Kα Fluorescence Statistics

Table 21. Fly Ash Sample BO-1 Kα Fluorescence Analysis.

Kα Counts	15KeV	15KeV	15KeV	15KeV	15KeV	μ	σ	Lower 95%	Upper 95%	Cv
Fly Ash Sample BO-1										
Si	103.38	110.26	6.62	89.45	74.28	76.798	41.586	40.347	113.249	0.542
K	209.68	226.5	23.83	215.45	169.52	168.996	83.954	95.408	242.584	0.497
Ca	566.38	548.38	435.44	541.5	452.27	508.794	60.267	455.968	561.620	0.118
Mn	516.57	526.47	36.68	518.47	422.66	404.170	209.789	220.284	588.056	0.519
Fe	607.83	592.94	1365.97	628.35	509.24	740.866	352.366	432.008	1049.724	0.476
Kα Counts	**15KeV**	**15KeV**	**15KeV**	**15KeV**	**15KeV**	**μ**	**σ**	**Lower 95%**	**Upper 95%**	**Cv**
Si:K	0.493	0.487	0.278	0.415	0.438	0.422	0.087	0.346	0.499	0.206
Si:Ca	0.183	0.201	0.015	0.165	0.164	0.146	0.074	0.080	0.211	0.511
Si:Mn	0.200	0.209	0.180	0.173	0.176	0.188	0.016	0.173	0.202	0.086
Si:Fe	0.170	0.186	0.005	0.142	0.146	0.130	0.072	0.067	0.193	0.556
K:Si	2.028	2.054	3.600	2.409	2.282	2.475	0.649	1.906	3.043	0.262
K:Ca	0.370	0.413	0.055	0.398	0.375	0.322	0.150	0.190	0.454	0.467
K:Mn	0.406	0.430	0.650	0.416	0.401	0.460	0.106	0.367	0.554	0.231
K:Fe	0.345	0.382	0.017	0.343	0.333	0.284	0.150	0.152	0.416	0.529
Ca:Si	5.479	4.974	65.776	6.054	6.089	17.674	26.894	-5.899	41.247	1.522
Ca:K	2.701	2.421	18.273	2.513	2.668	5.715	7.021	-0.439	11.869	1.228
Ca:Mn	1.096	1.042	11.871	1.044	1.070	3.225	4.834	-1.012	7.462	1.499
Ca:Fe	0.932	0.925	0.319	0.862	0.888	0.785	0.262	0.555	1.015	0.334
Mn:Si	4.997	4.775	5.541	5.796	5.690	5.360	0.449	4.966	5.753	0.084
Mn:K	2.464	2.324	1.539	2.406	2.493	2.245	0.400	1.895	2.596	0.178
Mn:Ca	0.912	0.960	0.084	0.957	0.935	0.770	0.384	0.433	1.106	0.498
Mn:Fe	0.850	0.888	0.027	0.825	0.830	0.684	0.368	0.361	1.007	0.538
Fe:Si	5.880	5.378	206.340	7.025	6.856	46.295	89.470	-32.127	124.718	1.933
Fe:K	2.899	2.618	57.321	2.916	3.004	13.752	24.357	-7.598	35.101	1.771
Fe:Ca	1.073	1.081	3.137	1.160	1.126	1.516	0.907	0.720	2.311	0.599
Fe:Mn	1.177	1.126	37.240	1.212	1.205	8.392	16.127	-5.743	22.527	1.922

Appendix B
Fly Ash Kα Fluorescence Statistics

Table 22. Fly Ash Sample BO-2 Kα Fluorescence Analysis.

Fly Ash Sample BO-2										
Kα Counts	**15KeV**	**15KeV**	**15KeV**	**15KeV**	**15KeV**	**μ**	**σ**	**Lower 95%**	**Upper 95%**	**Cv**
Si	48.64	110.05	86.48	75.63	90.26	82.212	22.519	62.474	101.950	0.274
K	125.58	250.22	159.27	208.7	240.46	196.846	53.344	150.089	243.603	0.271
Ca	269.22	533.87	395.45	500.47	596.37	459.076	128.696	346.270	571.882	0.280
Mn	243.23	492.28	397.34	461.9	562.18	431.386	120.735	325.558	537.214	0.280
Fe	320.15	600.21	469.46	530.5	630.65	510.194	123.289	402.128	618.260	0.242
Kα Ratio	**15KeV**	**15KeV**	**15KeV**	**15KeV**	**15KeV**	**μ**	**σ**	**Lower 95%**	**Upper 95%**	**Cv**
Si:K	0.387	0.440	0.543	0.362	0.375	0.422	0.074	0.357	0.486	0.175
Si:Ca	0.181	0.206	0.219	0.151	0.151	0.182	0.031	0.154	0.209	0.170
Si:Mn	0.200	0.224	0.218	0.164	0.161	0.193	0.030	0.167	0.219	0.153
Si:Fe	0.152	0.183	0.184	0.143	0.143	0.161	0.021	0.143	0.180	0.131
K:Si	2.582	2.274	1.842	2.759	2.664	2.424	0.373	2.097	2.751	0.154
K:Ca	0.466	0.469	0.403	0.417	0.403	0.432	0.033	0.402	0.461	0.077
K:Mn	0.516	0.508	0.401	0.452	0.428	0.461	0.050	0.417	0.505	0.109
K:Fe	0.392	0.417	0.339	0.393	0.381	0.385	0.028	0.360	0.410	0.074
Ca:Si	5.535	4.851	4.573	6.617	6.607	5.637	0.957	4.798	6.475	0.170
Ca:K	2.144	2.134	2.483	2.398	2.480	2.328	0.176	2.174	2.482	0.076
Ca:Mn	1.107	1.084	0.995	1.084	1.061	1.066	0.043	1.029	1.104	0.040
Ca:Fe	0.841	0.889	0.842	0.943	0.946	0.892	0.051	0.847	0.937	0.058
Mn:Si	5.001	4.473	4.595	6.107	6.228	5.281	0.834	4.550	6.012	0.158
Mn:K	1.937	1.967	2.495	2.213	2.338	2.190	0.239	1.980	2.400	0.109
Mn:Ca	0.903	0.922	1.005	0.923	0.943	0.939	0.039	0.905	0.974	0.042
Mn:Fe	0.760	0.820	0.846	0.871	0.891	0.838	0.051	0.793	0.882	0.061
Fe:Si	6.582	5.454	5.429	7.014	6.987	6.293	0.796	5.595	6.991	0.127
Fe:K	2.549	2.399	2.948	2.542	2.623	2.612	0.204	2.433	2.791	0.078
Fe:Ca	1.189	1.124	1.187	1.060	1.057	1.124	0.065	1.067	1.180	0.058
Fe:Mn	1.316	1.219	1.182	1.149	1.122	1.197	0.076	1.131	1.264	0.063

Appendix B
Fly Ash Kα Fluorescence Statistics

Table 23. Fly Ash Sample BO-3 Kα Fluorescence Analysis.

Fly Ash Sample BO-3										
Kα Counts	**15KeV**	**15KeV**	**15KeV**	**15KeV**	**15KeV**	**μ**	**σ**	**Lower 95%**	**Upper 95%**	**Cv**
Si	104.61	111.45	104.81	75.33	103.98	100.036	14.142	87.641	112.431	0.141
K	221.73	239.99	201.38	185.65	247.06	219.162	25.778	196.567	241.757	0.118
Ca	519.24	609.47	526.81	452.56	587.56	539.128	61.917	484.856	593.400	0.115
Mn	525.64	604.36	536.06	452.76	581.55	540.074	58.526	488.774	591.374	0.108
Fe	621.79	711.82	635.72	504.16	653.03	625.304	75.912	558.765	691.843	0.121
Kα Ratio	**15KeV**	**15KeV**	**15KeV**	**15KeV**	**15KeV**	**μ**	**σ**	**Lower 95%**	**Upper 95%**	**Cv**
Si:K	0.472	0.464	0.520	0.406	0.421	0.457	0.045	0.417	0.496	0.099
Si:Ca	0.201	0.183	0.199	0.166	0.177	0.185	0.015	0.172	0.198	0.080
Si:Mn	0.199	0.184	0.196	0.166	0.179	0.185	0.013	0.173	0.196	0.071
Si:Fe	0.168	0.157	0.165	0.149	0.159	0.160	0.007	0.153	0.166	0.046
K:Si	2.120	2.153	1.921	2.464	2.376	2.207	0.216	2.017	2.396	0.098
K:Ca	0.427	0.394	0.382	0.410	0.420	0.407	0.019	0.390	0.423	0.046
K:Mn	0.422	0.397	0.376	0.410	0.425	0.406	0.020	0.388	0.424	0.050
K:Fe	0.357	0.337	0.317	0.368	0.378	0.351	0.025	0.330	0.373	0.070
Ca:Si	4.964	5.469	5.026	6.008	5.651	5.423	0.437	5.040	5.806	0.081
Ca:K	2.342	2.540	2.616	2.438	2.378	2.463	0.114	2.363	2.562	0.046
Ca:Mn	0.988	1.008	0.983	1.000	1.010	0.998	0.012	0.987	1.009	0.012
Ca:Fe	0.835	0.856	0.829	0.898	0.900	0.863	0.034	0.834	0.893	0.039
Mn:Si	5.025	5.423	5.115	6.010	5.593	5.433	0.396	5.086	5.780	0.073
Mn:K	2.371	2.518	2.662	2.439	2.354	2.469	0.126	2.358	2.579	0.051
Mn:Ca	1.012	0.992	1.018	1.000	0.990	1.002	0.012	0.992	1.013	0.012
Mn:Fe	0.845	0.849	0.843	0.898	0.891	0.865	0.027	0.842	0.889	0.031
Fe:Si	5.944	6.387	6.065	6.693	6.280	6.274	0.292	6.018	6.530	0.047
Fe:K	2.804	2.966	3.157	2.716	2.643	2.857	0.206	2.676	3.038	0.072
Fe:Ca	1.198	1.168	1.207	1.114	1.111	1.160	0.045	1.120	1.199	0.039
Fe:Mn	1.183	1.178	1.186	1.114	1.123	1.157	0.035	1.126	1.188	0.031

Table 24. Fly Ash Sample BO-4 Kα Fluorescence Analysis.

Fly Ash Sample BO-4										
Kα Counts	**15KeV**	**15KeV**	**15KeV**	**15KeV**	**15KeV**	**μ**	**σ**	**Lower 95%**	**Upper 95%**	**Cv**
Si	52.63	83.38	95.05	65.41	86.16	76.526	17.157	61.487	91.565	0.224
K	143.75	243.49	209.39	151.98	166.12	182.946	42.259	145.905	219.987	0.231
Ca	337.59	556.36	472.6	419.27	415.95	440.354	80.774	369.554	511.154	0.183
Mn	344.3	566.2	465.28	399.01	392.44	433.446	85.807	358.234	508.658	0.198
Fe	415.41	712.12	555.32	465.57	493.81	528.446	114.443	428.134	628.758	0.217
Kα Ratio	**15KeV**	**15KeV**	**15KeV**	**15KeV**	**15KeV**	**μ**	**σ**	**Lower 95%**	**Upper 95%**	**Cv**
Si:K	0.366	0.342	0.454	0.430	0.519	0.422	0.071	0.361	0.484	0.167
Si:Ca	0.156	0.150	0.201	0.156	0.207	0.174	0.028	0.150	0.198	0.159
Si:Mn	0.153	0.147	0.204	0.164	0.220	0.178	0.032	0.149	0.206	0.182
Si:Fe	0.127	0.117	0.171	0.140	0.174	0.146	0.026	0.123	0.169	0.177
K:Si	2.731	2.920	2.203	2.323	1.928	2.421	0.402	2.069	2.773	0.166
K:Ca	0.426	0.438	0.443	0.362	0.399	0.414	0.033	0.385	0.443	0.080
K:Mn	0.418	0.430	0.450	0.381	0.423	0.420	0.025	0.398	0.442	0.060
K:Fe	0.346	0.342	0.377	0.326	0.336	0.346	0.019	0.329	0.362	0.055
Ca:Si	6.414	6.673	4.972	6.410	4.828	5.859	0.884	5.085	6.634	0.151
Ca:K	2.348	2.285	2.257	2.759	2.504	2.431	0.207	2.249	2.612	0.085
Ca:Mn	0.981	0.983	1.016	1.051	1.060	1.018	0.037	0.985	1.050	0.036
Ca:Fe	0.813	0.781	0.851	0.901	0.842	0.838	0.045	0.798	0.877	0.053
Mn:Si	6.542	6.791	4.895	6.100	4.555	5.777	0.999	4.901	6.652	0.173
Mn:K	2.395	2.325	2.222	2.625	2.362	2.386	0.149	2.256	2.516	0.062
Mn:Ca	1.020	1.018	0.985	0.952	0.943	0.983	0.036	0.952	1.015	0.036
Mn:Fe	0.829	0.795	0.838	0.857	0.795	0.823	0.027	0.799	0.847	0.033
Fe:Si	7.893	8.541	5.842	7.118	5.731	7.025	1.238	5.940	8.110	0.176
Fe:K	2.890	2.925	2.652	3.063	2.973	2.901	0.153	2.766	3.035	0.053
Fe:Ca	1.231	1.280	1.175	1.110	1.187	1.197	0.063	1.141	1.252	0.053
Fe:Mn	1.207	1.258	1.194	1.167	1.258	1.217	0.040	1.181	1.252	0.033

Appendix B
Fly Ash Kα Fluorescence Statistics

Table 25. Fly Ash Sample BO-5 Kα Fluorescence Analysis.

Fly Ash Sample BO-5										
Kα Counts	**15KeV**	**15KeV**	**15KeV**	**15KeV**	**15KeV**	**μ**	**σ**	**Lower 95%**	**Upper 95%**	**Cv**
Si	97.18	99.54	67.1	82.87	97.44	88.826	13.841	76.694	100.958	0.156
K	180.1	219.16	162.96	155.87	194.53	182.524	25.423	160.240	204.808	0.139
Ca	473.7	503	352.79	427.22	469.83	445.308	58.358	394.156	496.460	0.131
Mn	490.13	539	404.12	446.5	534.17	482.784	57.791	432.129	533.439	0.120
Fe	586.05	652.55	460.97	488.07	603.48	558.224	80.777	487.421	629.027	0.145
Kα Ratio	**15KeV**	**15KeV**	**15KeV**	**15KeV**	**15KeV**	**μ**	**σ**	**Lower 95%**	**Upper 95%**	**Cv**
Si:K	0.540	0.454	0.412	0.532	0.501	0.488	0.054	0.440	0.535	0.111
Si:Ca	0.205	0.198	0.190	0.194	0.207	0.199	0.007	0.193	0.205	0.037
Si:Mn	0.198	0.185	0.166	0.186	0.182	0.183	0.012	0.173	0.193	0.063
Si:Fe	0.166	0.153	0.146	0.170	0.161	0.159	0.010	0.150	0.168	0.062
K:Si	1.853	2.202	2.429	1.881	1.996	2.072	0.242	1.860	2.284	0.117
K:Ca	0.380	0.436	0.462	0.365	0.414	0.411	0.040	0.377	0.446	0.096
K:Mn	0.367	0.407	0.403	0.349	0.364	0.378	0.025	0.356	0.400	0.067
K:Fe	0.307	0.336	0.354	0.319	0.322	0.328	0.018	0.312	0.343	0.054
Ca:Si	4.874	5.053	5.258	5.155	4.822	5.032	0.184	4.871	5.194	0.037
Ca:K	2.630	2.295	2.165	2.741	2.415	2.449	0.236	2.242	2.656	0.097
Ca:Mn	0.966	0.933	0.873	0.957	0.880	0.922	0.043	0.884	0.960	0.047
Ca:Fe	0.808	0.771	0.765	0.875	0.779	0.800	0.045	0.760	0.839	0.057
Mn:Si	5.044	5.415	6.023	5.388	5.482	5.470	0.353	5.161	5.779	0.064
Mn:K	2.721	2.459	2.480	2.865	2.746	2.654	0.177	2.499	2.810	0.067
Mn:Ca	1.035	1.072	1.145	1.045	1.137	1.087	0.052	1.042	1.132	0.047
Mn:Fe	0.836	0.826	0.877	0.915	0.885	0.868	0.037	0.836	0.900	0.042
Fe:Si	6.031	6.556	6.870	5.890	6.193	6.308	0.401	5.957	6.659	0.064
Fe:K	3.254	2.978	2.829	3.131	3.102	3.059	0.162	2.917	3.201	0.053
Fe:Ca	1.237	1.297	1.307	1.142	1.284	1.254	0.068	1.194	1.313	0.054
Fe:Mn	1.196	1.211	1.141	1.093	1.130	1.154	0.049	1.111	1.197	0.042

Appendix B
Fly Ash Kα Fluorescence Statistics

Table 26. Fly Ash Sample BO-6 Kα Fluorescence Analysis.

Fly Ash Sample BO-6										
Kα Counts	**15KeV**	**15KeV**	**15KeV**	**15KeV**	**15KeV**	**μ**	**σ**	**Lower 95%**	**Upper 95%**	**Cv**
Si	82.23	83.55	82.12	107.02	95.38	90.060	10.985	80.431	99.689	0.122
K	249.1	183.2	209.63	252.33	246.13	228.078	30.456	201.382	254.774	0.134
Ca	1210.17	1009.47	987.2	1218.04	1484.17	1181.810	200.694	1005.896	1357.724	0.170
Mn	505.59	465.33	451.29	519.46	633.43	515.020	71.868	452.026	578.014	0.140
Fe	1479.3	1212.52	1205.41	1420.75	1629.63	1389.522	181.600	1230.345	1548.699	0.131
Kα Ratio	**15KeV**	**15KeV**	**15KeV**	**15KeV**	**15KeV**	**μ**	**σ**	**Lower 95%**	**Upper 95%**	**Cv**
Si:K	0.330	0.456	0.392	0.424	0.388	0.398	0.047	0.357	0.439	0.118
Si:Ca	0.068	0.083	0.083	0.088	0.064	0.077	0.010	0.068	0.086	0.135
Si:Mn	0.163	0.180	0.182	0.206	0.151	0.176	0.021	0.158	0.195	0.120
Si:Fe	0.056	0.069	0.068	0.075	0.059	0.065	0.008	0.058	0.072	0.124
K:Si	3.029	2.193	2.553	2.358	2.581	2.543	0.314	2.267	2.818	0.124
K:Ca	0.206	0.181	0.212	0.207	0.166	0.195	0.020	0.177	0.212	0.103
K:Mn	0.493	0.394	0.465	0.486	0.389	0.445	0.050	0.401	0.489	0.113
K:Fe	0.168	0.151	0.174	0.178	0.151	0.164	0.013	0.153	0.175	0.077
Ca:Si	14.717	12.082	12.021	11.381	15.561	13.153	1.858	11.524	14.781	0.141
Ca:K	4.858	5.510	4.709	4.827	6.030	5.187	0.566	4.691	5.683	0.109
Ca:Mn	2.394	2.169	2.188	2.345	2.343	2.288	0.102	2.198	2.377	0.045
Ca:Fe	0.818	0.833	0.819	0.857	0.911	0.848	0.039	0.814	0.881	0.046
Mn:Si	6.148	5.569	5.495	4.854	6.641	5.742	0.681	5.145	6.338	0.119
Mn:K	2.030	2.540	2.153	2.059	2.574	2.271	0.265	2.039	2.503	0.117
Mn:Ca	0.418	0.461	0.457	0.426	0.427	0.438	0.020	0.421	0.455	0.045
Mn:Fe	0.342	0.384	0.374	0.366	0.389	0.371	0.019	0.355	0.387	0.050
Fe:Si	17.990	14.513	14.679	13.276	17.086	15.508	1.956	13.794	17.223	0.126
Fe:K	5.939	6.619	5.750	5.631	6.621	6.112	0.477	5.694	6.530	0.078
Fe:Ca	1.222	1.201	1.221	1.166	1.098	1.182	0.052	1.136	1.227	0.044
Fe:Mn	2.926	2.606	2.671	2.735	2.573	2.702	0.140	2.580	2.825	0.052

Appendix B
Fly Ash Kα Fluorescence Statistics

Table 27. Fly Ash Sample BO-7 Kα Fluorescence Analysis.

Kα Counts	15KeV	15KeV	15KeV	15KeV	15KeV	μ	σ	Lower 95%	Upper 95%	Cv
				Fly Ash Sample BO-7						
Si	82.6	74.94	58.72	90.94	71.65	75.770	12.095	65.169	86.371	0.160
K	250.61	199.78	221.46	310.09	210.21	238.430	44.333	199.571	277.289	0.186
Ca	2368.22	2074.94	2417.16	2834.22	1902.17	2319.342	357.359	2006.108	2632.576	0.154
Mn	485.43	425.2	478.9	579.21	413.91	476.530	65.544	419.079	533.981	0.138
Fe	2705.68	2258.14	2751.31	3089.13	2286.78	2618.208	348.794	2312.481	2923.935	0.133
Kα Ratio	**15KeV**	**15KeV**	**15KeV**	**15KeV**	**15KeV**	**μ**	**σ**	**Lower 95%**	**Upper 95%**	**Cv**
Si:K	0.330	0.375	0.265	0.293	0.341	0.321	0.043	0.283	0.358	0.133
Si:Ca	0.035	0.036	0.024	0.032	0.038	0.033	0.005	0.028	0.038	0.160
Si:Mn	0.170	0.176	0.123	0.157	0.173	0.160	0.022	0.140	0.179	0.138
Si:Fe	0.031	0.033	0.021	0.029	0.031	0.029	0.005	0.025	0.033	0.157
K:Si	3.034	2.666	3.771	3.410	2.934	3.163	0.432	2.784	3.542	0.137
K:Ca	0.106	0.096	0.092	0.109	0.111	0.103	0.008	0.095	0.110	0.081
K:Mn	0.516	0.470	0.462	0.535	0.508	0.498	0.031	0.471	0.526	0.063
K:Fe	0.093	0.088	0.080	0.100	0.092	0.091	0.007	0.084	0.097	0.079
Ca:Si	28.671	27.688	41.164	31.166	26.548	31.047	5.906	25.870	36.224	0.190
Ca:K	9.450	10.386	10.915	9.140	9.049	9.788	0.823	9.067	10.509	0.084
Ca:Mn	4.879	4.880	5.047	4.893	4.596	4.859	0.163	4.716	5.002	0.034
Ca:Fe	0.875	0.919	0.879	0.917	0.832	0.884	0.036	0.853	0.916	0.041
Mn:Si	5.877	5.674	8.156	6.369	5.777	6.370	1.033	5.465	7.276	0.162
Mn:K	1.937	2.128	2.162	1.868	1.969	2.013	0.127	1.902	2.124	0.063
Mn:Ca	0.205	0.205	0.198	0.204	0.218	0.206	0.007	0.200	0.212	0.034
Mn:Fe	0.179	0.188	0.174	0.187	0.181	0.182	0.006	0.177	0.187	0.033
Fe:Si	32.756	30.133	46.855	33.969	31.916	35.126	6.704	29.250	41.002	0.191
Fe:K	10.796	11.303	12.424	9.962	10.879	11.073	0.898	10.286	11.860	0.081
Fe:Ca	1.142	1.088	1.138	1.090	1.202	1.132	0.047	1.091	1.173	0.041
Fe:Mn	5.574	5.311	5.745	5.333	5.525	5.498	0.180	5.340	5.655	0.033

Appendix B
Fly Ash Kα Fluorescence Statistics

Table 28. Fly Ash Sample BO-8 Kα Fluorescence Analysis.

Fly Ash Sample BO-8										
Kα Counts	**15KeV**	**15KeV**	**15KeV**	**15KeV**	**15KeV**	**μ**	**σ**	**Lower 95%**	**Upper 95%**	**Cv**
Si	90.26	89.04	146.58	115.5	124.51	113.178	24.276	91.899	134.457	0.214
K	323.87	285.42	545.32	397.13	400.93	390.534	99.503	303.317	477.751	0.255
Ca	4455.47	3607.43	6565.67	5134.4	5143.73	4981.340	1086.746	4028.779	5933.901	0.218
Mn	562.08	483.51	866.69	629.57	656.55	639.680	143.467	513.927	765.433	0.224
Fe	5577.02	4701.94	8404.17	6517.63	6521.46	6344.444	1377.548	5136.987	7551.901	0.217
Kα Ratio	**15KeV**	**15KeV**	**15KeV**	**15KeV**	**15KeV**	**μ**	**σ**	**Lower 95%**	**Upper 95%**	**Cv**
Si:K	0.279	0.312	0.269	0.291	0.311	0.292	0.019	0.275	0.309	0.065
Si:Ca	0.020	0.025	0.022	0.022	0.024	0.023	0.002	0.021	0.024	0.077
Si:Mn	0.161	0.184	0.169	0.183	0.190	0.177	0.012	0.167	0.188	0.068
Si:Fe	0.016	0.019	0.017	0.018	0.019	0.018	0.001	0.017	0.019	0.067
K:Si	3.588	3.206	3.720	3.438	3.220	3.434	0.226	3.237	3.632	0.066
K:Ca	0.073	0.079	0.083	0.077	0.078	0.078	0.004	0.075	0.081	0.048
K:Mn	0.576	0.590	0.629	0.631	0.611	0.607	0.024	0.586	0.628	0.039
K:Fe	0.058	0.061	0.065	0.061	0.061	0.061	0.002	0.059	0.063	0.040
Ca:Si	49.363	40.515	44.792	44.454	41.312	44.087	3.497	41.021	47.153	0.079
Ca:K	13.757	12.639	12.040	12.929	12.829	12.839	0.618	12.297	13.381	0.048
Ca:Mn	7.927	7.461	7.576	8.155	7.834	7.791	0.278	7.547	8.034	0.036
Ca:Fe	0.799	0.767	0.781	0.788	0.789	0.785	0.012	0.775	0.795	0.015
Mn:Si	6.227	5.430	5.913	5.451	5.273	5.659	0.397	5.310	6.007	0.070
Mn:K	1.736	1.694	1.589	1.585	1.638	1.648	0.066	1.591	1.706	0.040
Mn:Ca	0.126	0.134	0.132	0.123	0.128	0.128	0.005	0.124	0.132	0.036
Mn:Fe	0.101	0.103	0.103	0.097	0.101	0.101	0.003	0.099	0.103	0.026
Fe:Si	61.788	52.807	57.335	56.430	52.377	56.147	3.830	52.790	59.505	0.068
Fe:K	17.220	16.474	15.411	16.412	16.266	16.357	0.645	15.791	16.922	0.039
Fe:Ca	1.252	1.303	1.280	1.269	1.268	1.274	0.019	1.258	1.291	0.015
Fe:Mn	9.922	9.725	9.697	10.353	9.933	9.926	0.262	9.696	10.156	0.026

Appendix B
Fly Ash Kα Fluorescence Statistics

Table 29. Fly Ash Sample BO-9 Kα Fluorescence Analysis.

Kα Counts	15KeV	15KeV	15KeV	15KeV	15KeV	μ	σ	Lower 95%	Upper 95%	Cv
				Fly Ash Sample BO-9						
Si	125.33	159.09	128	193.53	141.77	149.544	28.004	124.998	174.090	0.187
K	376.3	440.65	367.24	610.83	397.92	438.588	100.369	350.612	526.564	0.229
Ca	5174.69	7123.9	6294.69	9578.27	6135.71	6861.452	1669.062	5398.476	8324.428	0.243
Mn	615.77	822.22	699.15	1126.5	686.5	790.028	202.233	612.766	967.290	0.256
Fe	7478.01	9923.32	8552.66	13416.78	8591.2	9592.394	2307.027	7570.225	11614.563	0.241
Kα Ratio	15KeV	15KeV	15KeV	15KeV	15KeV	μ	σ	Lower 95%	Upper 95%	Cv
Si:K	0.333	0.361	0.349	0.317	0.356	0.343	0.018	0.327	0.359	0.053
Si:Ca	0.024	0.022	0.020	0.020	0.023	0.022	0.002	0.021	0.024	0.079
Si:Mn	0.204	0.193	0.183	0.172	0.207	0.192	0.014	0.179	0.204	0.075
Si:Fe	0.017	0.016	0.015	0.014	0.017	0.016	0.001	0.015	0.017	0.064
K:Si	3.002	2.770	2.869	3.156	2.807	2.921	0.159	2.782	3.060	0.054
K:Ca	0.073	0.062	0.058	0.064	0.065	0.064	0.005	0.060	0.069	0.083
K:Mn	0.611	0.536	0.525	0.542	0.580	0.559	0.036	0.528	0.590	0.064
K:Fe	0.050	0.044	0.043	0.046	0.046	0.046	0.003	0.043	0.048	0.061
Ca:Si	41.289	44.779	49.177	49.492	43.279	45.603	3.626	42.425	48.782	0.080
Ca:K	13.752	16.167	17.141	15.681	15.419	15.632	1.240	14.545	16.718	0.079
Ca:Mn	8.404	8.664	9.003	8.503	8.938	8.702	0.263	8.472	8.933	0.030
Ca:Fe	0.692	0.718	0.736	0.714	0.714	0.715	0.016	0.701	0.729	0.022
Mn:Si	4.913	5.168	5.462	5.821	4.842	5.241	0.405	4.886	5.597	0.077
Mn:K	1.636	1.866	1.904	1.844	1.725	1.795	0.111	1.698	1.892	0.062
Mn:Ca	0.119	0.115	0.111	0.118	0.112	0.115	0.003	0.112	0.118	0.030
Mn:Fe	0.082	0.083	0.082	0.084	0.080	0.082	0.002	0.081	0.083	0.018
Fe:Si	59.667	62.376	66.818	69.327	60.600	63.757	4.153	60.117	67.398	0.065
Fe:K	19.872	22.520	23.289	21.965	21.590	21.847	1.276	20.729	22.966	0.058
Fe:Ca	1.445	1.393	1.359	1.401	1.400	1.400	0.031	1.373	1.427	0.022
Fe:Mn	12.144	12.069	12.233	11.910	12.514	12.174	0.224	11.978	12.371	0.018

Appendix B
Fly Ash Kα Fluorescence Statistics

Table 30. Fly Ash Sample BO-10 Kα Fluorescence Analysis.

Kα Counts	15KeV	15KeV	15KeV	15KeV	15KeV	μ	σ	Lower 95%	Upper 95%	Cv
Si	348.02	347.97	281.71	302.17	246.94	305.362	43.640	267.110	343.614	0.143
K	645.82	647.12	527.7	549.36	442.81	562.562	86.331	486.891	638.233	0.153
Ca	13905.89	14259.38	11324.44	12886.39	9905.85	12456.390	1825.054	10856.683	14056.097	0.147
Mn	1048.97	1113.54	810.61	995.27	785.12	950.702	145.947	822.776	1078.628	0.154
Fe	14138.71	14339.28	11262.85	13008.57	9912.87	12532.456	1906.927	10860.985	14203.927	0.152
Kα Ratio	**15KeV**	**15KeV**	**15KeV**	**15KeV**	**15KeV**	**μ**	**σ**	**Lower 95%**	**Upper 95%**	**Cv**
Si:K	0.539	0.538	0.534	0.550	0.558	0.544	0.010	0.535	0.552	0.018
Si:Ca	0.025	0.024	0.025	0.023	0.025	0.025	0.001	0.024	0.025	0.027
Si:Mn	0.332	0.312	0.348	0.304	0.315	0.322	0.018	0.307	0.337	0.055
Si:Fe	0.025	0.024	0.025	0.023	0.025	0.024	0.001	0.024	0.025	0.029
K:Si	1.856	1.860	1.873	1.818	1.793	1.840	0.033	1.811	1.869	0.018
K:Ca	0.046	0.045	0.047	0.043	0.045	0.045	0.002	0.044	0.047	0.036
K:Mn	0.616	0.581	0.651	0.552	0.564	0.593	0.040	0.557	0.628	0.068
K:Fe	0.046	0.045	0.047	0.042	0.045	0.045	0.002	0.043	0.046	0.038
Ca:Si	39.957	40.979	40.199	42.646	40.114	40.779	1.116	39.801	41.757	0.027
Ca:K	21.532	22.035	21.460	23.457	22.370	22.171	0.810	21.461	22.881	0.037
Ca:Mn	13.257	12.805	13.970	12.948	12.617	13.119	0.530	12.655	13.584	0.040
Ca:Fe	0.984	0.994	1.005	0.991	0.999	0.995	0.008	0.987	1.002	0.008
Mn:Si	3.014	3.200	2.877	3.294	3.179	3.113	0.166	2.968	3.258	0.053
Mn:K	1.624	1.721	1.536	1.812	1.773	1.693	0.112	1.595	1.792	0.066
Mn:Ca	0.075	0.078	0.072	0.077	0.079	0.076	0.003	0.074	0.079	0.039
Mn:Fe	0.074	0.078	0.072	0.077	0.079	0.076	0.003	0.073	0.078	0.038
Fe:Si	40.626	41.208	39.980	43.051	40.143	41.002	1.241	39.914	42.090	0.030
Fe:K	21.893	22.159	21.343	23.679	22.386	22.292	0.868	21.532	23.053	0.039
Fe:Ca	1.017	1.006	0.995	1.009	1.001	1.005	0.008	0.998	1.013	0.008
Fe:Mn	13.479	12.877	13.894	13.070	12.626	13.189	0.502	12.749	13.630	0.038

Appendix B
Fly Ash Kα Fluorescence Statistics

Table 31. Fly Ash Sample BO-11 Kα Fluorescence Analysis.

Fly Ash Sample BO-11										
Kα Counts	**15KeV**	**15KeV**	**15KeV**	**15KeV**	**15KeV**	**μ**	**σ**	**Lower 95%**	**Upper 95%**	**Cv**
Si	106.45	118.17	111.75	93.06	123.95	110.676	11.850	100.289	121.063	0.107
K	320.89	307.31	317.52	312.89	416.15	334.952	45.677	294.915	374.989	0.136
Ca	9930.99	9766.62	9921.15	9763.28	11899.85	10256.378	922.261	9447.992	11064.764	0.090
Mn	538.5	578.23	585.96	549.1	671.57	584.672	52.421	538.724	630.620	0.090
Fe	8185.2	8504.8	8391.24	8241.14	9980.07	8660.490	748.295	8004.590	9316.390	0.086
Kα Ratio	**15KeV**	**15KeV**	**15KeV**	**15KeV**	**15KeV**	**μ**	**σ**	**Lower 95%**	**Upper 95%**	**Cv**
Si:K	0.332	0.385	0.352	0.297	0.298	0.333	0.037	0.300	0.365	0.112
Si:Ca	0.011	0.012	0.011	0.010	0.010	0.011	0.001	0.010	0.012	0.089
Si:Mn	0.198	0.204	0.191	0.169	0.185	0.189	0.013	0.178	0.201	0.071
Si:Fe	0.013	0.014	0.013	0.011	0.012	0.013	0.001	0.012	0.014	0.077
K:Si	3.014	2.601	2.841	3.362	3.357	3.035	0.331	2.745	3.325	0.109
K:Ca	0.032	0.031	0.032	0.032	0.035	0.033	0.001	0.031	0.034	0.042
K:Mn	0.596	0.531	0.542	0.570	0.620	0.572	0.037	0.540	0.604	0.064
K:Fe	0.039	0.036	0.038	0.038	0.042	0.039	0.002	0.037	0.040	0.053
Ca:Si	93.293	82.649	88.780	104.914	96.005	93.128	8.306	85.848	100.408	0.089
Ca:K	30.948	31.781	31.246	31.204	28.595	30.755	1.245	29.664	31.846	0.040
Ca:Mn	18.442	16.891	16.931	17.781	17.719	17.553	0.651	16.982	18.123	0.037
Ca:Fe	1.213	1.148	1.182	1.185	1.192	1.184	0.023	1.164	1.205	0.020
Mn:Si	5.059	4.893	5.243	5.900	5.418	5.303	0.388	4.963	5.643	0.073
Mn:K	1.678	1.882	1.845	1.755	1.614	1.755	0.112	1.657	1.853	0.064
Mn:Ca	0.054	0.059	0.059	0.056	0.056	0.057	0.002	0.055	0.059	0.037
Mn:Fe	0.066	0.068	0.070	0.067	0.067	0.068	0.002	0.066	0.069	0.023
Fe:Si	76.892	71.971	75.089	88.557	80.517	78.605	6.364	73.027	84.184	0.081
Fe:K	25.508	27.675	26.427	26.339	23.982	25.986	1.362	24.793	27.180	0.052
Fe:Ca	0.824	0.871	0.846	0.844	0.839	0.845	0.017	0.830	0.860	0.020
Fe:Mn	15.200	14.708	14.320	15.008	14.861	14.820	0.333	14.528	15.111	0.022

Table 32. Fly Ash Sample BO-12 Kα Fluorescence Analysis.

Fly Ash Sample BO-12										
Kα Counts	15KeV	15KeV	15KeV	15KeV	15KeV	μ	σ	Lower 95%	Upper 95%	Cv
Si	138.1	91.13	84.48	119.16	116.45	109.864	21.922	90.648	129.080	0.200
K	386.27	258.43	271.91	374.47	307.85	319.786	58.330	268.658	370.914	0.182
Ca	9636.34	6794.36	6741.77	9654.66	8184.01	8202.228	1438.888	6941.005	9463.451	0.175
Mn	654.46	474.27	490.37	709.95	565.67	578.944	102.278	489.294	668.594	0.177
Fe	7646.88	5279.02	5444.6	7373.98	6495.04	6447.904	1080.543	5500.780	7395.028	0.168
Kα Ratio	15KeV	15KeV	15KeV	15KeV	15KeV	μ	σ	Lower 95%	Upper 95%	Cv
Si:K	0.358	0.353	0.311	0.318	0.378	0.343	0.028	0.319	0.368	0.082
Si:Ca	0.014	0.013	0.013	0.012	0.014	0.013	0.001	0.013	0.014	0.069
Si:Mn	0.211	0.192	0.172	0.168	0.206	0.190	0.019	0.173	0.207	0.102
Si:Fe	0.018	0.017	0.016	0.016	0.018	0.017	0.001	0.016	0.018	0.066
K:Si	2.797	2.836	3.219	3.143	2.644	2.928	0.243	2.714	3.141	0.083
K:Ca	0.040	0.038	0.040	0.039	0.038	0.039	0.001	0.038	0.040	0.031
K:Mn	0.590	0.545	0.554	0.527	0.544	0.552	0.023	0.532	0.573	0.042
K:Fe	0.051	0.049	0.050	0.051	0.047	0.050	0.001	0.048	0.051	0.028
Ca:Si	69.778	74.557	79.803	81.023	70.279	75.088	5.221	70.511	79.665	0.070
Ca:K	24.947	26.291	24.794	25.782	26.584	25.680	0.794	24.984	26.376	0.031
Ca:Mn	14.724	14.326	13.748	13.599	14.468	14.173	0.481	13.752	14.594	0.034
Ca:Fe	1.260	1.287	1.238	1.309	1.260	1.271	0.028	1.247	1.295	0.022
Mn:Si	4.739	5.204	5.805	5.958	4.858	5.313	0.549	4.831	5.794	0.103
Mn:K	1.694	1.835	1.803	1.896	1.837	1.813	0.074	1.748	1.878	0.041
Mn:Ca	0.068	0.070	0.073	0.074	0.069	0.071	0.002	0.069	0.073	0.034
Mn:Fe	0.086	0.090	0.090	0.096	0.087	0.090	0.004	0.086	0.093	0.046
Fe:Si	55.372	57.928	64.448	61.883	55.775	59.081	3.958	55.612	62.551	0.067
Fe:K	19.797	20.427	20.024	19.692	21.098	20.207	0.572	19.706	20.709	0.028
Fe:Ca	0.794	0.777	0.808	0.764	0.794	0.787	0.017	0.772	0.802	0.022
Fe:Mn	11.684	11.131	11.103	10.387	11.482	11.157	0.495	10.723	11.591	0.044

Appendix B
Fly Ash Kα Fluorescence Statistics

Table 33. Fly Ash Sample BO-13 Kα Fluorescence Analysis.

Fly Ash Sample BO-13										
Kα Counts	**15KeV**	**15KeV**	**15KeV**	**15KeV**	**15KeV**	**μ**	**σ**	**Lower 95%**	**Upper 95%**	**Cv**
Si	67.47	63.08	116.3	78.93	104.66	86.088	23.372	65.602	106.574	0.271
K	261.68	303.5	450.53	289.67	389.63	339.002	78.540	270.159	407.845	0.232
Ca	5221.19	6726.92	9314.26	6527.14	7824.46	7122.794	1534.803	5777.499	8468.089	0.215
Mn	385.38	495.39	685.01	512.12	594.63	534.506	112.401	435.983	633.029	0.210
Fe	5223.3	6553.09	9321.45	6571.9	7881.21	7110.190	1552.789	5749.130	8471.250	0.218
Kα Ratio	**15KeV**	**15KeV**	**15KeV**	**15KeV**	**15KeV**	**μ**	**σ**	**Lower 95%**	**Upper 95%**	**Cv**
Si:K	0.258	0.208	0.258	0.272	0.269	0.253	0.026	0.230	0.276	0.103
Si:Ca	0.013	0.009	0.012	0.012	0.013	0.012	0.002	0.011	0.013	0.130
Si:Mn	0.175	0.127	0.170	0.154	0.176	0.160	0.020	0.143	0.178	0.128
Si:Fe	0.013	0.010	0.012	0.012	0.013	0.012	0.001	0.011	0.013	0.120
K:Si	3.878	4.811	3.874	3.670	3.723	3.991	0.468	3.581	4.401	0.117
K:Ca	0.050	0.045	0.048	0.044	0.050	0.048	0.003	0.045	0.050	0.056
K:Mn	0.679	0.613	0.658	0.566	0.655	0.634	0.045	0.594	0.674	0.071
K:Fe	0.050	0.046	0.048	0.044	0.049	0.048	0.002	0.045	0.050	0.052
Ca:Si	77.385	106.641	80.088	82.695	74.761	84.314	12.828	73.070	95.558	0.152
Ca:K	19.953	22.164	20.674	22.533	20.082	21.081	1.196	20.033	22.129	0.057
Ca:Mn	13.548	13.579	13.597	12.745	13.159	13.326	0.372	13.000	13.651	0.028
Ca:Fe	1.000	1.027	0.999	0.993	0.993	1.002	0.014	0.990	1.014	0.014
Mn:Si	5.712	7.853	5.890	6.488	5.682	6.325	0.914	5.524	7.126	0.145
Mn:K	1.473	1.632	1.520	1.768	1.526	1.584	0.118	1.480	1.688	0.075
Mn:Ca	0.074	0.074	0.074	0.078	0.076	0.075	0.002	0.073	0.077	0.028
Mn:Fe	0.074	0.076	0.073	0.078	0.075	0.075	0.002	0.074	0.077	0.024
Fe:Si	77.417	103.885	80.150	83.262	75.303	84.003	11.508	73.916	94.091	0.137
Fe:K	19.961	21.592	20.690	22.688	20.227	21.031	1.114	20.055	22.008	0.053
Fe:Ca	1.000	0.974	1.001	1.007	1.007	0.998	0.014	0.986	1.010	0.014
Fe:Mn	13.554	13.228	13.608	12.833	13.254	13.295	0.310	13.023	13.567	0.023

REFERENCES

Armands, G., 1972, Geochemical Studies of Uranium, Molybednum, and Vanadium in a Swedish Alum Shale: Doctoral Thesis at Stockholm University, 148p.

Berwick, B., 2008, Depositional Environment, Mineralogy, and Sequence Stratigraphy of the Late Devonian Sanish Member (Upper Three Forks Formation), Williston Basin, North Dakota: Master's Thesis, Colorado School of Mines, 263 p.

Blount, C.W., and Leyden, D.E., 1973, Application of Chelating Ion Exchange Resins for Trace Element Analysis of Geological Samples using X-Ray Fluoresence: Journal of Analytical Chemistry., 45, 7, p. 1045-2050.

Bottjer, R.J., Sterling, R., Grau, A., Dea, P., 2011, Stratigraphic Relationships and Reservoir Quality at the Three-Forks-Bakken Unconformity, Williston Basin, North Dakota. The Rocky Mountain Association of Geologists (RMAG), 2013.

Chelchenko, E.R., and Kelly, D.C., 2007, Terrestrial Records of a Regional Weathering Profile at the Paleocene-Eocene Boundary in the Williston Basin of North Dakota: Geological Society of America Bulletin. 125, p. 428-442.

Croudace, I.W., Rothwell, R.G., 2006, ITRAX: Description and Evaluation of a New Multi-Function X-Ray Core Scanner. Special Publication-Geological Society of London. 267, 51.

Dow, W.G., 1974, Application of Oil-Correlation and Source-Rock Data to Exploration in the Williston Basin: AAPG Bulletin. 58, p. 1253-1262.

Egenhoff, S., Facies Architecture and Sequence Stratigraphy of the Middle Bakken Member, North Dakota: The Bakken-Three Forks Petroleum System in the Williston Basin, Rocky Mountain Association of Geologists Special Publication, p. 27-47.

Frenkel, M.A., Walker, M., Wolters, F., 2004, Integration of LWD and Wireline Array Technologies to Improve Estimation of Hydrocarbon Reserves. Presented at SPE Asia Pacific Oil and Gas Conference, Perth, Australia, October 18-20.

Gaswirth, S.B., Marra, K.R., Cook, T.A, Charpentier, R.R., Gautier, D.L., Higley, D.K., Klett, T.R., Lewan, M.D., Lillis, P.G., Schenk, C.J., Tennyson, M.E., and Whidden, K.J., 2013, Assessment of Undiscovered Oil Resources in the Bakken and Three Forks Formations, Williston Basin Province, Montana, North Dakota, and South Dakota, 2013: U.S. Geological Survey Fact Sheet 2013–3013, 4 p.

Giauque, R.D., Garrett, R.B., and Goda, L.Y., 1979, Determination of Trace Elements in Light Element Matrices by X-Ray Fluorescence Spectrometry. Journal of Analytical Chemistry. 51, 4, p. 511-516.

Ge L, Zhang Y, Cheng Y, Zhou S, Xie T, Hou S, 1997, Proposed Correction and Influence of Drilling fluids in X-ray Fluorescence Logging. X-Ray Spectrum, 303, 8.

Gerhard, L.C., 1982, Geological Development, Origin, and Energy Mineral Resources of the Williston Basin, North Dakota: AAPG Bulletin. 66, p. 989-1020.

Gordon, D., 2012, Understanding Conventional Oil: Energy and Climate, Carnegie Endowment for International Peace, Washington D.C., 34 p.

Haskett, W., Brown, P., 2005, Evaluation of Unconventional Resource Plays. SPE Annual Technical Conference and Exhibition, Dallas, Texas, October 9-12.

Hassan, Z., Amar, B.T., 1998, The Benefits of Logging While Drilling (LWD) for Formation Evaluation in The Dulang West Field. SPE Reservoir Evaluation and Engineering, December, p. 497-503.

Hayes, J.M., and Waldbauer, J.R., 2006, The Carbon Cycle and Associated Redox Processes Through Time, Philosophical Transactions of the Royal Society B: Biological Sciences 361. 1470, p. 931-950.

Heck, T.J., LeFever, R.D., LeFever, J.A., 1998, Overview of the Petroleum Geology of the North Dakota Williston Basin: A North Dakota Geological Survey Publication, Oil & Gas Division, 14p.

Karner, F.R., Benson, S.A., Schobert, H.H., and Roaldson, R.G., 1984, Geochemical Variation of Inorganic Constituents in a North Dakota Lignite. US Department of Energy. Grand Forks, North Dakota, p. 123-137.

Kubo, H., 1978, Energy Dispersive X-Ray Fluorescence Spectrometric Determination of Trace Elements in Oil Samples: Journal of Analytical Chemistry. 50, 7, p. 899-903.

Kundert, D. and Mullen, M, 2009, Proper Evaluation of Shale Gas Reservoirs Leads to a More Effective Hydraulic-Fracture Stimulation. Paper SPE 123586 presented at SPE Rocky Mountain Petroleum Technology Conference, Denver Colorado, USA, 14-16 April.

LeFever, J.A., LeFever, R.D., and Nordeng, S.H., 2011, Revised Nomenclature for the Bakken Formation (Mississiippian-Devonian), North Dakota. The Bakken-Three Forks Petroleum System in the Williston Basin: Denver, Colorado, Rocky Mountain Association of Geologists, p. 11-26.

LeFever, J.A., Martinuik, C.D., Dancsok, E.F.R., and Mahnic, P.A., 1991, Petroleum Potential of the Middle Member, Bakken Formation, Williston Basin: in Saskatchewan Geological Society Special Publications 6, p. 74-94.

LeFever, R.D., LeFever, J.A., and Anderson, S.B., 1987, Structural Evolution of the Central and Southern Portions of the Nesson Anticline, North Dakota: Fifth International Williston Basin Symposium, p. 147-156.

Lineback, J.A., and Davidson, M.L., 1982, The Williston Basin-Sediment-Starved During the Early Mississippian, in Christopher, J.E., and Kaldi, J., Fourth International Williston Basin Symposium: Regina, Saskatchewan, Saskatchewan Geological Society Special Publication 6, p. 125-130.

Lo, K.Y., 2001, Basic Rock Mechanics and Testing: Geotechnical and Geoenvironmental Engineering Handbook, 1088p.

Lorah, M. M., Cozzarelli, I.M., and Bohlke, J.K., 2012, Evaluating Nutrient Fate and Redox Controls in Groundwater in Riparian Areas, USGS National Research Program, Virginia, SIR 2012-5235.

Market, J., Quirein, J. Hinz, D., Pitcher, J. Logging-While-Drilling in Unconventional Shales., 2010, Paper SPE 133685 presented at the SPE Annual Technical Conference and Exhibition, Florence, Italy, 19-22 September.

Meissner, F.F., 1984, Petroleum Geology of the Bakken Formation, Williston Basin, North Dakota and Montana. Petroleum Geochemistry and Basin Evaluation. AAPG Memoir. 35, p. 159-179.

Nicolas, M.P.B., 2006, Petroleum Geology of the Devonian Three Forks Formation, Sinclair Field and Surrounding Area, Southwestern Manitoba: Saskatchewan and Northern Plains Oil and Gas Symposium Core Workshop, 26 p.

Nicolas, M.P.B., 2007, Devonian Three Forks Formation, Manitoba: Preliminary Hydrocarbon and Stratigraphic Investigations: Manitoba Geological Survey 2007 Report of Activities, p. 175-185.

Nordeng, S.H., and Helms, L.D., 2010, Bakken Source System, Three Forks Formation Assessment: North Dakota Industrial Comission, Department of Mineral Resources Report, 9p.

Pollastro, R.M., Cook, T.A., Roberts, L.N.R., Schenk, C.J., Lewman, M.D., Lawrence, O.A., 2008, Assessment of Undiscovered Oil Resources in the Devonian-Mississippian Bakken Formation, Williston Basin Province, Manitoba and North Dakota, 2008: U.S. Geological Survey Fact Sheet, 2008:3021, 2p.

Prammer, M., Morys, M., Knizhnik, S., 2007, Field Testing of an Advanced LWD Imaging/Resistivity Tool. Paper AA presented at the SPWLA 48th Annual Logging Symposium, Austin, Texas, USA, 3-6 June.

Ramakrishna, S. Balliet, R. Sarvotham, S., 2007, Formation Evaluation in the Bakken Complex Using Laboratory Core Data and Advanced Logging Technologies. Paper presented at the SPWLA 51st Annual Logging Symposium, Perth, Australia, 19-24 June.

Rider, M.H., 2011, The Geological Interpretations of Well Logs, Published by Rider-French Consulting Ltd. 440p. ISBN: 0954190688

Rose, H.J., 1963, X-Ray Fluorescence Analysis of the Light Elements in Rocks and Minerals: Applied Spectroscopy, 17, 4, p. 81-85.

Schlumberger Corporation, 2011, Evaluation Brochure-Schlumberger Platform Express, www.connect.slb.com, SMP-5177, 15p.

Schwab, G.M., Philins, J., 1947, Reactions of Iron Pyrite: Its Thermal Decompositional, Reduction by Hydrogen, and Oxidation. Journal of American Chemical Societies. 69, 11, p. 2588-2596.

Smith, M.G., and Bustin, R.M., 1995, Sequence Stratigraphy of the Bakken and Exshaw Formations; a Continuum of Black Shale Formations in the Western Canada Sedimentay Basin: Saskatchewan Geological Society Special Publication 12, p. 299-409.

145

Smith, M.G. and Bustin, R.M., 1996, Lithofacies and Paleoenvironments of the Upper Devonian and Lower Mississippian Bakken Formation, Williston Basin: Bulletin of Canadian Petroleum Geology, v. 44, p. 495-507.

Sonnenberg, S.A., Pramudito, A., 2009, Petroleum Geology of the Giant Elm Coulee Field, Williston Basin. AAPG Bulletin, 93, 9, p. 1127-1153.

Sutiyono, S., 1992, Evaluation of Logging While Drilling Technology, Offshore, East Kalimantan: Indonesian Petroleum Association: in 21st Annual AAPG Convention Proceedings, 2, p. 1-19.

Tebo, B.M., Orbaztsova, A.Y., 1998, Sulfate-Reducing Bacterium Grows with Cr (VI), U (VI), Mn (IV), and Fe (III) as Electron Acceptors. FEMS Microbiology Letters 162.1, p. 193-198.

Thrasher, L.C., 1987, Macrofossils and Stratigraphic Subdivisions of the Bakken Formation (Devonian-Mississippian), Williston Basin, North Dakota. Saskatchewan GS, Fifth International Williston Basin Symposium, p. 53-67.

Wangwe, E.M., 2013, The Usefulness of Rock Quality Designation (RQD) in Determining Strength of the Rock: International Refereed Journal of Engineering and Science. 2, p. 36-40.

Webster, R.L., 1984, Petroleum Source Rocks and Stratigraphy of the Bakken Formation in North Dakota: Hydrocarbon Source Rocks of the Greater Rock Mountain Region, p. 57-64.